NASA/TM—2019–220142

A Meteoroid Handbook for Aerospace Engineers and Managers

A. Moorhead and B. Cooke
Marshall Space Flight Center, Huntsville, Alabama

R. Blaauw and D. Moser
Jacobs Space Exploration Group, Huntsville, Alabama

S. Ehlert
Jacobs Space Exploration Group, Qualis Corporation, Huntsville, Alabama

December 2019

The NASA STI Program…in Profile

Since its founding, NASA has been dedicated to the advancement of aeronautics and space science. The NASA Scientific and Technical Information (STI) Program Office plays a key part in helping NASA maintain this important role.

The NASA STI Program Office is operated by Langley Research Center, the lead center for NASA's scientific and technical information. The NASA STI Program Office provides access to the NASA STI Database, the largest collection of aeronautical and space science STI in the world. The Program Office is also NASA's institutional mechanism for disseminating the results of its research and development activities. These results are published by NASA in the NASA STI Report Series, which includes the following report types:

- TECHNICAL PUBLICATION. Reports of completed research or a major significant phase of research that present the results of NASA programs and include extensive data or theoretical analysis. Includes compilations of significant scientific and technical data and information deemed to be of continuing reference value. NASA's counterpart of peer-reviewed formal professional papers but has less stringent limitations on manuscript length and extent of graphic presentations.

- TECHNICAL MEMORANDUM. Scientific and technical findings that are preliminary or of specialized interest, e.g., quick release reports, working papers, and bibliographies that contain minimal annotation. Does not contain extensive analysis.

- CONTRACTOR REPORT. Scientific and technical findings by NASA-sponsored contractors and grantees.

- CONFERENCE PUBLICATION. Collected papers from scientific and technical conferences, symposia, seminars, or other meetings sponsored or cosponsored by NASA.

- SPECIAL PUBLICATION. Scientific, technical, or historical information from NASA programs, projects, and mission, often concerned with subjects having substantial public interest.

- TECHNICAL TRANSLATION. English-language translations of foreign scientific and technical material pertinent to NASA's mission.

Specialized services that complement the STI Program Office's diverse offerings include creating custom thesauri, building customized databases, organizing and publishing research results…even providing videos.

For more information about the NASA STI Program Office, see the following:

- Access the NASA STI program home page at <http://www.sti.nasa.gov>

- E-mail your question via the Internet to <help@sti.nasa.gov>

- Phone the NASA STI Help Desk at 757–864–9658

- Write to:
  NASA STI Information Desk
  Mail Stop 148
  NASA Langley Research Center
  Hampton, VA 23681–2199, USA

NASA/TM—2019–220142

A Meteoroid Handbook for Aerospace Engineers and Managers

A. Moorhead and B. Cooke
Marshall Space Flight Center, Huntsville, Alabama

R. Blaauw and D. Moser
Jacobs Space Exploration Group, Huntsville, Alabama

S. Ehlert
Jacobs Space Exploration Group, Qualis Corporation, Huntsville, Alabama

National Aeronautics and
Space Administration

Marshall Space Flight Center • Huntsville, Alabama 35812

December 2019

Acknowledgments

The authors would like to thank Rob Suggs, Aaron Kingery, and Peter Brown for their helpful review of and suggestions for this handbook.

Available from:

NASA STI Information Desk
Mail Stop 148
NASA Langley Research Center
Hampton, VA 23681–2199, USA
757–864–9658

This report is also available in electronic form at
<http://www.sti.nasa.gov>

TABLE OF CONTENTS

1. INTRODUCTION TO METEOROIDS 1

   1.1 Terminology 2
   1.2 Preparing to Assess Risk 4
   1.3 References 5

2. METEOROID OBSERVATIONS 6

   2.1 Direct Detection 6
   2.2 In Situ Meteoroid Observations 7
   2.3 Meteor Observations 13
   2.4 Impact Observations 25
   2.5 Meteorite Recovery 28
   2.6 Simultaneous Detection by Multiple Methods 29
   2.7 References 30

3. METEOROID ENVIRONMENT 39

   3.1 Sources of Meteoroids 39
   3.2 Sporadic Environment 41
   3.3 Meteor Showers and Streams 50
   3.4 Model Overviews 53
   3.5 References 58

4. SPACECRAFT EFFECTS 61

   4.1 Types of Meteoroid-Induced Anomalies 61
   4.2 Notable Meteoroid-Associated Anomalies 67
   4.3 Risk Evaluation and Mitigation 73
   4.4 References 75

5. EFFECTS ON THE GROUND 80

   5.1 Types of Effects 80
   5.2 Impact Frequency as a Function of Size/Energy 88
   5.3 Notable Events 92
   5.4 Impacts on the Moon and Mars 96
   5.5 References 99

TABLE OF CONTENTS (Continued)

6. CURRENT AND FUTURE WORK 103

6.1 The Luminous and Ionization Efficiency of Meteors 103
6.2 Ballistic Effects of Meteoric Material 105
6.3 Material Properties 107
6.4 Uncertainties in the Near-Earth Sporadic Meteoroid Environment 109
6.5 Uncertainties in the Near-Earth Shower Meteoroid Environment 111
6.6 The Interplanetary Meteoroid Environment 113
6.7 References 116

LIST OF FIGURES

1. Artist's conception of the Pegasus meteoroid detection satellite. 8

2. Photograph of a Pegasus satellite prior to launch. 8

3. Panels of pressurized gas cells mounted on the back of the main antenna of Pioneer 10. 9

4. This image shows pressurized gas cells on the back of Pioneer 10's antenna as it's being readied for its mission. 10

5. Time-lapse image of Perseid meteors illustrating the term "radiant." 14

6. A map of observers and cameras that spotted a bright meteor over the state of New York in March of 2019. 16

7. Bright bolides detected via satellite over the period 1988–2019. 18

8. Brightness (or instrument voltage) as a function of time (in seconds) for a meteor in six different band-passes measured by a multi-spectral radiometer. 19

9. Beam pattern of CMOR and SAAMER. 21

10. Diagram of radar reflection geometry. 22

11. Part of an infrasound barometer at a station operated by the CTBTO in Greenland. 24

12. Image of a fragment of Comet Shoemaker-Levy 9 impacting Jupiter. 27

13. Meteoroid flux at 1 au as a function of limiting meteoroid mass. 42

14. Diagram of Sun-Earth configuration and corresponding values of Sun-centered ecliptic longitude. 43

15. Meteor radiant distribution observed by CMOR. 44

16. Meteor radiant distribution observed by CMOR. Observational biases have been taken into account and the results have been weighted to a constant limiting mass. .. 45

LIST OF FIGURES (Continued)

17. Meteor radiant distribution observed by CMOR. Observational biases have been taken into account and the results have been weighted to a constant limiting kinetic energy. 45

18. Distribution of meteoroid speeds at the top of the atmosphere as observed by meteor radars. 46

19. Density distribution for meteoroids on long-period and short-period orbits. 48

20. Average meteoroid speed as a function of direction (ecliptic latitude and longitude) at 1 au calculated using MEM 3. 55

21. Annual meteor shower forecast for 2015. 57

22. Meteoroid impact on window 6 of Endeavor, incurred during Space Shuttle mission STS-126. 62

23. Damage on an EVA glove caused by pitting of an International Space Station handrail by meteoroids or orbital debris. 63

24. A visual scan of the Moon's surface by a Narrow Angle Camera on board LRO, disrupted by a meteoroid strike. 64

25. Secondary debris from a dust particle impacting the thermal blanket of the STEREO spacecraft. 66

26. Diagram of the Mariner IV spacecraft. The Cosmic Dust Detector is highlighted in yellow and comprises a small portion of the spacecraft's total surface area. 68

27. Finite element model of the International Space Station used for BUMPER meteoroid and orbital debris analysis. 73

28. An image of the atmosphere taken from the International Space Station. The yellow sodium layer can clearly be seen. 81

29. Three meteorites illustrating meteorite categories. 82

30. A small dent in the roof of a house caused by a falling meteorite. 85

31. Airbursts occurring between 2000 and 2013 that were equivalent to one kiloton of TNT or greater. 86

LIST OF FIGURES (Continued)

32. Barringer crater (also known as Meteor Crater). 87

33. The frequency at which meteoroids and asteroids hit the Earth's atmosphere as a function of kinetic energy. 89

34. A Chelyabinsk superbolide seen from Kamensk-Uralsky in Sverdlovsk Oblast, Russia. 94

35. Damage to the zinc plant in the city of Chelyabinsk. 94

36. Trees toppled by the Tunguska explosion. 96

37. Iron meteorite "Lebanon" on Mars imaged by MER Curiosity. 98

38. Five sample luminous efficiency profiles. 104

39. The result of a hypervelocity impact test using a metal projectile and metal target. .. 106

LIST OF TABLES

1. Example combinations of typical meteoroid sizes and speeds that will produce a magnitude 0 meteor. 2

2. Basic characteristics for each major meteor showers. These characteristics include peak ZHR, date of activity (both peak date and time span), radiant, and geocentric velocity. 51

3. Meteor shower outburst summary. 52

4. Particle diameter that corresponds to each listed kinetic energy assuming a density of 1 g/cc and a speed of 20 km/s. 72

5. PE classification scheme for fireballs. 82

6. List of meteorite falls/finds that caused damage or produced a crater from 1950 to 2014. 90

LIST OF ACRONYMS

AMOR	Advanced Meteor Orbit Radar
AMS	American Meteor Society
ANSMET	Antarctic Search for Meteorites
CCD	charge-coupled device
CME	Chemistry of Micrometeoroids Experiment
CMOR	Canadian Meteor Orbit Radar
CTBTO	Comprehensive Test Ban Treaty Organization
DRAGONS	Debris Resistive/Acoustic Grid Orbital Navy-NASA Sensor
EMP	electromagnetic pulse
GIADA	Grain Impact Analyser and Dust Accumulator
HPLA	high-power, large-aperture
IMEM	Interplanetary Meteoroid Environment Model
IMO	International Meteor Organization
KBO	Kuiper belt object
LDEF	Long Duration Exposure Facility
LEO	low Earth orbit
MAARSY	Middle Atmosphere Alomar Radar System
MEM	Meteoroid Engineering Model
MEO	Meteoroid Environment Office
MER	Mars Exploration Rover

LIST OF ACRONYMS (Continued)

METEM	the Divine-based meteoroid engineering model
MORP	Meteorite Observation and Recovery Program
OSIRIS-Rex	Origins, Spectral Interpretation, Resource Identification, Security, Regolith Explorer
PNP	probability of no penetration
SAAMER	Southern Argentina Agile Meteor Radar
ZHR	zenithal hourly rate

TECHNICAL MEMORANDUM

A METEOROID HANDBOOK FOR AEROSPACE ENGINEERS AND MANAGERS

1. INTRODUCTION TO METEOROIDS

At the beginning of the Space Age, spacecraft designers and mission planners were very concerned about meteoroids. They envisioned vehicles being ripped to pieces by streams of fast-moving space rocks, a notion promoted by the science fiction novels and movies of the time. The reality is, of course, different—the meteoroid streams that produce meteor showers are not dense by laypeople's standards, having spatial densities of just a handful of particles per cubic kilometer, even during meteor outbursts. The ever-present, diffuse, sporadic background, which produces observed meteor rates of only 5 to 8 meteors per hour, makes up 90% of the meteoroid risk to spacecraft that spend at least a year in low Earth orbit (LEO), whereas the visually spectacular but short-lived meteor showers make up the other 10%.

Still, meteoroids do pose a significant risk to spacecraft. At Earth, they can travel 12 to 72 km/s. These high speeds cause even small meteoroids to carry enormous kinetic energy, making them capable of doing serious damage to spacecraft. For example, a 1-mm-diameter meteoroid moving at 25 km/s can inflict the same damage as a bullet fired from a 0.357 Magnum pistol. An exterior wire can be severed by a 0.1-mm (100 μm) particle, a spacesuit can be penetrated by a 0.5-mm meteoroid, and an unshielded pressure wall (like the cabin of the Space Shuttle) can be perforated by centimeter-sized particles.

Along with mechanical damage, meteoroids can also cause other types of spacecraft anomalies. Meteoroids can transfer their momentum to the spacecraft, which can destroy or damage equipment such as shunt resistors and charge-coupled device (CCD) detectors with a clear view of space. Meteoroid impacts can also generate plasma. The impact vaporizes material, producing a crater and an expanding plasma, which can in turn provide a conductive path for any charge accumulated on the spacecraft. This effect is thought to be responsible for the demise of a satellite in one case: the OLYMPUS communications satellite was sent tumbling out of control during the 1993 Perseid outburst, and a Perseid meteoroid strike has been posited as a possible cause (McDonnell et al. 1993; Caswell et al. 1995). Other researchers have suggested that very fast meteoroids could produce a small electromagnetic pulse capable of disrupting spacecraft function (Close et al. 2010).

1.1 Terminology

1.1.1 Interplanetary Dust, Meteoroids, Meteors, and Meteorites

A meteor occurs when a solid particle passes through a gaseous planetary atmosphere and produces light, ionization, shock waves, and other physical phenomena, while a meteoroid is a natural particle moving in interplanetary space. More specifically, a meteoroid is a particle in interplanetary space that is smaller than an asteroid and larger than a dust particle; Commission F1 of the International Astronomical Union gives the relevant size range as roughly between 30 μm and 1 m. Finally, a meteorite is any fragment of a natural object that survived the meteor phase or impact with an atmosphere or planetary or lunar surface.

Interplanetary dust particles generally come from comets. They are small and may or may not produce meteors, depending on the speed of entry. Typically, the dust particle is quickly decelerated high in the atmosphere, where the atmospheric density is low and the body does not get hot enough to evaporate. The remnants may float down through the atmosphere and gradually reach the ground undetected. Dust can be collected both in space and in the terrestrial environment (Brownlee 1985).

Most meteoroids are fragile and are destroyed in the atmosphere, never reaching the ground to become macroscopic meteorites. During atmospheric entry, they produce meteors often detectable via optical and radio sources (see chapter 2). Typically, meteors observed by the naked eye and by meteor cameras are caused by meteoroids between 50 mm and 0.2 m; the exact size limit depends on the velocity (Ceplecha et al. 1998). Table 1 lists example combinations of meteoroid sizes and speeds that typically create a meteor as bright as the planet Saturn or the star Vega (visual magnitude 0).

Table 1. Example combinations of typical meteoroid sizes and speeds that will produce a magnitude 0 meteor. Adapted from Ceplecha et al. (1998)

Meteoroid Size (cm)	Speed (km/s)
2	15
1	30
0.5	60

Meteors are divided into subgroups based on their brightness. The term *fireball* or *bolide* is used when the meteor's brightness surpasses stellar magnitude –4 (which is as bright as the planet Venus). If a meteor's visual magnitude is –17 or brighter, it is called a *superbolide* (the full moon has a visual magnitude of –12, whereas that of the Sun is –27). Fireballs are usually produced when the meteoroid is larger than 2 cm (assuming a 15 km/s speed; Ceplecha et al. 1998). Superbolides are produced by the entry of massive objects a meter or larger in diameter. These events often draw the attention of the public, as they are visually very impressive. They can also be detected by: optical cameras, radars, acoustic detectors, seismic detectors, and even satellites orbiting the Earth and looking down. The Chelyabinsk meteor of February, 2013, is an example of a superbolide.

Meteorites are classified into types based on their mineral composition. There are three broad classes: stony, iron, and stony-iron. Iron meteorites are a mixture of iron and nickel. They are more likely to survive atmospheric entry than stony meteoroids. Stony meteorites, composed of silicates, are the most commonly found, and are further subdivided into chondrites and achondrites. Most stony meteorites are chondrites, which contain small spherical structures called chondrules, which are in turn melted droplets of material formed during the early stages of the Solar System. Achondrites do not contain chondrules. The last class of meteorites, the stony-irons, contains both iron-nickel alloys and silicates, as the name implies.

The Meteoroid Environment Office (MEO) refers to meteoroids larger than 10^{-6} g being within the *threat regime*. This is the mass threshold above which meteoroids can typically puncture spacecraft parts or Extravehicular Activity (EVA) suits. However, smaller dust particles can abrade the surfaces and solar arrays of a spacecraft, as well as exposed optical surfaces.

1.1.2 Meteor Showers and Sporadic Meteors

When most people think of meteors, they think of meteor showers, such as the Perseids, which put on a beautiful visual display every August. The Perseids are simply the most well-known example of a meteor shower; the full list of known or reported meteor showers numbers in the hundreds. *Meteor showers* occur when the Earth passes through a trail of debris left behind by a comet or asteroid as it orbits the Sun; the shower lasts for the length of time it takes for the Earth to pass through this trail, which can range from a few hours to many weeks. The particles in this debris trail, which is usually comprised of individual meteor streams produced in years when the parent body is close to perihelion, have similar orbits. Therefore, these trails encounter the Earth with the same geometrical circumstances and will appear to radiate from a common point in the night sky, referred to as the meteor shower radiant, with similar speeds. The name of the meteor shower is derived from the constellation in which the radiant is located: the Leonid radiant is located within Leo, the Taurids in Taurus, and so forth. While some meteor showers produce large numbers of meteors, others are barely noticeable; meteor astronomers measure the level of activity in terms of zenithal hourly rate (ZHR). This quantity represents the number of meteors seen per hour by an observer when the radiant is directly overhead. The observed hourly rate will be smaller if the radiant is near the horizon. Even though there are now several hundred meteor showers in databases, the vast majority are classed as minor, with ZHRs on the order of 1; chapter 3 lists the most significant meteor showers in terms of visual activity.

It is a mistake, however, to think that the meteoroid environment consists entirely, or even mostly, of meteor showers. The vast majority of meteoroids are so-called *sporadic meteoroids*, which may be encountered throughout the year. The sporadic background consists of particles that have been in space for many millennia, during which time their orbits have evolved to the point where they have lost most of their similarity to the orbits of their parent bodies. Sporadic meteoroids account for the bulk of the meteoroid flux encountered by Solar System bodies and spacecraft; chapter 3 describes this in detail.

1.2 Preparing to Assess Risk

The first step in assessing the risk a meteoroid impact poses to a spacecraft is characterizing the meteoroid environment seen by that spacecraft on a given mission. Environment models describe the rate at which particles encounter the spacecraft, along with their properties, such as speed, impact angle, and bulk density. Risk assessments must also consider the spacecraft's properties, such as size, orientation, and material components. Risk assessment codes such as BUMPER take an environment description, spacecraft design (often in the form of a computer-aided design [CAD] model), and mission trajectory as inputs to calculate the probability of no penetration or the probability of no critical failure. These calculations use ballistic limit equations (BLEs) to compute the level of damage for a given material or component.

Accurately computing the risk is challenging because spacecraft are made of diverse materials and components. Furthermore, the difficulty of conducting impact testing at speeds typical of meteors means that the effect of meteoroid impacts on most materials is unknown or poorly constrained. This can and has led to programs questioning whether the risk posed by micrometeoroid and orbital debris (MMOD) is over-reported, given the observed spacecraft failure rate or anomaly rate. A common first assumption in these cases is that the environment models are in error, but this is not necessarily the case. The fault often lies in improper use of the BLEs. For example, an aluminum particle upon aluminum single-wall surface BLE is not adequate for assessing the damage done by a meteoroid to a composite fuel tank, yet designers will often apply such BLEs regardless because no appropriate meteoroid-specific BLE exists. The notion that some number is better than no number can result in extraordinarily high risk levels and can create debate and delay within the programs (Squire 2015).

It is also important to remember that environment models have limitations. For example, NASA's Meteoroid Engineering Model (MEM) is valid only between Mercury and the asteroid belt. Using it in the design of a vehicle headed to Europa would be a mistake. Similarly, MEM specifically models particles in the threat regime. Artificially extending MEM to smaller particle sizes would likely produce inaccurate results.

Finally, there are uncertainties and gaps in our understanding of the meteoroid environment. Meteoroids are small, fast, and destroyed by their entry into the atmosphere or their impacts onto spacecraft. Therefore, we never directly observe meteoroids. Rather, we observe their proxies: the light emitted by a meteor, its ionization trail, the spacecraft attitude disturbances they can cause, and the craters they create on returned spacecraft surfaces. Because we only observe these proxies, characterizations of meteoroid density, speed, and size involve assumptions and the use of theories that can have significant built-in unknowns. In assembling the MEM model, we have tried to minimize the impact of these unknowns by building a model that is consistent across all particle sizes in the threat regime and that matches cratering results from returned surfaces.

1.3 References

Brownlee, D.E.: "Cosmic Dust - Collection and Research," *Annual Review of Earth and Planetary Sciences*, Vol. 13, *No. 1*, pp. 147–173, 1985

Caswell, R.D.; McBride, N.; and Taylor, A.D.: "Olympus End of Life Anomaly-A Perseid Aeteoroid Event?" *International Journal of Impact Engineering*, Vol. 17, pp. 139–150, 1995.

Ceplecha, Z.; Borovička, J.; Elford, G.W.; et al.: "Meteor Phenomena and Bodies," *Space Science Reviews*, Vol. 84, No. 3, pp. 327–471, 1998.

Close, S.; Colestock, P.; Kelley, M.; and Lee, N.: "Electromagnetic Pulses Generated by Meteoroid Impacts on Spacecraft," *Journal of Geophysical Research: Space Physics,* Vol. 115, No. A12, p. A12328, https://doi.org/10.1029/2010JA015921, 2010.

McDonnell, J.A.M. et al.: "The Olympus Satellite Anomaly: Hypervelocity Impact Effects and Meteoroid Collision Assessment," pp. 1–35, 1993.

Squire, M.D.; Cooke, W.J.; Williamsen, J.; et al.: "Joint Polar Satellite System (JPSS) Micrometeoroid and Orbital Debris (MMOD) Assessment," Technical Report NASA/TM-2015-218780, NASA Langley Research Center, Hampton, VA, 2015.

2. METEOROID OBSERVATIONS

Meteors have been observed and recorded throughout history (Yang et al. 2005; Kronk 2014), but modern meteor observations began in earnest in 1833. During the four hours before dawn on November 13, the eastern half of North America was treated to a spectacular meteor storm. Observers claimed to see up to a thousand meteors per minute radiating from a point within the constellation Leo. The experience inspired several American scientists (including Denison Olmsted and Alexander Catlin Twining) to begin studying the then-unexplained phenomena of meteors and meteor showers. At first, meteor data consisted simply of visual observations, but has since expanded to include video, radar, lidar, telescopic, and infrasound observations. Meteoroids may be observed prior to entering the atmosphere via impact detectors mounted on spacecraft, and we can, in some cases, also recover and study the remnants of meteors in the form of meteorites. This chapter is dedicated to describing the different types of meteor observations, the type of equipment (in broad terms) used in each case, and the information that can be extracted.

Although meteor astronomy began with the visual observation of meteors in the atmosphere, the first section of this chapter will discuss space-based meteoroid detections. These *in situ* experiments provide valuable measurements of the meteoroid cratering rate on spacecraft, but are expensive and the data are often limited. Thus, we heavily supplement *in situ* data with meteor observations, described in section 2.3. Meteor observations are the largest source of meteoroid data and correspondingly make up the largest fraction of this chapter. Finally, we briefly discuss meteorite recovery and the information it contributes to our understanding of the meteoroid environment.

2.1 Direct Detection

It is not possible to directly detect potentially hazardous meteoroids with the current technology. Our telescopes do not always detect asteroids before they enter the atmosphere (see, e.g., the Chelyabinsk impactor discussion in section 5.3.4); detecting millimeter-sized meteoroids is out of the question.

We can, however, directly detect particles that are either larger or smaller than meteoroids. Asteroids can be observed individually with telescopes, and small particles can be observed in the aggregate as zodiacal light. This latter phenomenon occurs when particles ranging in size from 10 to 300 microns in diameter—i.e., dust and sub-hazardous meteoroids—reflect and scatter sunlight. Studies of the zodiacal light can be used to probe the distribution of small particles in the Solar System and can be used to constrain dynamical models of dust particles (e.g., Nesvorný et al. 2010) or, assuming that the distribution of dust and meteoroids is similar, meteoroid models (Jones 2004).

2.2 *In Situ* Meteoroid Observations

In situ observations are those in which a spacecraft detects meteoroids (or man-made orbital debris) striking a detector. Such observations directly measure the rate at which meteoroids strike and/or damage a spacecraft surface and therefore provide valuable constraints on meteoroid environment models. A well-designed *in situ* experiment can measure multiple meteoroid properties; examples include impact speed, meteoroid or crater size, composition, and velocity. A dedicated *in situ* experiment is not strictly necessary for collecting meteoroid impact data; meteoroid cratering rates can sometimes be extracted from the pattern of damage on returned or inspected spacecraft surfaces. Both planned and incidental observations will be discussed in this section.

Deriving meteoroid rates, masses, speeds, and other properties from *in situ* detections requires an understanding of how the impactor and detector interact. For instance, ballistic limit equations, or BLEs, describe quantities such as the depth and width of an impact crater or the limiting thickness that can be penetrated by a given projectile. In many cases, these equations are derived empirically from tests of aluminum spheres striking targets at sub-meteoroid speeds (see, for example, Cour-Palais 1985); aluminum spheres are a poor stand-in for meteoroids, but it is not currently possible to accelerate fragile meteoritic material to 20 km/s in a laboratory. Other BLEs are derived from theoretical models of impact physics (e.g., Watts & Atkinson 1995), but depend on quantities, such as the speed of sound within a meteoroid, that are not known. As a result, meteoroid fluxes derived from impact experiments are uncertain, and the level of uncertainty is not known.

2.2.1 Penetration Detectors

Perhaps the most obvious method for detecting particle impacts is to measure the rate at which an exposed surface is damaged or penetrated. The three Pegasus satellites (see figures 1 and 2), launched in 1965, used this basic approach to measure the meteoroid impact flux. Each satellite had large extendable wings covered with meteoroid impact detectors; these detectors consisted of aluminum-copper-mylar parallel plate capacitors that would discharge when punctured by a meteoroid. The detectors were produced in three thicknesses, each of which required a different minimum meteoroid energy for penetration, thus producing a simple size distribution. However, because each capacitor stopped working when punctured, the usable area decreased gradually over time as the spacecraft collected impacts. No meteoroid properties were measured other than the ability to penetrate these detectors: velocity, density, and impact angle were all unknown.

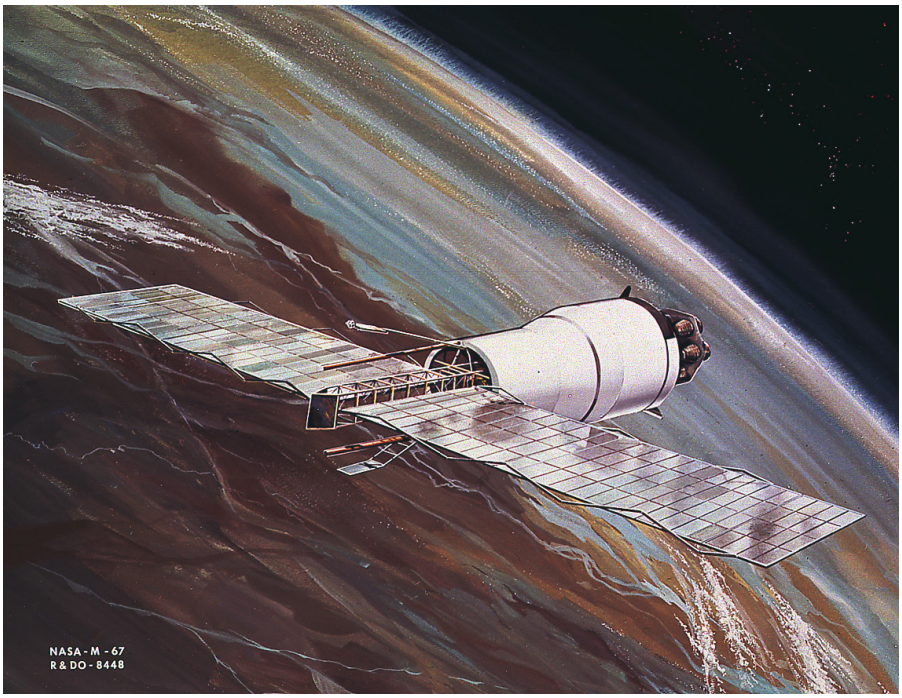

Figure 1. Artist's conception of the Pegasus meteoroid detection satellite. The large wings of aluminum-covered meteoroid detection panels extend outward from the spacecraft's axis in the foreground.

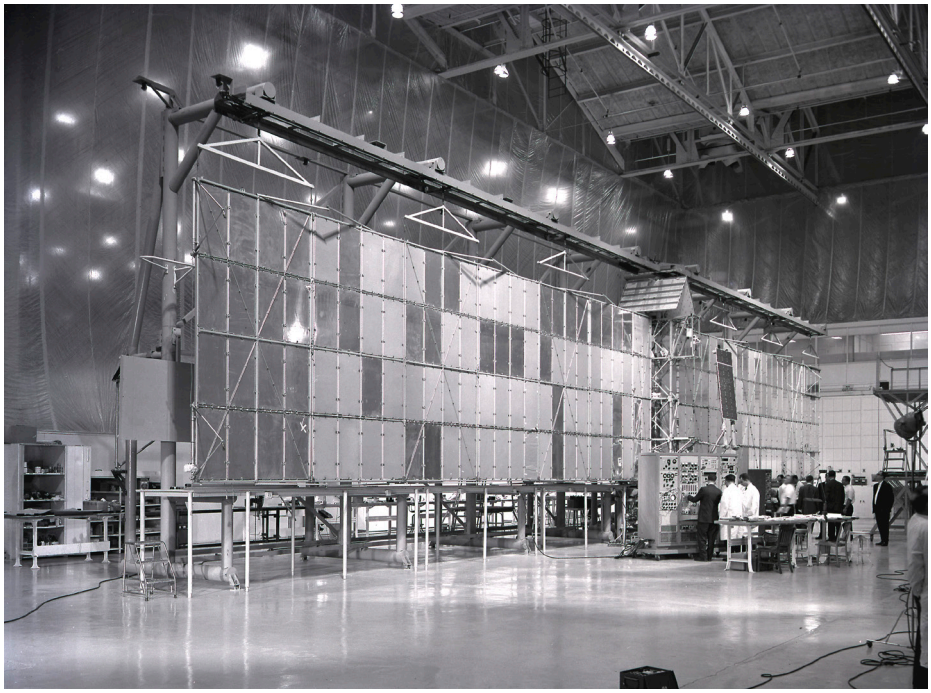

Figure 2. Photograph of a Pegasus satellite prior to launch. Note the large wings covered in rectangular meteoroid impact detector panels.

Each Pegasus satellite had over 200 square meters of impact detectors, totaling more than 600 square meters of collecting area. The sheer size of these detector arrays, combined with their two-year operation, produced one of the best measurements of the near-Earth meteoroid cratering flux ever made. The Pegasus data have the additional advantage of being uncontaminated by orbital debris. In 1965, orbital debris was virtually nonexistent, and it was therefore safe to assume that any impacting particle was a natural one.

Pioneer 10 and Pioneer 11 conducted another measurement of the meteoroid flux 7–8 years after Pegasus. Unlike the Pegasus satellites, which remained in low Earth orbit, Pioneer 10 and 11 flew outward to the asteroid belt, Jupiter, and Saturn. Pioneer 10 was in fact the first mission to pass through the asteroid belt and visit Jupiter, and Pioneer 11 was the first to visit Saturn. Each satellite carried panels of gas-filled cells attached to the back of its main dish antenna (see figures 3 and 4). When punctured by a meteoroid, the gas would leak out of the cell, and the impact would be detected as a drop in pressure. A large hole was assumed to produce a faster rate of leakage and thus the gas loss rate provided a crude measure of impactor size (or, rather, kinetic energy).

Figure 3. Panels of pressurized gas cells were mounted on the back of the main antenna for the purposes of detecting meteoroids; particles larger than 10^{-9} g could puncture Pioneer 10's cells and cause a detectable drop in gas pressure.

Figure 4. This image shows pressurized gas cells on the back of Pioneer 10's antenna as it's being readied for its mission.

Pioneer 10 and 11 made the first measurements of the meteoroid environment outside 1.6 au (Humes et al. 1974) and confirmed that Jupiter's gravity produces a massive enhancement in its local meteoroid environment (Humes et al. 1975). However, the small number of total impacts (for Pioneer 10, 67 impacts were recorded between 1 and 5.1 au) provided for a cruder measurement than that obtained by Pegasus. Additionally, these spacecraft probed the meteoroid environment at much smaller sizes than Pegasus. With approximate limiting masses of 10^{-9} g for Pioneer 10 and 10^{-8} g for Pioneer 11 (Humes et al. 1975), the particles that these spacecraft detected were several orders of magnitude too small to be hazardous to spacecraft.

Meteoroid impacts can penetrate electrical wires as well as flat plates; thus, one possible method of detection is to expose grids of conductive or resistive wires and measure impacts through changes in current. For instance, the Debris Resistive/Acoustic Grid Orbital Navy-NASA Sensor (DRAGONS) uses resistive grids to measure the timing, direction, and puncture size resulting from debris impacts (Liou et al. 2015).

2.2.2 Surface Return or Inspection

More than 10 years after Pioneer, NASA flew the Long Duration Exposure Facility (LDEF) to collect a variety of space environment data. LDEF followed a nearly circular orbit with an altitude of 500 km and inclination of 28.5° (Zook 1990) for almost six years, maintaining a constant orientation relative to its orbit (for example, the same surface faced away from the Earth for the entire mission). Unlike the Pegasus and Pioneer spacecraft, LDEF had no communication with the Earth while in orbit. Instead, the entire spacecraft was retrieved at the end of its mission and analyzed.

LDEF carried several dedicated impact experiments, including the Meteoroid and Space Debris Impact Experiment, which exposed a series of aluminum plates to the space environment (Humes 1991), and the Chemistry of Micrometeoroids Experiment (CME), which exposed both aluminum and gold targets. The data from these experiments were supplemented by impact crater data observed on other parts of the spacecraft surface. The crater dimensions were measured, counted, and incorporated into meteoroid models (see, for example, Love & Brownlee 1993). Residues in impact craters on CME targets were subjected to Scanning Electron Microscopy (SEM) and Energy Dispersive X-ray Analysis (EDXA) to determine their composition and could in many cases be attributed to orbital debris or meteoroids based on composition (Hörz et al. 1995).

LDEF was followed by a European Space Agency (ESA) mission named the European Retrievable Carrier (EURECA). Its purpose was to study space environment effects, including meteoroid and orbital debris impacts, through post-flight examination. Unlike LDEF, EURECA kept one face pointing towards the Sun, rather than the Earth, throughout its mission, and EURECA was largely covered with thermal blankets rather than aluminum plating (Drolshagen et al. 1995). These thermal blankets, along with solar panels, aluminum signs, and scuff plates (McDonnell et al. 1998), were examined for meteoroid impacts. EURECA also carried a dedicated impact experiment—the Timeband Capture Cell Experiment (TiCCE)—that consisted of thin aluminum foil. Meteoroids and debris punched holes through this thin foil; thus, diameters could be extracted but not penetration depth. EURECA was exposed to the environment at an orbital altitude of 508 km for 326 days between mid-1992 and mid-1993 (Mandeville & Berthoud 1995).

A dedicated mission is not required, however, for obtaining meteoroid impact data from spacecraft surfaces. Particle impact data has also been obtained from Space Shuttle windows, Hubble Space Telescope solar arrays, and International Space Station hardware (Hyde et al. 2017). The utility of these data for meteoroid analyses varies depending on the degree of orbital debris contamination, exposure time and area, and the way the surface material responds to impacts. This type of data collection can be particularly important for reusable spacecraft; at least 17 meteoroid impacts on shuttle windows were large enough to warrant window replacements (Hyde et al. 2001).

2.2.3 Impact Ionization Detectors

Impact ionization detectors do not detect the impact itself but rather collect electrons and other ions from the plasma produced by a particle impact. The strength of the signal strongly depends on the speed of the impactor; an example dependence of $v^{3.48}$ is quoted by McBride & McDonnell (1999). Some speed information can be extracted from the signal, although speed measurements typically are uncertain to a factor of two. Impact ionization detectors are not only heavily biased towards faster particles, but are also usually quite small—the largest impaction ionization detectors, on the Ulysses and Galileo spacecraft, had 0.1 m^2 of sensitive area (Grün et al. 1992). Typical detectors are closer to 0.01 m^2 (e.g., DEBIE: Kuitunen et al. 2001). Thus, this detection method has not produced meteoroid flux measurements within the threat regime.

2.2.4 Piezoelectric Impact Detectors

Piezoelectricity is a phenomenon whereby electric charge accumulates in certain materials when they are subjected to mechanical stress. These materials can act as transducers by converting mechanical energy, such as that imparted by a hypervelocity impact, to electrical current (Simpson & Tuzzolino 1985). One such material that is commonly used as an impact detector is polyvinylidene fluoride (PVDF); it has been employed in numerous dust detectors, including Vega 1 and 2 (Perkins et al. 1985), ARGOS (Tuzzolino et al. 2001), Cassini (Srama et al. 2004), Stardust (Tuzzolino 2003), New Horizons (Horányi et al. 2007), and the Aeronomy of Ice in the Mesosphere (AIM) mission (Russell et al. 2009). Lead zirconate titanate (PZT) is also used, although less commonly, as a piezoelectric detector (Tuzzolino et al. 2004; Corte et al. 2016; Kuznetsov et al. 2018).

Like impact ionization detectors, PVDF detectors tend to be small in area; the examples cited above range from 0.005 m^2 (Cassini: Bradley et al. 1996) to 0.102 m^2 (SDC: Horányi et al. 2007; AIM: Russell et al. 2009). Thus, like impact ionization, this is a detection mechanism that has yet to produce meteoroid flux measurements within the threat regime.

2.2.5 Acoustic Sensors

When a particle impacts a spacecraft surface, it sends sound waves through the material. A microphone attached to the surface can detect these acoustic signals and thus detect the impact. Multiple microphones located at different points on the surface may be able to triangulate the impact location and/or determine the size of the impact.

Acoustic sensors (microphones) can be attached to a variety of other materials and thus can detect impacts over a larger area, but these data may have larger uncertainties associated with them (Tuzzolino 2003), and it is challenging to design a detector for large impacts (Corsaro et al. 2016).

Acoustic data may be combined with other detector types to overcome the uncertainty issue; for instance, DRAGONS attaches multiple acoustic sensors to both thin films and a backplate to assist in impact detection and characterization (Liou et al. 2015). When combined with the data from a resistive grid and an absorptive backplate, the acoustic data contribute to a detailed description of the time, angle, speed, and size of an impact.

2.2.6 Other Methods

This section focuses on a few of the more commonly used meteoroid detection mechanisms, but there are numerous others. For instance, meteoroids may be detected as sudden changes in a spacecraft's momentum or attitude; a press release indicated that the Gaia spacecraft saw large numbers of attitude disturbances and attributed them to meteoroid strikes, although no detailed account of their analysis has been published. In order to correctly interpret attitude strikes, it is important to know whether the momentum imparted to the spacecraft is magnified by a "kick back" effect; this has been estimated to enhance the momentum by a factor of 2–3 (Squire 2017).

It is also possible to capture small particles in Aerogel, which is a type of solid foam (Burchell et al. 2008). Dust particles are decelerated and captured by the soft material without being completely destroyed (although volatiles are typically lost) and can thus be retrieved and studied in a lab. However, Aerogel cannot capture particles large enough to be hazardous, and so we will not discuss Aerogel dust capture experiments further in this handbook

Nondestructive particle detection can also be accomplished using a light curtain, in which laser diodes are placed side by side. Particles passing through this curtain block or scatter light and are thus detected. The Grain Impact Analyser and Dust Accumulator (GIADA) instrument on *Rosetta* made use of such a light curtain, although one with a very small 0.01 cm^2 area (Colangeli et al. 2007).

2.3 Meteor Observations

Meteoroids enter the Earth's atmosphere at phenomenal speeds. The air heats up dramatically as a result and strips away the surface of the meteoroid in a process called ablation. From the ground, we see this process in the form of a streak of light known as a meteor. Meteors are far more visible than the meteoroids themselves; a meteoroid the weight of a penny can create a fireball visible hundreds of miles away. As a result, meteor observations provide the most extensive—and the oldest—sets of data on the meteoroid environment. Optical meteor observations take many forms, from simple naked-eye observations to video recordings to satellite observations. The first part of this section is devoted to the various methods of detecting meteors optically.

Meteors do not only produce light, however; they also generate long trails of ions and electrons capable of reflecting radio waves. The long, thin trail of ionization produced by a meteoroid the size of a grain of sand can reflect a radar signal with a radar cross-section equivalent to that of a large ship (Ceplecha et al. 1998; Skolnik 2001). In fact, radar networks can observe meteors caused by meteoroids smaller than the width of a human hair. Meteors also produce shock waves in the air that can be detected with infrasound microphones, sometimes from incredible distances. Radar and infrasound observations are discussed in sections 2.3.2 and 2.3.3, respectively.

If the same meteor is detected by multiple observers or instruments at different locations, these observations can usually be combined to determine a trajectory, including distance, height, speed, and direction of motion. If the true distance is known, the apparent brightness of a meteor can be converted to a "true" or absolute brightness. Meteor observation networks therefore usually consist of multiple stations to make this triangulation possible.

A single observer, camera, or other optical instrument can see the apparent brightness of a meteor and its general direction of motion, but not measure its true velocity or brightness. However, if multiple meteors from the same meteor shower are seen by a single observer, that observer can determine a radiant and a population index. The radiant is the point in the sky from which the shower meteors appear to originate (see figure 5); these meteors move in parallel, creating a one-point perspective that reflects their direction of motion. The population index is a single number that measures the ratio of dim to bright meteors within a group. It can be converted to a mass index, a power-law exponent expressing the ratio of smaller meteoroids to larger (Koschack & Rendtel 1990). Finally, single-station observations can be used to measure meteor rates; these rates can sometimes be converted to meteor fluxes (Koschack & Rendtel 1990; Campbell-Brown & Jones 2006).

Figure 5. This time-lapse image of Perseid meteors illustrates how meteors belonging to the same shower appear to "radiate" out from a single point in the sky, giving rise to the term "radiant." Image credit: NASA/JPL.

Meteors may be produced whenever a meteoroid strikes a sufficiently thick atmosphere at high speed. This includes the atmospheres of other celestial objects, such as Mars and Venus. In fact, it's thought that meteors could be visible at heights of about 90 km above the Martian surface (Adolfsson et al. 1996) and about 120 km above the Venusian surface (McAuliffe & Christou 2006). A possible meteor trail was seen by the OUVS instrument on Pioneer Venus Orbiter (Huestis & Slanger 1993), and a possible optical meteor in the Martian atmosphere was thought to be seen by the Spirit Rover (Selsis et al. 2005), although it was later shown to be most likely a cosmic ray (Domokos et al. 2007).

2.3.1 Optical Observations

Optical meteor detectors include a wide variety of instruments ranging in complexity from intensified cameras and spectrometers to the naked human eye. These instruments detect the light produced by a meteor; they do not image the meteoroid itself. We therefore usually quote not the minimum mass but the minimum brightness (or "limiting magnitude") detectable by an optical system.

While *in situ* detectors may be limited to a few square meters, or even a few square centimeters, of collecting area, optical detectors essentially use the Earth's atmosphere to intercept meteoroids. The entire atmosphere is not visible from one spot on the globe, of course, but a typical visual effective collecting area can exceed 10,000 square miles (Koschack & Rendtel 1990). Cameras with a narrower field of view will have a smaller collecting area but will still far exceed that of *in situ* detectors.

Optical detectors also carry certain disadvantages. For instance, clouds lie in the troposphere, the lowest 4–11 miles of the Earth's atmosphere. Meteors occur at altitudes of about 100 km (or 60 miles) and therefore cannot be seen except in clear weather. They also cannot be seen during the day unless they are exceptionally bright (at least several times brighter than the planet Venus). Another critical limitation of optical detection methods is that the relationship between a meteor's brightness and a meteoroid's mass is not at all certain. The percentage of a meteoroid's kinetic energy that is converted to visible light is called the luminous efficiency and varies by an order of magnitude or more between competing models (for a comparison, see Weryk & Brown 2013).

2.3.1.1 Visual Observations. The oldest and simplest way to collect meteor data is through visual observation: watching meteors using the naked eye. Observers can use a watch and notebook to record when meteors occur, their brightness, and, optionally, the apparent direction of their motion. Visual observations have historically played a prominent role in meteor astronomy and have influenced many meteor terms, such as radiant, which refers to the point from which meteors appear to radiate. Another example is the zenithal hourly rate (ZHR), or the rate at which a visual observer might count meteors under perfect sky conditions when the radiant is directly overhead (i.e., at the zenith).

There are two organizations that collect and analyze amateur visual observations on a large scale. The first of these, the International Meteor Organization (IMO), provides amateurs with basic instructions and collects the results via an electronic report form. From these visual reports, the IMO publishes ZHR profiles for most major meteor showers. These ZHR graphs can help assess whether a meteor shower is exhibiting normal activity or is in outburst. Due to the number of participating observers, the IMO can often produce activity profiles with finer time resolution than dedicated networks. In fact, the initial activity profiles used by the MEO to generate meteor shower forecasts were derived from visual meteor data (Jenniskens 1994).

The second organization that collects visual meteor observations is the American Meteor Society (AMS). The AMS collects reports of individual bright fireballs and, when multiple

reports are available, calculates crude meteor trajectories. While a single visual observer cannot determine the true position or speed of a meteor, a combination of many visual reports can be used to derive a rough trajectory (Moser 2017); see figure 6 for an example. The MEO regularly uses visual reports from the AMS to derive locations, speeds, and heights of bright fireballs of public interest.

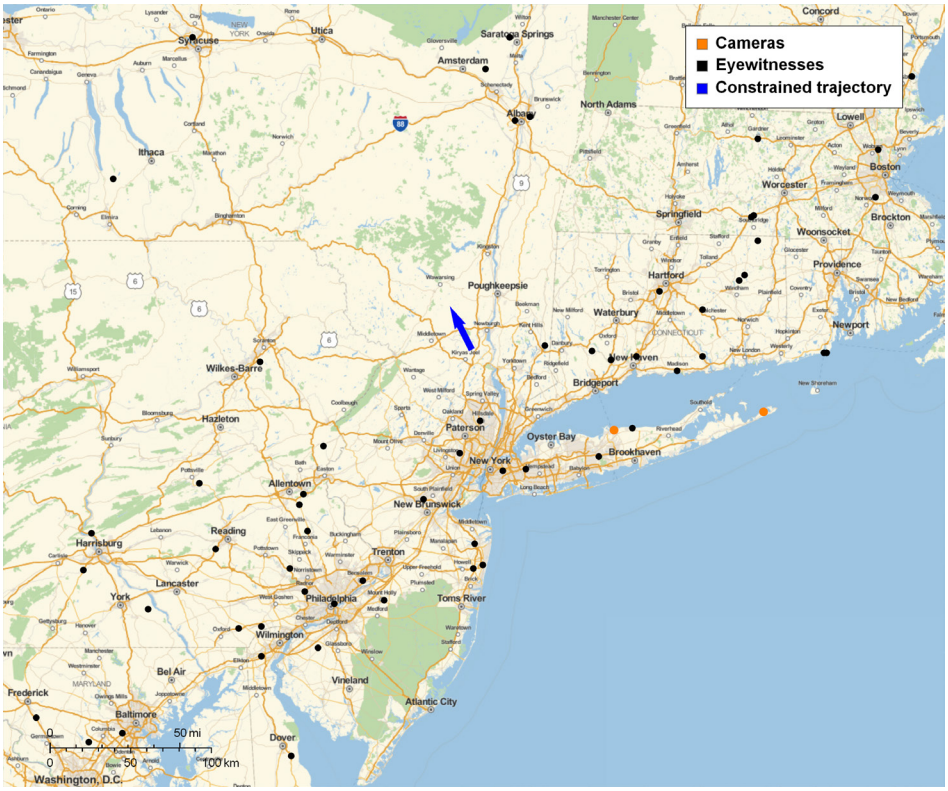

Figure 6. A map of observers (black dots) and cameras (orange dots) that spotted a bright meteor over the state of New York in March of 2019. The blue arrow marks the meteor trajectory derived from the eyewitness and camera data.

2.3.1.2 Photographic (Film and Electronic) Observations. Like visual observers, photographic networks (i.e., networks of cameras, whether film-based or digital) can detect optical meteor signatures. Unlike visual observers, photographic networks create permanent records that can be carefully analyzed at leisure. Cameras can also be placed at set locations at distances ideal for triangulating meteor trajectories. Depending on the quality and resolution of the camera, the resulting photographs can produce extremely precise trajectories and are therefore favored for meteorite recovery projects.

A simple still photograph of a meteor provides information about its brightness, radiant, and apparent position relative to the stars but reveals nothing about the speed of the meteor. To overcome this limitation, meteor cameras can be paired with a "shutter" that creates a strobe effect in the photograph. Meteors then appear as a dashed, rather than solid, streak in the image, and the

length and separation of the dashes will be longer for faster meteors. Some of the meteor's light will be lost, but velocity measurements are often worth this trade-off. One of the earliest systems to use this setup was the Harvard Meteor Project's Super-Schmidt cameras (Jacchia & Whipple 1956), which recorded 3-5 meteors per hour (Jenniskens 2006) using a rotating shutter and produced what was for decades the highest resolution meteor data set available. Today, photographic networks make use of CCD cameras rather than film and liquid crystal shutters rather than spinning blades. For instance, the Desert Fireball Network uses liquid crystal shutters that blink on and off in a unique, non-repeating pattern known as a de Bruijn sequence (Bland et al. 2012; Howie et al. 2017). The irregular shutter pattern essentially overlays a time stamp onto the meteor, measuring both its position and absolute time to determine a speed.

Photographs are sometimes combined with secondary detectors; for instance, a sky brightness sensor (radiometer) can supplement the photograph with time information and, potentially, a detailed light curve. The European Fireball Network takes this approach with its fireball cameras (Spurný et al. 2007).

2.3.1.3 Video Observations. Meteor networks increasingly use video cameras to observe meteors, including the NASA All Sky Fireball Network (Cooke & Moser 2012), the Southern Ontario Meteor Network (Weryk et al. 2008), and the Fireball Recovery and Interplanetary Observation Network in France (Colas et al. 2015). Video meteor cameras are generally inexpensive (security cameras can be used) and detection is relatively easily automated. Videos record the time as well as the position and brightness of the meteor and therefore can be used to derive trajectories and orbits. The relatively low cost and ease of use allows amateur meteor astronomers to make significant contributions to meteor astronomy (see, e.g., Molau et al. 2011).

Video observations involve a trade-off between resolution, frame rate, and computer hardware limitations. The bandwidth of the attached computer system, including wired or internet connections between the camera and the computer, limits the frequency and resolution with which images can be recorded. Additionally, it can be challenging to permanently store accumulated meteor video data; possible solutions include keeping only those video clips that include meteors and discarding the original video data after a trajectory and light curve has been extracted.

Both photography and videography involve a tradeoff between field of view and focal length (or "zoom"). A wide field of view and short focal length is optimal for capturing a landscape, while a narrow field of view and long focal length is better for zooming in on a distant bird. Similarly, meteor cameras may choose to use a lens with a wide field of view and a short focal length for surveying a large portion of the sky for bright meteors. For instance, the NASA All Sky Fireball Network uses all-sky cameras to monitor the entire visible sky for very bright meteors (Cooke & Moser 2012). On the other end of the spectrum, telescopic systems monitor a tiny portion of the sky for very faint meteors (e.g., Watanabe et al. 2014).

One can increase a photographic or video camera's sensitivity to faint meteors without changing the focal length or field of view by using a more sensitive CCD or by adding an image intensifier to the system. The trade-offs are an increase in the cost of the system and saturation of bright meteors. Saturation can be reduced by increasing the bit depth, at the cost of generating

large amounts of data and increasing monetary costs. A bright meteor or other object, if intensified, may even damage the camera.

Meteor astronomers can combat these various trade-offs by building networks that combine multiple methods or instruments. For instance, the Canadian Automated Meteor Observatory (CAMO) combines two sets of video cameras with different specifications. Two cameras with a fixed position, wider field of view, higher frame rate, and higher bit depth are coupled to image intensifiers. These cameras are used to automatically detect faint meteors (i.e., those that are as dim as magnitude +7.5) and rapidly compute their trajectory. This information is then fed to two movable mirrors that track the meteor and reflect the light into a telescope with a much narrower field of view. This system thus combines the detection capabilities of a fixed video camera with the fine resolution of a telescope to obtain entire meteor trajectories in fine detail (Weryk et al. 2013).

2.3.1.4 Satellite Observations. Occasionally, meteors are bright enough to be observed by orbiting satellites. In most cases, all that can be measured is the brightness of the meteor; without a second observer, the true distance and speed cannot be triangulated. In rare cases, satellite observations can determine a trajectory if a persistent meteor trail is observed, as it was for the Chelyabinsk fireball in 2013 (Miller et al. 2013). Meteors can even be detected by satellites designed for other purposes. For instance, the Geostationary Lightning Mapper (GLM) satellites have recently been employed as meteor detectors by both the MEO and by personnel affiliated with NASA Ames (Jenniskens et al. 2018).

More often, satellites simply measure the frequency of bright bolides and their brightness or energy. Figure 7 shows the location of bolides from 1988-2019 detected by US government sensors, which, according to Jenniskens et al. (2018), includes satellite detections. Both the size and the color of the symbol indicates the energy released.

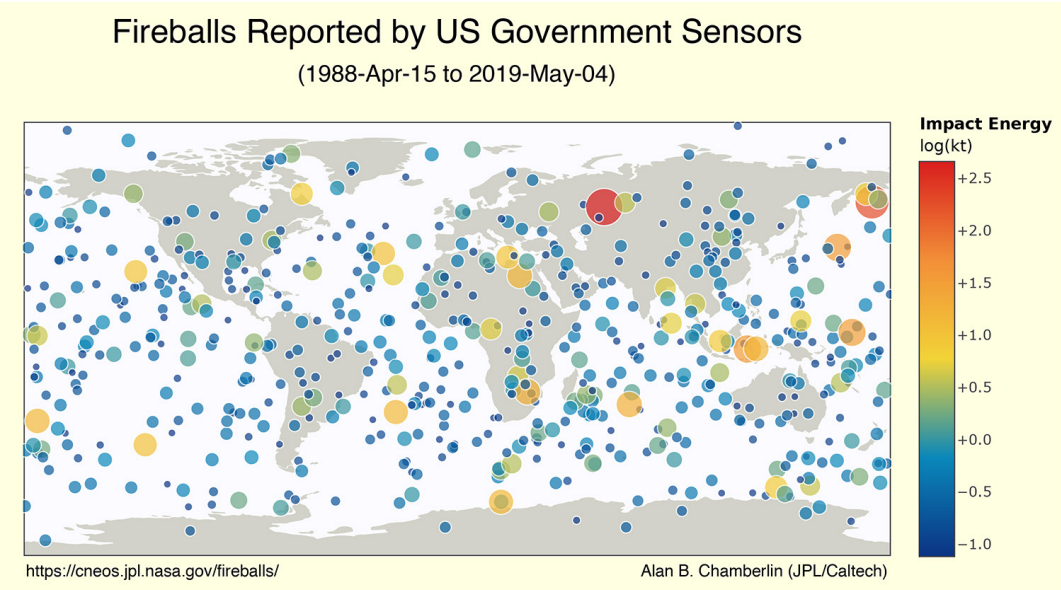

Figure 7. Bright bolides detected via satellite over the period 1988–2019.

2.3.1.5 Radiometers and Spectrometers. Radiometers measure the light level as a function of time and can be used to obtain detailed meteor light curves. They may measure the total light present within a fairly wide range of wavelengths, or they may focus on measuring light in a narrow band of wavelengths. However, they provide no spatial information whatsoever—they are essentially a one-pixel camera. Thus, radiometers are often paired with cameras in a photographic or video network; by combining the results from the radiometer with the camera, one can obtain both a trajectory and a detailed light curve (see, for instance, Spurný et al. 2007) and even speeds in some cases (Shrbený and Spurný 2013).

Meteors can vary in color, and their light can be concentrated at certain wavelengths where there are emission lines. These emission lines correspond to specific elements present in the meteoroid such as magnesium, sodium, calcium, and iron (Vojáček et al. 2015). Oxygen and nitrogen emission lines are also produced by the hot air surrounding the meteoroid. A radiometer that measures a single light level will not be able to capture this information from a meteoroid; instead, one must use a spectrometer.

Spectrometers use either a prism or a grating to physically separate different wavelengths of light. This information can then be collected separately or projected onto an image (for an example of the latter, see Jenniskens 2007). A multi-spectral radiometer combines some of the functionality of a spectrometer with a radiometer. Figure 8 shows data from a multi-spectral radiometer that measures brightness as a function of time within six distinct wavelength ranges (or band-passes).

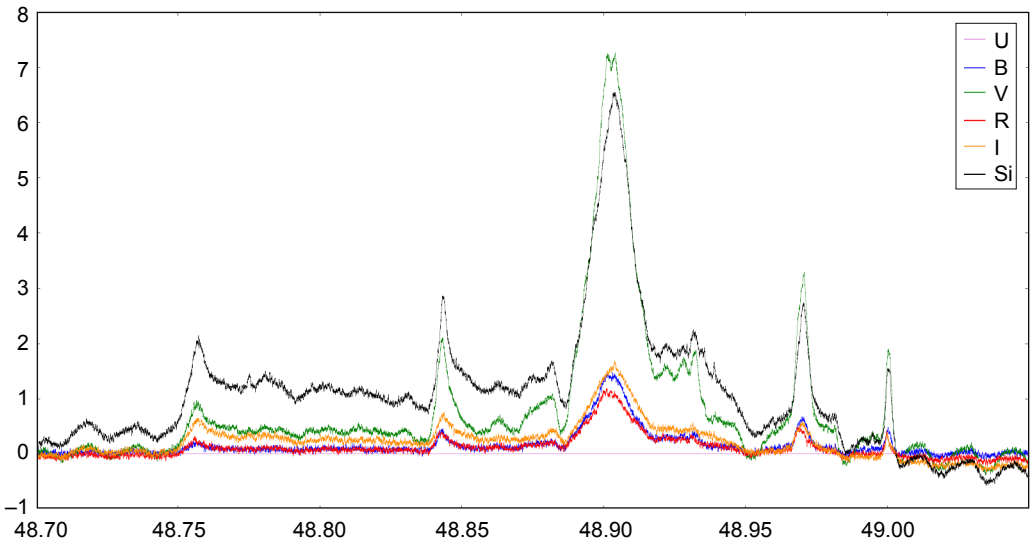

Figure 8. Brightness (or instrument voltage) as a function of time (in seconds) for a meteor in six different band-passes measured by a multi-spectral radiometer.

2.3.2 Radar Observations

When a meteoroid ablates in the Earth's atmosphere, meteoritic and atmospheric atoms are ionized and the cloud of ions and free electrons can be *millions* of times larger than the meteoroid itself. The electrons in this cloud also reflect radio waves; as a result, meteors may be detected by radar systems. Meteor radars can be placed in two categories: high-power, large-aperture (HPLA) radars and patrol radars (for a summary of the characteristics of these two types of radars, see Janches 2003). Both types emit radio waves and detect the portion that is reflected by the meteor, but HPLAs emit a narrow, powerful beam while patrol radars emit a low-power, wide beam. Patrol radars typically focus on detecting the reflections of radio waves off the ionization trail of a meteor, while HPLAs typically detect the reflection off the high-density plasma "head" around the meteoroid. Patrol radars do detect head echoes, however, and HPLAs can detect meteor trails. If the electron line density is less than about 2×10^{14} electrons per meter, the trail is called "underdense" and the radio wave can partially penetrate the trail and reflect off both the front and back edge of the cylindrical trail. Brighter meteors produce a higher line density and are opaque to radar; these trails are referred to as "overdense." In the underdense case, the total scattered radiation is proportional to the density of the electrons along the line of sight (i.e., the line density), and the signal therefore probes the total ionization more directly (Ceplecha et al. 1998). In the overdense case, the radar cannot penetrate the trail and thus some line density profile must be assumed.

Meteor radars detect the reflection of waves off of meteors; they do not detect radio waves emitted by the meteors. Thus, radio waves must travel first a distance r to the meteor, dropping in intensity by a factor of r^2, then return the same distance r to the detector, dropping in intensity by another factor of r^2. In total, radar sensitivity is inversely proportional to distance taken to the fourth power; in contrast, optical sensitivity is inversely proportional to the square of the distance. Thus, radars are not an ideal method for detecting bright but distant bolides on the horizon.

One of the greatest advantages of observing meteors via radar is that this method does not require a clear, dark sky. Instead, meteors can be detected day and night and radars thus provide the only observations of many daytime meteor showers, such as the Daytime Sextantids. In fact, one of the most significant meteor showers in terms of flux is the Daytime Arietid meteor shower. However, daytime radar meteor observations are affected by Faraday rotation, in which the free electrons in the ionosphere together with the Earth's magnetic field rotates the polarization of the radar beam so that it is no longer parallel to the radar receiving antennas, somewhat reducing their detectability (Elford & Taylor 1997).

Meteor radars can also detect meteors in cloudy weather. While weather radars detect the reflection of radio waves off of the water droplets in clouds, they do so with a radio wavelength of 1-10 cm. At the much longer 10-meter wavelength used by the Canadian Meteor Orbit Radar (CMOR; Jones et al. 2005), clouds are transparent. Weather can still pose certain challenges, however. Lightning produces ionization in the atmosphere that can reflect radio waves and sometimes produces false positives for meteor detection. The powerful transmitter antennas may need to be powered off if they become covered in ice and reflect energy back to the transmit unit, producing gaps in the data.

2.3.2.1 Patrol Radars. Patrol radars emit a broad beam of radio waves in an effort to "cover" as much of the sky as possible. Emission is not, however, uniform; the power is greater in the "lobes" of the transmission beam (see figure 9). Similarly, the receiver is more sensitive to reflections from certain angles; together, this pattern of sensitivity as a function of angle is called the "gain pattern." Gain pattern varies depending on the radar array. Patrol radars typically use Yagi antennas to transmit and receive the radar signal. Yagi antennas consist of parallel metal rods; they can transmit and detect in any direction, but the sensitivity tends to be greater in the direction perpendicular to the rods. Each transmission frequency produced by CMOR is generated by a single antenna and received by five parallel antennas, resulting in a relatively simple pattern with two lobes. The Southern Argentina Agile Meteor Radar (SAAMER) transmits from a circle of eight antennas and thus has a more complex, eight-lobed transmission gain pattern (Janches et al. 2015). This gain pattern must be considered to properly calculate meteor fluxes. However, both CMOR and SAAMER are capable of detecting meteors across a very broad range of angles.

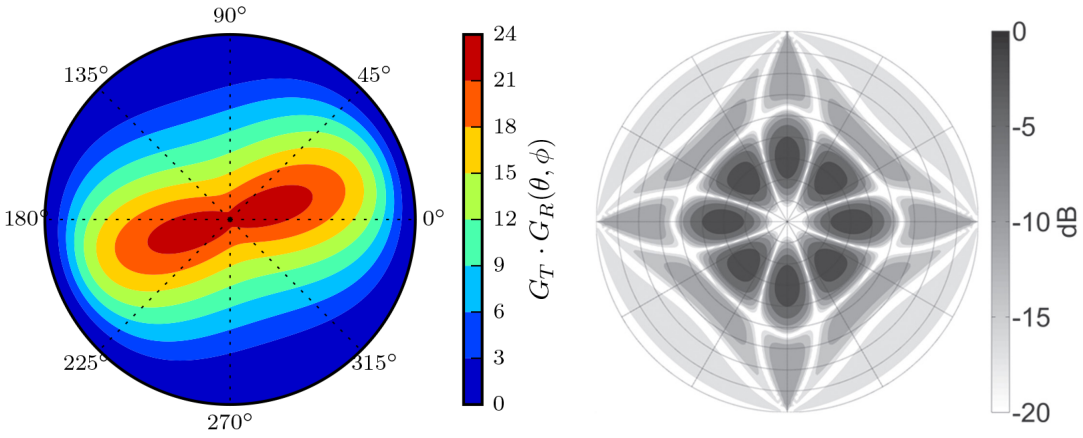

Figure 9. Beam pattern of CMOR (left) and SAAMER (right).

A single transmitter and receiver array can detect meteors and their angular position in the sky; the latter is derived from the phase difference in the reflected radio wave when it is detected by each receiver in the array. Reflected radio waves can be detected only when the meteor trail is perpendicular to the line of sight between the array and the meteor (see figure 10). Thus, a given detected meteor must originate from a radiant that lies within the plane perpendicular to the line of sight. Similarly, meteors belonging to a particular shower (which therefore share a common radiant) will all be detected along a great circle in the sky. If the shower is strong enough to be clearly distinguishable, one can then use angular position alone to measure meteor shower activity with a single meteor radar station (Campbell-Brown & Jones 2006).

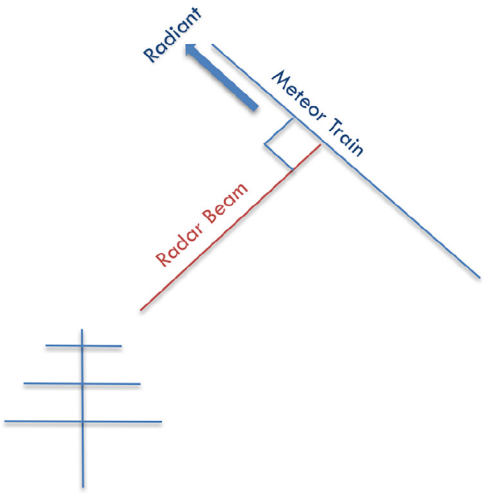

Figure 10. Diagram of radar reflection geometry.

Theoretically, one can also measure the speed of the meteor from the radar diffraction pattern, but in practice it is more effective to employ multiple receiving stations that are physically separated and measure time-of-flight speeds (Baggaley et al. 1994). CMOR, SAAMER, and the defunct Advanced Meteor Orbit Radar (AMOR; Baggaley et al. 1994, Baggaley 2001) all make use of multiple receiver sites to measure time-of-flight speed.

Some radars continually monitor the sky for meteors; examples include CMOR and AMOR. In other cases, multi-purpose radars dedicate a portion of their time to meteor research; SAAMER falls into this category. Constant meteor detection is of course preferable for monitoring sporadic activity and detecting previously unknown showers and unexpected outbursts, but splitting time between experiments can be financially advantageous.

Most patrol radars are derived from designs which measure upper atmospheric winds, and they come equipped with software that select only those meteor trails that are strictly underdense. Strictly underdense echoes come from a specific point on the trail, one at which the angle between the transmitted beam and the receiver line of sight is 90°, which enables the wind speed measurement to be tied to a specific altitude. Unless the default software is modified to handle trails that do not meet the strict underdense criteria—entailing a considerable amount of work—overdense echoes are not counted, resulting in a much lower number of observed meteors.

2.3.2.2 High-power, Large-aperture (HPLA) Radars. A meteor essentially produces a tube of ionization as it streaks through the atmosphere; the side of this tube presents a much larger reflective area to a radar than the end, or "head," does. Thus, regularly detecting these "head echoes" requires a much higher transmitter power and narrower gain pattern, which so-called HPLA radars provide, in order to focus all the energy into a small part of the sky. HPLA radars can also be employed to detect the trail echoes of extremely small meteors, but are more frequently used to detect meteor head echoes as these are much more common per unit area of sky.

Probably the best-known HPLA radar is the Arecibo radio telescope in Puerto Rico. This facility can operate as either a radio telescope (which passively detects radio waves emitted by distant astronomical sources such as quasars) or a radar (which transmits radio waves and detects their reflection off much closer objects such as asteroids). In radar mode, Arecibo can detect meteoroids passing through its beam (see, e.g., Janches 2000). The Jicamarca radar, the Middle Atmosphere Alomar Radar System (MAARSY), the European Incoherent Scatter (EISCAT) radar system, the Advanced Research Projects Agency Long Range Tracking and Instrumentation Radar (ALTAIR), and the Middle and Upper Atmosphere (MU) radar have also been employed to detect meteor head echoes (Chapin & Kudeki 1994; Fujiwara et al. 1995; Pellinen-Wannberg & Wannberg 1994; Brown et al. 2001; Janches 2000; Schult et al. 2018).

HPLA radars can obtain meteoroid speeds through range-rate measurements, Doppler shifts in the reflected radar frequency, or a combination of the two (Pellinen-Wannberg 2001). Some radars (Jicamarca, MAARSY, MU, and, to some extent, ALTAIR) have interferometric capability and can therefore track the echo within the beam and, in some cases, measure its deceleration. HPLA radars have the ability to detect extremely faint meteors and, when in head-detection mode, are not affected by the initial trail radius effect (in which the radius of the trail is comparable to the radar wavelength and thus leads to destructive interference and reduced detectability).

Unlike patrol radars, HPLA radars are massive, multi-million-dollar instruments with many non-meteor applications. Time on these instruments is competitive and meteor observing campaigns are very short in duration, with rare exceptions (e.g., Brown et al. 2017). Thus, while HPLAs can detect the smallest meteors of any known method, they are not used to systematically monitor the entire sky.

2.3.3 Infrasound and Seismic Detectors

Objects with a diameter of one meter, and sometimes those as small as 10 cm, produce low-frequency sound waves when they hit the atmosphere. These sound waves are too low-pitched (less than 20 Hz) to be heard with the human ear, but can be picked up by infrasound microphones. Low frequency sound waves can propagate great distances through the atmosphere; in fact, the Comprehensive Test Ban Treaty Organization (CTBTO) uses infrasound to monitor the globe for nuclear detonations and detects meteors as well as nuclear explosions. Large meteors can also be detected at great distances; the Chelyabinsk meteor was detected by an infrasound station in Antarctica.

Infrasound can be detected by either a traditional microphone (albeit one that has been tuned to pick up lower-than-usual frequencies) or a barometer (in this case, one that has been

tuned to pick up higher-than-usual frequencies; Evers & Haak 2003). Barometers are more frequently used for detecting natural and artificial atmospheric explosions. Each barometer is typically connected to a series of pipes or porous hoses to sample changes in pressure over a large area (see fig. 11); this is done to reduce the effects of wind noise. Noise can be further reduced by placing the arrays in quiet locations away from urban centers. These barometers are arranged in arrays, and trajectory information from the acoustic wave (its arrival direction and angle of incidence to the ground) can be derived from the times at which a signal reaches each barometer in the array (Silber et al. 2015). As mentioned above, meteors are detected incidentally by the CTBTO arrays; dedicated meteor infrasound arrays are operated by organizations such as the University of Western Ontario (ELFO; Edwards et al. 2008) and by the Royal Netherlands Meteorological Institute (Evers & Haak 2003).

Figure 11. Part of an infrasound barometer at a station operated by the CTBTO in Greenland. Image credit: The Official CTBTO Photostream.

Shock waves can also propagate into the ground and be transmitted as seismic waves; these waves can be detected by seismic stations rather than by microphones or barometers (Cevolani 1994). The shock wave produced by a fireball tends to produce a "reverse N" seismographic signature in which the vertical ground velocity takes a sharp downturn, followed by a rapid upturn (see, e.g., Ishihara et al. 2003). The time at which the signal reaches different seismic stations can be used to determine the location of the fireball; if available, wave polarization information can be used as an additional constraint (Langston 2004).

The velocity of a meteor is more difficult to constrain with infrasound or seismic data. Normally, an object traveling at supersonic speeds produces a shock cone; the shape of this cone is determined by the ratio of the sound speed to the object's speed. However, a meteor's speed exceeds the sound speed by a huge ratio: the speed of a meteor is at least 10 km/s, or 10,000 m/s, while the speed at which the resulting shockwave travels through the air is about 320 m/s (Kumar et al. 2017). As a result, the shock "cone" resembles a cylinder (Langston 2004), making it difficult to determine the meteor speed from the shape of the shock wave. The ratio of meteor speed to sound speed also obscures any velocity information that is contained in the timing of the signals. For instance, one fireball seen in 1989 produced two shock waves, possibly as it fragmented twice, that were seen by 12 seismic stations. However, because the second shock wave was produced at a lower altitude, it reached the seismic stations *first* (Qamar 1995), and all that could be determined about the meteor's speed from the seismic data was that it must exceed 3 km/s. Fluctuations in the sound speed or even the physical parameters of the ground (Langston 2004) can further muddy the waters.

The velocities derived from infrasound and seismic signals can therefore be crude compared to cutting-edge optical meteor observations. In some cases, it may only be possible to derive a location and an energy. Speed or directionality can only be obtained through detailed modeling (for a review, see Silber et al. 2018), through the analysis of signals from a large number of stations (Pujol et al. 2005), or if distinct fragmentation events occur (Edwards & Hildebrand 2004). Additionally, infrasound and seismic detectors only pick up the largest fireballs; the object must be at least 10 cm in size to produce a signal. On the other hand, infrasound may be the only possible method of detection for remote events. For instance, a fireball over Indonesia in 2009 left no instrumental records other than 17 infrasound detections (Silber et al. 2011). A similar event may have occurred in northern Taiwan in late 2013; explosions were heard, but no fireball seen. This event was recorded by 12 seismometers and 3 infrasound sensors, enabling scientists to locate the site of the fireball and derive a trajectory (Kumar et al. 2017). These rate measurements can be incorporated into the distributions of meteoroid sizes (Brown et al. 2002).

2.4 Impact Observations

When very large meteoroids (or small asteroids or comets) impact a planet or moon, the flash can potentially be seen from another planet. Flashes can be produced whether the meteoroid impacts the surface of an airless body or a thick atmosphere. In some cases, changes may also be seen on the surface of the planet or moon. This section discusses a few such cases: meteoroid impacts on the surface of the Moon, and impacts on the atmosphere of Jupiter and rings of Saturn.

2.4.1 Lunar Impacts

The Moon lacks an atmosphere and thus meteoroids crash into the lunar surface at full speed. These hypervelocity impacts, especially those involving larger meteoroids, produce a short-lived flash of visible light that can be seen from the Earth's surface nearly 240,000 miles away.

The MEO observes the unlit portions of the Moon using ground-based telescopes in order to detect these flashes (Suggs et al. 2014; Suggs et al. 2017). These 14–20 inch telescopes watch the surface of the new or mostly dark Moon; the huge collecting area involved (the camera's field of view covers about a million square km) makes this technique well-suited for detecting rare, massive meteoroids. However, these flashes can only be observed on the dark, unlit surface of the Moon. Furthermore, the total illuminated fraction of the Moon must be less than 50%, or the glare from the illuminated fraction contaminates the field of view. As a result, only 8–12 nights per month are suitable for lunar impact flash observations, assuming perfect weather.

The analysis of Suggs et al. (2014) demonstrates that lunar impact observations are complete to masses larger than about 30 grams; this threshold lies above and complements the MEO's all-sky and wide-field camera systems. A study of 126 impact flashes (Suggs et al. 2014) was able to measure the flux of meteoroids down to this 30 cm threshold and found that the result agreed with the large bolide flux curve of Brown et al. (2002).

One can derive the location of the impact on the Moon's surface, as well as brightness, from lunar impact observations. The MEO has developed a process to locate impacts on the lunar surface to within about 7 km in uncertainty (Moser et al. 2015). Accurate locations can make it possible to link impact flashes to changes in the lunar surface. For instance, a particularly bright flash on March 17, 2013 was later linked to an 18.8 m crater detected by NASA's Lunar Reconnaissance Orbiter Camera (LROC; Robinson et al. 2015).

On the other hand, quantities such as speed, directionality, and material properties cannot be derived from an impact flash. At most, one can rule out half of all possible meteoroid radiants; after all, the meteoroid cannot have passed *through* the Moon. Without speed and radiant information, it is impossible to definitely associate flashes with a particular meteor shower or sporadic source. However, Suggs et al. (2014) concocted a figure of merit for meteor shower membership that takes shower activity, timing, and radiant geometry into account. Using this figure of merit, they estimated that more than half of observed flashes were associated with a meteor shower.

The lunar monitoring program at NASA Marshall Space Flight Center, currently operated by the MEO, is the first such program established. However, several other groups have also begun impact flash projects. A group in Spain published a paper in 2015 (Ortiz et al. 2015) reporting 12 observed flashes, 9 of which occurred during the Geminid meteor shower. More recently, a group in Greece started the NEO Lunar Impacts and Optical TrAnsients (NELIOTA) project, which started to publish scientific results in 2018 (Bonanos et al.).

2.4.2 Jovian and Saturnian Impacts

Fireballs were seen on the surface of Jupiter as early as 1979, when Voyager I recorded one during its encounter with the giant planet (Cook & Duxbury 1981). In July 1994, the impact of Comet Shoemaker-Levy 9 onto Jupiter garnered a great deal of public interest. Observatories around the word imaged the event and the Hubble Space Telescope captured high-resolution images of the multiple fireballs produced as fragments of the comet hit the Jovian atmosphere (Crawford et al. 1995); see figure 12.

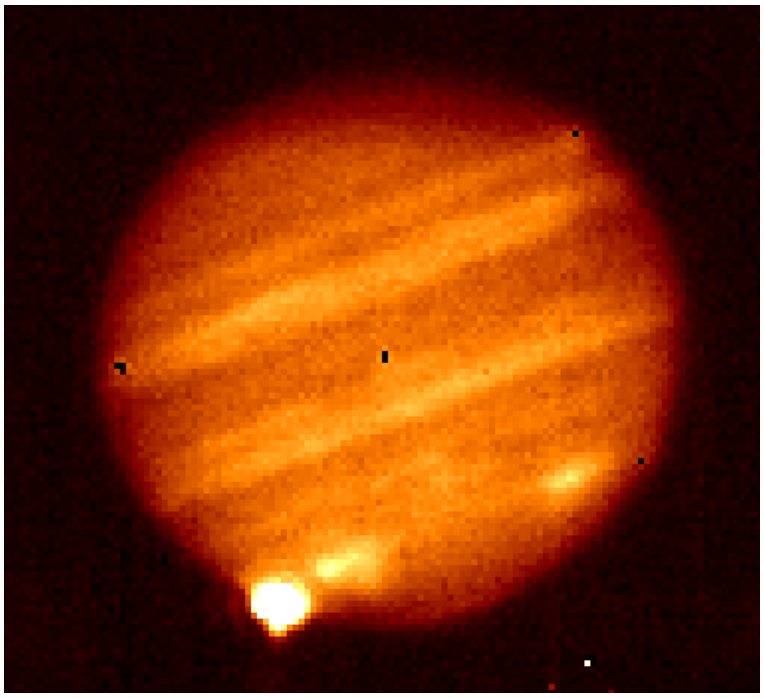

Figure 12. Image of a fragment of Comet Shoemaker-Levy 9 impacting Jupiter (lower left). This is a two-second exposure taken by the NASA Infrared Telescope Facility.

Later, several smaller flashes on Jupiter were observed by amateur observers and linked to impacts by researchers (Hueso et al. 2013; Hueso et al. 2018). Between 2010 and 2018, five impacts were reported (Hueso et al. 2018), but the small number of impacts makes it difficult to determine a flux. Hueso also suggests that impacts could produce observable debris fields, which could be used as a secondary or alternative detection method.

Elongated clouds of debris in Saturn's rings have also been attributed to meteoroid impacts (Tiscareno et al. 2013). These clouds are not the result of a single meteoroid impact. Rather, meteoroids are thought to first impact Saturn's rings with minimal debris production but with enough force to break up the meteoroid itself and capture it into Saturnian orbit. Then, the meteoroid again impacts the ring, this time as a collection of particles capable of producing the observed debris clouds. These impacts were used to estimate the flux of particles onto Saturn's rings.

2.5 Meteorite Recovery

Most meteoroids that enter the Earth's atmosphere are completely destroyed by ablation and fragmentation, but occasionally a remnant falls to the ground as a meteorite. Most known meteorites are found on the ground some time later (this is termed a "meteorite find"; see section 5.1.3.1). A precious few are caught in the process of falling and recovered based on their trajectory (a "meteorite fall"; see section 5.1.3.2).

Meteoroids with a slow atmospheric entry speed and a strong or dense composition are much more likely to produce meteorites (Halliday et al. 1989; Ceplecha et al. 1998). Thus, meteorites in general tend to represent only a small portion of objects that enter the atmosphere. Most meteoroids are thought to originate from comets; these objects are thought to be fragile and enter the atmosphere at high speeds and thus rarely if ever survive passage through the atmosphere. The much rarer asteroidal objects constitute most known meteorites. Even fragments of the Moon and Mars, which constitute a increasingly small portion of the meteoroid environment, are represented in meteorite collections.

Passage through the atmosphere alters the outer layer of the meteoroid/meteorite and generally creates a "fusion crust." Any significant amount of time on the ground can further alter the meteorite: water tends to rust or oxidize metals and, over longer time periods, minerals can gradually alter or replace silicates in the meteorite (Wlotzka 1993). Despite this, meteorite studies have led to many valuable insights into the formation of our Solar System. For instance, most meteorites contain small round grains called chondrules; these objects are thought to have formed as free-floating molten droplets in the early Solar System and are believed to be the fundamental building blocks of planets (Bollard et al. 2017), asteroids, and possibly comets (Swindle & Campins 2004). Iron meteorites are thought to originate from the cores of shattered asteroids (for a discussion, see Goldstein et al. 2009).

Meteorite falls provide both compositional and orbital information and are thus of particular value to the community. For this reason, a number of networks have been established within the past 60 years with the goal of capturing meteorite-producing events. The first multiple-camera observation of a meteorite-producing fireball was made in 1959 by a meteor network at Ondrejov Observatory in Czechoslovakia (founded in 1951). The trajectory obtained from the camera observations assisted in the recovery of the meteorite east of the city of Příbram (Ceplecha et al. 1959a; Ceplecha et al. 1959b; Ceplecha 1960; Ceplecha 1961). The Příbram meteorite fall spurred a great deal of interest and prompted the establishment of several other networks. The Prairie Network in the midwestern United States operated from 1964 to 1975 and detected one meteorite fall: the Lost City meteorite (McCrosky et al. 1971). The Meteorite Observation and Recovery Program (MORP) in western Canada operated from 1970 to 1985 and also detected one meteorite fall (the Innisfree meteorite; Halliday et al. 1981), although 50 fireballs were thought to have dropped meteorites. Some more modern networks have had a higher rate of success; Australia's Desert Fireball Network captured five meteorite falls in a ten-year period (Devillepoix et al. 2018).

Although meteorite falls are rare even with top-of-the-line equipment, meteor networks also produce a wealth of other data. For instance, fireball data from the Prairie Network were used to develop the "PE" criterion discussed in section 5.1.3 (Ceplecha & McCrosky 1976). Meteors observed by MORP were used to construct meteoroid and meteorite flux measurements and derive early density estimates for large meteoroids (Halliday et al. 1996). NASA's own All-Sky Fireball Network (Cooke & Moser 2012), which was modeled after a meteorite-focused network and does occasionally record meteorite falls such as the Dishchii'bikoh meteorite, focuses primarily on bright meteors, not meteorites.

2.6 Simultaneous Detection by Multiple Methods

In many cases, two or more observation methods can be combined to maximize the amount of information gleaned from meteor events or to mitigate the limitations associated with a single method. Simultaneous observations can also be used to characterize a new detection method. An early example is available in Grygar et al. (1968), who supplemented telescopic observations of meteors with visual observers using either the naked eye or binoculars. The visual data was used to derive relations for correcting quantities such as the brightness and angular length of meteors seen via telescope.

Some individual bright events are detected by numerous systems; for instance, the Park Forest meteorite fall was seen by orbiting satellites, ground-based observers, and acoustic, infrasound, and seismic detectors (Brown et al. 2004). The optical video data were used to determine the meteor's trajectory, while the acoustic, infrasound, and seismic data were used to obtain estimates of the kinetic energy and mass of the object. Another example is the Carancas meteorite impact, which had few optical observations but was detected by several infrasound and seismic sensors (see, e.g., Tancredi et al. 2009). The data from these sensors helped to better constrain the trajectory.

In recent decades, a number of researchers have combined radar and optical meteor detections to accomplish a number of goals. Meteor radars, particularly patrol radars, can detect very large numbers of meteors but tend to have low precision when measuring trajectories. Simultaneous optical observations can be used to provide higher-resolution trajectories for individual events (see, e.g., Michell et al. 2015), or to investigate whether systematic errors exist in the radar trajectories (Brown et al. 2017). Because radar observations probe the amount of ionization produced by the meteor, while optical observations measure the amount of light produced, the two methods can be combined to place different constraints on the ablation of the meteor. For example, Weryk & Brown (2013) used a number of dually detected meteors to develop an alternative model of luminous efficiency that was tied to the ionization efficiency.

Simultaneous detections do not necessarily have to involve completely different detection methods to be of value. For instance, Jones & Campbell-Brown (2005) used dual-frequency radar observations to quantify the initial trail radius effect, in which high-speed meteors ablate at high altitudes, creating a large trail radius that can approach the radar wavelength and result in destructive interference.

2.7 References

Adolfsson, L.G.; Gustafson, B.Å.S.; and Murray, C.D.: "The Martian Atmosphere as a Meteoroid Detector," *Icarus*, Vol. 119, No. 1, pp. 144–152, 1996.

Baggaley, W.J.: "The AMOR Radar: An Efficient Tool for Meteoroid Research," *Advances in Space Research*, Vol. 28, No. 9, pp. 1277–1282, 2001.

Baggaley, W.J.; Bennett, R.G.T.; Steel, D.I.; and Taylor, A.D.: "The Advanced Meteor Orbit Radar Facility – AMOR," *Quarterly Journal of the Royal Astronomical Society*, Vol. 35, No. 3, pp. 293, 1994

Bland, P.A.; Spurny, P.; Bevan, A.W.R.; et al.: "The Australian Desert Fireball Network: A New Era for Planetary Science," *Australian Journal of Earth Sciences*, Vol. 59, No. 2, pp. 177–187, 2012.

Bollard, J.; Connelly, J.N.; Whitehouse, M.J.; et al.: "Early Formation of Planetary Building Blocks Inferred from Pb Isotopic Ages of Chondrules," *Science Advances*, Vol. 3, No. 8, pp. e1700407, 2017.

Bonanos, A.Z.; Avdellidou, C.; Liakos, A.; et al.: "NELIOTA: First Temperature Measurement of Lunar Impact Flashes," *Astronomy and Astrophysics*, Vol. 612, 2018.

Bradley, J.G.; Grün, E.; and Srama, R.: "Cosmic Dust Analyzer for Cassini," *Proc. SPIE* Vol. 2803, International Symposium on Optical Science, Engineering, and Instrumentation, October 7, 1996.

Brown, P.G.; Hunt, S.; and Close, S.: "Astronomical and Physical Data for Meteoroids Recorded by the ALTAIR Radar," *Proceedings of the Meteoroids 2001 Conference*, pp. 469–474, August 6–10, 2001.

Brown, P.G.; Pack, D.; Edwards, W.N.; et al.: "The Orbit, Atmospheric Dynamics, and Initial Mass of the Park Forest Meteorite," *Meteoritics & Planetary Science*, Vol. 39, No. 1, pp. 1781–1796, 2004.

Brown, P.G.; Spalding, R.E.; ReVelle, D.O.; et al.: "The Flux of Small Near-Earth Objects Colliding with the Earth," *Nature*, Vol. 420, No. 6, pp. 294–296, 2002.

Brown, P.G.; Stober, G.; Schult, C.; et al.: "Simultaneous Optical and Meteor Head Echo Measurements Using the Middle Atmosphere Alomar Radar System (MAARSY): Data Collection and Preliminary Analysis," *Planetary and Space Science*, Vol. 141, pp. 25–34, 2017.

Burchell, M.J.; Fairey, S.A.J.; Wozniakiewicz, D.E.; et al.: "Characteristics of Cometary Dust Tracks in Stardust Aerogel and Laboratory Calibrations," *Meteoritics & Planetary Science*, Vol. 43, No. 1, pp. 23–40, 2008.

Campbell-Brown, M.D.; and Jones, J.: "Annual Variation of Sporadic Radar Meteor Rates," *Monthly Notices of the Royal Astronomical Society*, Vol. 367, No. 2, pp. 709–716, 2006.

Ceplecha, Z.: "Experimental Data on the Final Mass of the Body Landed on the Earth after Penetrating the Atmosphere at Cosmical Velocity," *Bulletin of the Astronomical Institute of Czechoslovakia*, Vol. 11, pp. 9, 1960.

Ceplecha, Z.: "Multiple Fall of Přibram Meteorites Photographed. 1. Double-Station Photographs of the Fireball and Their Relations to the Found Meteorites," *Bulletin of the Astronomical Institute of Czechoslovakia*, Vol. 12, pp. 21, 1961.

Ceplecha, Z.; Borovička, J.; Elford, W.G.; et al.: "Meteor Phenomena and Bodies," *Space Science Reviews*, Vol. 84, No. 3, pp. 327–471, 1998.

Ceplecha, Z.; and McCrosky, R.E.: "Fireball End Heights - A Diagnostic for the Structure of Meteoric Material," *Journal of Geophysical Research*, Vol. 81, No. 35, pp. 6257–6275, 1976.

Ceplecha, Z.; Rajchl, J.; and Sehnal, L.: "New Czechoslovak Meteorite 'Luhy'," *Bulletin of the Astronomical Institute of Czechoslovakia*, Vol. 10, pp. 147, 1959a.

Ceplecha, Z.; Rajchl, J.; and Sehnal, L.: "Complete Data on Bright Meteor 15761," *Bulletin of the Astronomical Institute of Czechoslovakia*, Vol. 10, pp. 204, 1959b.

Cevolani, G.: "The Explosion of the Bolide over Lugo di Romagna (Italy) on 19 January 1993," *Planetary and Space Science*, Vol. 42, No. 9, pp. 767–775, 1994.

Chapin, E.; and Kudeki, E.: "Radar Interferometric Imaging Studies of Long-Duration Meteor Echoes Observed at Jicamarca," *Journal of Geophysical Research*, Vol. 99, No. A), pp. 8937–8949, 1994.

Colangeli, L.; Moreno, J.J.; Palumbo, P.; et al.: "GIADA: The Grain Impact Analyser and Dust Accumulator for the Rosetta Space Mission," *Advances in Space Research*, Vol. 39, No. 3, pp. 446–450, 2007.

Colas, F.; Zanda, B.; Bouley, S.; et al.: "FRIPON, the French Fireball Network," *European Planetary Science Congress 2015*, i.d. EPSC2015–800, September 27-October 2, 2015.

Cook, A.F.; and Duxbury, T.C.: "A Fireball in Jupiter's Atmosphere," *Journal of Geophysical Research*, Vol. 86, No. A10, pp. 8815–8817, 1981.

Cooke, W.J.; and Moser, D.E.: "The Status of the NASA All Sky Fireball Network," *International Meteor Conference Publication*, pp. 9–12, 2012.

Corsaro, R.D.; Giovane, F.; Liou, J.; et al.: "Characterization of Space Dust Using Acoustic Impact Detection," *The Journal of the Acoustical Society of America*, Vol. 140, No. 2, pp. 1429–1438, 2016.

Corte, D.V.; Sordini, R.; Accolla, M.; et al.: "GIADA – Grain Impact Analyzer and Dust Accumulator – Onboard Rosetta Spacecraft: Extended Calibrations," *Acta Astronautica*, Vol. 126, pp. 205–214, 2016.

Cour-Palais, B.G.: "Hypervelocity Impact Investigations and Meteoroid Shielding Experience Related to Apollo and Skylab," Paper presented at Orbital Debris, NASA Johnson Space Center, Houston, TX, March 01, 1985.

Crawford, D.A.; Boslough, M.B.; Trucano, T.G.; and Robinson, A.C.: "The Impact of Periodic Comet Shoemaker-Levy 9 on Jupiter," *International Journal of Impact Engineering*, Vol. 17, No. 1-3, pp. 253–262, 1995.

Devillepoix, H.A.R.; Bland, P.A.; Sansom, E.K.; et al.: "Observation of Metre-scale Impactors by the Desert Fireball Network," *Monthly Notices of the Royal Astronomical Society*, Vol. 483, No. 4, pp. 5166–5178, 2018.

Domokos, A.; Bell, J.F.; Brown, P.; et al.: "Measurement of the Meteoroid Flux at Mars," *Icarus*, Vol. 191, No. 1, pp. 141–150, 2007.

Drolshagen, G.; McDonnell, J.A.M.; Stevenson, T.; et al.: "Post-flight Measurements of Meteoroid/Debris Impact Features on EURECA and the Hubble Solar Array," *Advances in Space Research*, Vol. 16, No. 1, pp. 85–89, 1995.

Edwards, W.N.; Brown, P.G.; Weryk, R.J.; and ReVelle, D.O.: "Infrasonic Observations of Meteoroids: Preliminary Results from a Coordinated Optical-radar-infrasound Observing Campaign," *Earth, Moon, and Planets*, Vol. 102, No. 1, pp. 221–229, 2008.

Edwards, W.N.; and Hildebrand, A.R.: "SUPRACENTER: Locating Fireball Terminal Bursts in the Atmosphere Using Seismic Arrivals," *Meteoritics & Planetary Science*, Vol. 39, No. 9, pp. 1449–1460, 2004.

Elford, W.G.; and Taylor, A.D.: "Measurement of Faraday Rotation of Radar Meteor Echoes for the Modelling of Electron Densities in the Lower Ionosphere," *Journal of Atmospheric and Terrestrial Physics*, Vol. 59, No. 9, pp. 1021–1024, 1997.

Evers, L.G.; and Haak, H.W.: "Tracing a Meteoric Trajectory with Infrasound," *Geophysical Research Letters*, Vol. 30, No. 24, pp. 294–4, 2003.

Fujiwara, Y.; Ueda, M; Nakamura, T.; and Tsutsumi, M.: "Simultaneous Observations of Meteors with the Radar and TV Systems,". *Earth, Moon, and Planets*, Vol. 68, No. 1, pp. 277–282, 1995.

Goldstein, J.I.; Scott, E.R.D.; and Chabot, N.L.: "Iron Meteorites: Crystallization, Thermal History, Parent Bodies, and Origin," *–Geochemistry (Chemie der Erde): Interdisciplinary Journal for Chemical Topics of the Geosciences*, Vol. 69, No. 4, pp. 293–325, 2009.

Grün, E.; Fechtig, H.; Hanner, M.S.; et al.: "The Galileo Dust Detector," *Space Science Reviews*, Vol. 60, No. 1–4, pp. 317–340, 1992.

Grygar, J.; Kohoutek, L.; and Plavcová, Z.: "Simultaneous Radar and Optical Observation of Meteors at ONDrEJOV in 1962," Paper Presented at the Physics and Dynamics of Meteors. Symposium No. 33, Tatranska Lomnica, 1968.

Halliday, I.; Blackwell, A.T.; and Griffin, A.A.: "The Flux of Meteorites on the Earth's Surface," *Meteoritics*, Vol. 24, pp. 173–178, 1989.

Halliday, I.; Griffin, A.A.; and Blackwell, A.T.: "Detailed Data for 259 Fireballs from the Canadian Camera Network and Inferences Concerning the Influx of Large Meteoroids," *Meteoritics & Planetary Science*, Vol. 31, No. 2, pp. 185–217, 1996.

Halliday, I.; Griffin, A.A.; and Blackwell, A.T.: "The Innisfree Meteorite Fall - A Photographic Analysis of Fragmentation, Dynamics and Luminosity," *Meteoritics*, Vol. 16, pp. 153–170, 1981.

Horányi, M.; Hoxie, V.; James, D.; et al.: "The Student Dust Counter on the New Horizons Mission," *Space Science Reviews*, Vol. 140, No. 1–4, pp. 387–402, 2007.

Howie, R.M.; Paxman, J.; Bland, P.A.; et al.: "How to Build a Continental Scale Fireball Camera Network," *Experimental Astronomy*, Vol. 43, No. 3, pp. 1711–266, 2017.

Hörz, F.; See, T.H.; Bernhard, R.P.; and Brownlee, D.E.: "Natural and Orbital Debris Particles on LDEF's Trailing and Forward-facing Surfaces," Paper Presented at the Third LDEF Post-Retrieval Symposium, NASA Langley Research Center, February 01, 1995.

Hueso, R.; Perez-Hoyos, S.; Sánchez-Lavega, A.; et al.: "Impact Flux on Jupiter: From Superbolides to Large-scale Collisions," *Astronomy and Astrophysics*, Vol. 560, pp. A55–14, 2013.

Hueso, R.; Delcroix, M.; Sánchez-Lavega, A; et al.: "Small Impacts on the Giant Planet Jupiter," *Astronomy and Astrophysics*, Vol. 617, pp. A68–13, 2018.

Huestis, D.L.; and Slanger, T.G.: "New Perspectives on the Venus Nightglow," *Journal of Geophysical Research*, Vol. 98, No. E6, pp. 10839–10847, 1993.

Humes, D.H.: "Large Craters on the Meteoroid and Space Debris Impact Experiment," Paper Presented at the Third LDEF Post-Retrieval Symposium, NASA Langley Research Center, January 01, 1992.

Humes, D.H.; Alvarez, J.M.; Kinard, W.H.; and O'Neal, R.L.: "Pioneer 11 Meteoroid Detection Experiment - Preliminary Results," *Science*, Vol. 188, No. 4187, pp. 473–474, 1975.

Humes, D.H.; Alvarez, J.M.; O'Neal, R.L.; and Kinard, W.H.: "The Interplanetary and Near-Jupiter Meteoroid Environments," *Journal of Geophysical Research*, Vol. 79, No. 2, pp. 3677–3684, 1974.

Hyde, J.L.; Christiansen, E.L.; Barnhard, R.P.; et al.: "A History of Meteoroid and Orbital Debris Impacts on the Space Shuttle," in *Proceedings of the Third European Conference on Space Debris*, H. Sawaya-Lacoste (ed.), ESA SP-473, Vol. 1, Noordwijk, Netherlands, pp. 191–196, 2001.

Hyde, J.L.; Christiansen, E.; Lear, D.; et al.: "Surveys of Returned ISS Hardware for MMOD Impacts," in *Proceedings of the 7th European Conference on Space Debris*, ESA Space Debris Office, pp. 1–8, 2017.

Ishihara, Y.; Tsukada, S.; Sakai, S.; et al.: "The 1998 Miyako Fireball's Trajectory Determined from Shock Wave Records of a Dense Seismic Array," *Earth Planets Space*, Vol. 55, pp. e9–e12, 2003.

Jacchia, L.G.; and Whipple, F.L.: "The Harvard Photographic Meteor Programme," *Vistas in Astronomy*, Vol. 2, No. 1, pp. 982–994, 1956.

Janches, D.: "Micrometeor Observations Using the Arecibo 430 MHz Radar I. Determination of the Ballistic Parameter from Measured Doppler Velocity and Deceleration Results," *Icarus*, Vol. 145, No. 1, pp. 53–63, 2000.

Janches, D.: "On the Geocentric Micrometeor Velocity Distribution," *Journal of Geophysical Research*, Vol. 108, No. A6, pp. 1222–14, 2003.

Janches, D.; Close, S.; Hormaechea, J.L.; et al.: "The Southern Argentina Agile Meteor Radar Orbital System (SAAMER-OS): An Initial Sporadic Meteoroid Orbital Survey in the Southern Sky," *The Astrophysical Journal*, Vol. 809, No. 1, p. 36, 2015.

Jenniskens, P.; *Meteor Showers and their Parent Comets*, Cambridge University Press, pp. 802, 2006.

Jenniskens, P.; "Meteor Stream Activity I. The Annual Streams," *Astronomy and Astrophysics*, Vol. 287, pp. 990–1013, 1994.

Jenniskens, P.: "Quantitative Meteor Spectroscopy: Elemental Abundances," *Advances in Space Research*, Vol. 39, No. 4, pp. 491–512, 2007.

Jenniskens, P.; Albers, J.; Clemens, E.T.; et al.: "Detection of Meteoroid Impacts by the Geostationary Lightning Mapper on the GOES-16 Satellite," *Meteoritics & Planetary Science*, Vol. 53, No. 12, pp. 627–25, 2018.

Jones, J.; and Campbell-Brown, M.D.: "The Initial Train Radius of Sporadic Meteors," *Monthly Notices of the Royal Astronomical Society*, Vol. 359, No. 3, pp. 1131–1136, 2005.

Jones, J.; Brown, P.; Webster, A.R.; et al.: "The Canadian Meteor Orbit Radar: System Overview and Preliminary Results," *Planetary and Space Science*, Vol. 53, No. 4, pp. 413–421, 2005.

Koschack, R.; and Rendtel, J.: "Determination of Spatial Number Density and Mass Index from Visual Meteor Observations (I)," *WGN*, Vol. 18, pp. 44–58, 1990.

Kronk, G.W.: *Meteor Showers*, Springer Press, New York, NY, 2014.

Kuitunen, J.; Drolshagen, G.; McDonnell, J.A.M.; et al.: "DEBIE - First Standard In-situ Debris Monitoring Instrument," in *Proceedings of the Third European Conference on Space Debris*, ESA, Vol. 3, No. 1, pp. 185–190, 2001.

Kumar, U.; Chao, B.F.; Hsieh, Y.; and Chang, E.T.Y.: "A Meteor Shockwave Event Recorded at Seismic and Infrasound Stations in Northern Taiwan," *Geoscience Letters*, Vol. 4, No. 1, pp. 1–8, 2017.

Kuznetsov, I.A.; Hess, S.L.G.; Zakharov, A.V.; et al.: "Numerical Modelling of the Luna-Glob Lander Electric Charging on the Lunar Surface with SPIS-DUST," *Planetary and Space Science*, Vol. 156, pp. 62–70, 2018.

Langston, C.A.: "Seismic Ground Motions from a Bolide Shock Wave," *Journal of Geophysical Research: Solid Earth*, Vol. 109, No. B, p. B12309, 2004.

Liou, J.-C.; Corsaro, R.; Giovane, F.; et al.: "DRAGONS - A Micrometeoroid and Orbital Debris Impact Sensor," *Proceedings 30th International Symposium on Space Technology and Science (ISTS); 34th International Electric Propulsion Conference (IEPC); 6th Nano-Satellite Symposium (NSAT)*, NASA Johnson Space Center JSC-CN-33620, pp. 1–6, 2015.

Love, S.G.; and Brownlee, D.E.: "A Direct Measurement of the Terrestrial Mass Accretion Rate of Cosmic Dust," *Science*, Vol. 262, No. 5, pp. 550–553, 1993.

Mandeville, J.C.; and Berthoud, L.: "From LDEF to EURECA: Orbital Debris and Meteoroids in Low Earth Orbit," *Advances in Space Research*, Vol. 16, No. 1, pp. 67–72, 1995.

McAuliffe, J.P.; and Christou, A.A.; "Modelling Meteor Ablation in the Venusian Atmosphere," *Icarus*, Vol. 180, No. 1, pp. 8–22, 2006.

McBride, N.; and McDonnell, J.A.M.: "Meteoroid Impacts on Spacecraft: Sporadics, Streams, and the 1999 Leonids," *Planetary and Space Science*, Vol. 47, No. 8, pp. 1005–1013, 1999.

McCrosky, R.E.; Posen, A.; Schwartz, G.; and Shao, C.Y.: "Lost City Meteorite - Its Recovery and a Comparison with Other Fireballs, *Journal of Geophysical Research*, Vol. 76, No. 17, pp. 4090–4108, 1971.

McDonnell, J.A.M.; Griffiths, A.D.; Zarnecki, J.C.; et al.: "Meteoroid and Debris Flux and Ejecta Models: Summary Report," Technical Report 11887/96/NL/JG, ESA, Unispace Kent, 1998.

Michell, R.G.; Janches, D.; Samara, M.; et al.: "Simultaneous Optical and Radar Observations of Meteor Head-echoes Utilizing SAAMER," *Planetary and Space Science*, Vol. 118, pp. 95–101, 2015.

Miller, S.D.; Straka, W.C.; Bachmeier, A.S.; et al.: "Earth-viewing Satellite Perspectives on the Chelyabinsk Meteor Event," in *Proceedings of the National Academy of Sciences*, 2013.

Molau, S.; Javor, K.; Crivello, S.; et al.; "Results of the IMO Video Meteor Network - May 2011," *WGN*, Vol. 39, pp. 105–109, 2011.

Moser, D.E.: "Comparing Eyewitness-derived Trajectories of Bright Meteors to Instrumentally-observed Data," *Planetary and Space Science*, Vol. 143, pp. 182–191, 2017.

Moser, D.E.; Suggs, R.M.; Kupferschmidt, L.; and Feldman, J.: "Lunar Impact Flash Locations," Technical Memorandum 218213, NASA, 2015.

Ortiz, J.L.; Madiedo, J.M.; Morales, N.; et al.: "Lunar Impact Flashes from Geminids: Analysis of Luminous Efficiencies and the Flux of Large Meteoroids on Earth," *Monthly Notices of the Royal Astronomical Society*, Vol. 454, No. 1, pp. 344–352, 2015.

Pellinen-Wannberg, A.: "The High Power Large Aperture Radar Method for Meteor Observations," in: *Proceedings of the Meteoroids 2001 Conference*, Swedish Insitute of Space Physics, Kiruna, Sweden, pp. 443–450, 2001.

Pellinen-Wannberg, A.; and Wannberg, G.: "Meteor Observations with the European Incoherent Scatter UHF Radar," *Journal of Geophysical Research*, Vol. 99, No. A, pp. 11379–11390, 1994.

Perkins, M.A.; Simpson, J.A.: and Tuzzolino, A.J.: "A Cometary and Interplanetary Dust Experiment on the Vega Spacecraft Missions to Halley's Comet," *Nuclear Instruments and Methods in Physics Research*, Vol. 239, No. 2, pp. 310–323, 1985.

Pujol, J.; Rydelek, P.; and Bohlen, T.: "Determination of the Trajectory of a Fireball Using Seismic Network Data," *Bulletin of the Seismological Society of America*, Vol. 95, No. 4, pp. 1495–1509, 2005.

Qamar, A.: "Space Shuttle and Meteoroid -Tracking Supersonic Objects in the Atmosphere with Seismographs," *Seismological Research Letters*, Vol. 66, No. 5, pp. 6–12, 1995.

Robinson, M.S.; Boyd, A.K.; Denevi, B.W.; et al.: "New Crater on the Moon and a Swarm of Secondaries," *Icarus*, Vol. 252, No. C, pp. 229–235, 2015.

Russell, J.M.; Bailey, S.M.; Gordley, L.L.; et al.: "The Aeronomy of Ice in the Mesosphere (AIM) Mission: Overview and Early Science Results," *Journal of Atmospheric and Solar-Terrestrial Physics*, Vol. 71, No. 3–4, pp. 289–299, 2009.

Schult, C.; Brown, P.; Pokorny; et al.: "A Meteoroid Stream Survey Using Meteor Head Echo Observations from the Middle Atmosphere ALOMAR Radar System (MAARSY)," *Icarus*, Vol. 309, pp. 177–186, 2018.

Selsis, F.; Lemmon, M.T.; Vaubaillon, J.; and Bell, J.F.: "Extraterrestrial Meteors: A Martian Meteor and Its Parent Comet," *Nature*, Vol. 435, No. 7, pp. 581–581, 2005.

Shrbený, L.; and Spurný, P.: "Determination of Atmospheric Velocity of Bright Meteors on the Basis of High-resolution Light Curves," *Astronomy and Astrophysics*, Vol. 550, pp. A31-6, 2013.

Silber, E.A.; Bosloughm M.; Hocking, W.K.; et al.: "Physics of Meteor Generated Shock Waves in the Earth's Atmosphere - A Review," *Advances in Space Research*, Vol. 62, No. 3, pp. 489–532, 2018.

Silber, E.A.; Brown, P.G.; and Krzeminski, Z.: "Optical Observations of Meteors Generating Infrasound: Weak Shock Theory and Validation," *Journal of Geophysical Research: Planets*, Vol. 120, No. 3, pp. 413–428, 2015.

Silber, E.A.; Le Pichon, A.; and Brown, P.G.: "Infrasonic Detection of a Near-Earth Object Impact over Indonesia on 8 October 2009," *Geophysical Research Letters*, Vol. 38, No. 1, 2011.

Simpson, J.A.; and Tuzzolino, A.J.: "Polarized Polymer Films as Electronic Pulse Detectors of Cosmic Dust Particles," *Nuclear Instruments and Methods in Physics Research Section A*, Vol. 236, No. 1, pp. 187–202, 1985.

Spurný, P.; Borovička, J.; and Shrbený, L.: "Automation of the Czech Part of the European Fireball Network: Equipment, Methods and First Results," *Near Earth Objects*, Vol. 236, No. S236, pp. 121–130, 2007.

Squire, M.: "Evaluating Micrometeoroid and Orbital Debris Risk Assessments Using Anomaly Data," Technical Report NF1676L-28197, NASA Langley Research Center, Hampton, VA, 2017.

Srama, R.; Ahrens, T.J.; Altobelli, S.; et al.: "The Cassini Cosmic Dust Analyzer," *Space Science Reviews*, Vol. 114, No. 1, pp. 465–518, 2004.

Suggs, R.M.; Moser, D.E.; Cooke, W.J.; and Suggs, R.J.: "The Flux of Kilogram-sized Meteoroids from Lunar Impact Monitoring," *Icarus*, Vol. 238, pp. 23–36, 2014.

Suggs, R.M.; Ehlert, S.R.; and Moser, D.E.: "A Comparison of Radiometric Calibration Techniques for Lunar Impact Flashes," *Planetary and Space Science*, Vol. 143, pp. 225–229, 2017.

Swindle, T.D.; and Campins, H.: "Do Comets Have Chondrules and CAIs? Evidence from the Leonid Meteors," *Meteoritics & Planetary Science*, Vol. 39, No. 10, pp. 1733–1740, 2004.

Tancredi, G.; Ishitsuka, J.; Schultz, P.H.; et al.: "A Meteorite Crater on Earth Formed on September 15, 2007: The Carancas Hypervelocity Impact," *Meteoritics & Planetary Science*, Vol. 44, No. 1, pp. 1967–1984, 2009.

Tiscareno, M.S.; Mitchell, C.J.; Murray, C.D.; et al.: "Observations of Ejecta Clouds Produced by Impacts onto Saturn's Rings," *Science*, Vol. 340, No. 6, pp. 460–464, 2013.

Tuzzolino, A.J.; "Dust Flux Monitor Instrument for the Stardust Mission to Comet Wild 2," *Journal of Geophysical Research*, Vol. 108, No. E10, pp. 41–24, 2003.

Tuzzolino, A.J.; Economou, T.E.; Clark, B.C.; et al.: Dust Measurements in the Coma of Comet 81P/Wild 2 by the Dust Flux Monitor Instrument," *Science*, Vol. 304, No. 5, pp. 1776–1780, 2004.

Tuzzolino, A.J.; McKibben, R.B.; Simpson, J.A.; et al.: "The Space Dust (SPADUS) Instrument aboard the Earth-orbiting ARGOS Spacecraft: I—Instrument Description," *Planetary and Space Science*, Vol. 49, No. 7, pp. 689–703, 2001.

Vojáček, V.; Borovička, J.; Koten, P.; et al.: "Catalogue of Representative Meteor Spectra," *Astronomy and Astrophysics*, Vol. 580, p. A67, 2015.

Watanabe, J.; Kasuaga, T.; Terai, T.; et al.: "Faint Meteor Observation by Large-format CMOS Sensor with 1.05-m Kiso Schmidt Telescope," in *The Meteoroids 2013*, *Proceedings of the Astronomical Conference*, T.J. Jopek, F.J.M. Rietmeijer, J. Watanabe, I.P. Williams (ed.), A.M. University Press, Poznań, Poland, pp. 325–328, 2014.

Watts, A.J.; and Atkinson, D.R.: "Dimensional Scaling for Impact Cratering and Perforation," *Internation Journal of Impact Engineering*, Vol. 17, No. 4–6, pp. 925-935, 1995.

Weryk, R.J.; and Brown, P.G.: "Simultaneous Radar and Video Meteors—II Photometry and Ionisation," *Planetary and Space Science*, Vol. 81, No. C, pp. 32–47, 2013.

Weryk, R.J.; Campbell-Brown, M.D.; Wiegart, P.A.; et al.: "The Canadian Automated Meteor Observatory (CAMO): System Overview," *Icarus*, Vol. 225, No. 1, pp. 614–622, 2013.

Weryk, R.J.; Brown; P.G.; Domokos, A.; et al.: "The Southern Ontario All-sky Meteor Camera Network," *Earth, Moon, and Planets*, Vol. 102, No. 1, pp. 241–246, 2008.

Wlotzka, F.: "A Weathering Scale for the Ordinary Chondrites," *Meteoritics*, Vol. 28, No. 3, pp. 460, 1993.

Yang, H.J.; Park, C.; and Park, M.G.: "Analysis of Historical Meteor and Meteor Shower Records: Korea, China, and Japan," *Icarus*, Vol. 175, No. 1, pp. 215–225, 2005.

Zook, H.A.: "Flux vs. Direction of Impacts on LDEF by Meteoroids and Orbital Debris,"*Abstracts of the Lunar and Planetary Science Conference*, Vol. 21, pp. 1385, 1990.

3. METEOROID ENVIRONMENT

Unlike asteroids and large orbital debris, meteoroids cannot currently be individually tracked; all detection methods involve meteoroid removal and/or destruction. Therefore, environment models describe only the population, rather than individual, characteristics of meteoroids. This chapter describes these population characteristics (specifically flux, directionality, speed, and density) as well as known and theorized processes of meteoroid production and the leading environment models.

3.1 Sources of Meteoroids

Meteoroids can potentially originate from almost any rocky body in the Solar System, but some bodies, such as comets, produce meteoroids much more readily than others. This section presents the classes of parent bodies as well as the mechanisms through which they produce meteoroids.

3.1.1 Comets

Comets were the first celestial bodies linked to meteor showers (Schiaparelli 1867), and the majority of meteoroids are still thought to originate from comets. In fact, a dynamical study by Wiegert et al. (2009) provides evidence that the bulk of the background meteor flux (or sporadic complex; see section 3.2) could be produced by just a couple of comets, specifically 2P/Encke and 55P/Tempel-Tuttle.

The same processes that generate comets' characteristic comae liberate meteoroids and dust from cometary surfaces. Comets contain volatile materials such as water, carbon dioxide, and carbon monoxide. At the same time, comets have eccentric orbits—and in some cases parabolic or hyperbolic orbits, in which the comet approaches the Sun only once. They spend the bulk of their time in the distant reaches of the Solar System, only occasionally swinging inward toward the Sun for a brief period. When this occurs, previously frozen volatiles are exposed to the Sun's heat and vaporize, lifting debris off the surface of the comet's nucleus and accelerating it outwards. This growing cloud of gas and debris, illuminated by the Sun, constitutes the comet's coma and is much brighter than the nucleus itself. Due to small differences in the particles' velocity, the coma spreads and elongates over time, forming a dust trail that roughly follows the comet's orbit. This dust trail marks the birth of a meteoroid stream.

Because comets produce the majority of meteoroids, the study of comet activity is critical to meteor astronomy. Observations of comets can yield useful information; the brightness of the coma provides information about how much material it is releasing, and the size of the coma depends on the speed at which material is ejected from the nucleus. The better these quantities are known, the more accurately meteoroid streams can be modeled.

3.1.2 Asteroids

It is commonly assumed that meteoroids also originate from asteroids. There are several meteor showers whose orbit most closely resembles that of an asteroid; for instance, the Quadrantids are thought to originate from 2003 EH1.

There are several possible mechanisms through which an asteroid can produce meteoroids. In the first scenario, the asteroid is actually an extinct comet, and produced meteoroids in the past through the usual cometary process (section 3.1.1). This hypothesis is often applied to 2003 EH1.

In the second scenario, collisions between asteroids produce debris. In the inner Solar System, such collisions would occur most frequently within the asteroid belt and this debris would initially remain within the belt. However, as solar photons are absorbed and reemitted from small particles, tiny amounts of angular momentum are removed, and the particles then spiral inward toward the Sun over tens or hundreds of thousands of years (Burns et al. 1979). Eventually, some of these particles will intersect the Earth and produce meteors.

In the third scenario, an individual asteroid can produce debris by "spinning up." This section mentions several ways in which radiative forces can affect the motion of meteoroids, and solar radiation can also affect the motion of asteroids. The Sun can heat the sunward-facing side of an asteroid; this heat is then dispersed through the asteroid itself and re-emitted as radiation. If the asteroid is irregular, the emitted radiation can be uneven in direction, resulting in a very small torque on the asteroid (this is known as the Yarkovsky effect; Öpik, 1951). Over long enough time scales, this effect can increase the asteroid's rotation rate. If the asteroid is a rubble pile, or if it has a surface layer of rubble, it may fling particles off its surface as it rotates faster and faster. This process was recently observed for asteroid P/2013 P5, which shows six distinct dust tails radiating away from the object in different directions. These tails are short-lived and new ones appear as the object rotates, indicating that the asteroid has been spun to breakup speed by radiative forces (Jewitt et al. 2015). Once again, particles could spiral in slowly towards the Earth.

Asteroids tend towards more circular, less-inclined orbits than comets. Their debris drifts gradually towards the Earth on nearly circular orbits within the ecliptic plane. Just before they collide with the Earth, they are on orbits very similar to that of our planet and produce relatively slow meteors. This is analogous to the relative lack of motion between two cars travelling side-by-side on the freeway. While fast meteoroids produce much brighter meteors, slow meteors of asteroidal origin are harder to detect.

Although detecting asteroidal meteors in the atmosphere is a challenge, finding asteroidal meteorites on the ground is common. The fraction of *meteors* that are asteroidal is estimated to be 5%, but the majority of *meteorites* are classified as asteroidal (Borovicka et al. 2015). This is because asteroidal material is more durable and more likely to survive atmospheric entry. A comparatively "gentle" entry speed also improves the odds of producing a meteorite.

3.1.3 Planets and moons

Larger celestial bodies such as planets and moons can also serve as sources of meteoroids. The cratered surfaces of rocky bodies in the Solar System provide clear evidence of asteroid and comet impacts. If these impacts have sufficiently high energy, they can eject material from the planet or moon.

Meteorites of both lunar and Martian origin have been found on Earth. Allan Hills A81005, the first rock to be identified as a lunar meteorite, was collected in Antarctica in 1982. Its chemical composition demonstrated a lunar origin (Marvin 1983). At around the same time, meteoriticists began to suspect that some meteorites were Martian in origin. In 2013, the Curiosity Rover made high-precision measurements of argon isotopes in the Martian atmosphere. These measurements matched argon levels in gas bubbles trapped within some meteorites, definitively linking them to the red planet and demonstrating that material can be transferred from Mars to Earth. At the time of writing, the Meteoritical Bulletin Database lists 160 meteorites as having a Martian origin (The Meteoritical Society 2019).

3.1.4 Kuiper Belt Objects

The asteroid belt is one of the most notable features of the inner Solar System, containing hundreds of thousands of known asteroids. In comparison, the outer Solar System's Kuiper belt is 20 times as wide (ranging from 30 to 50 au) and 200 times as massive. Its members are known as Kuiper belt objects (KBOs), the most famous of which is the erstwhile-planet Pluto. These objects are similar to comets in that they are primarily made of various ices, but are distinguished from comets in that they remain frozen and distant from the Sun.

Much like asteroids and planets, KBOs can produce meteoroids as the result of collisions. KBOs also produce dust in response to impacts by interstellar dust grains (Han et al. 2011). In fact, KBOs are thought to be one of the main sources of dust exterior to Saturn; these grains migrate inward under the influence of radiative forces. As they approach Jupiter, the giant planet's gravity often expels KBO dust and meteoroids from the Solar System.

3.2 Sporadic Environment

Most young meteoroids recently ejected from a parent comet will be initially concentrated in a trail of particles. Over time, this trail will elongate and eventually meteoroids will be distributed along an entire stream orbit. If this orbit intersects the Earth's path around the Sun, meteoroids collide with the Earth and produce meteors. If Earth-bound observers measure the radiant—or apparent direction—and speed of the meteor, the orbit of the meteoroid stream can be determined. In many cases, the parent body of a meteoroid stream can be identified using the similarity of the meteor stream orbit to the parent body orbit.

Meteoroids originate from parent bodies and their orbits therefore initially resemble those of their parent bodies. Small differences in velocity between meteoroids cause them to spread out along and away from the "average" orbit. The gravitational effects of the planets, especially

Jupiter, perturb the meteoroids' motion, distorting meteoroid streams and sometimes splitting them into sub-streams. The Sun's radiation also plays a role. Photons carry momentum, and, as they are absorbed or reflected by meteoroids, they transfer that momentum to the meteoroid. This effect is known as "radiation pressure" and can partially or completely counteract gravity for small particles (Burns et al. 1979). Radiation pressure on meteoroids in the threat regime is small, but may still alter their orbital motion.

Eventually, meteoroid streams can become so dispersed that they are no longer really streams but rather become part of the omnipresent meteor background, which meteoriticists call the *sporadic complex*. In this chapter, we distinguish between these sporadic meteors and meteors that still clearly belong to showers. This boundary can be somewhat fuzzy in practice, as we discuss in section. 3.2.5.

3.2.1 Flux

In 1985, Eberhard Grün developed a meteoroid flux model based on lunar craters, zodiacal light, and *in situ* meteoroid detectors such as Pegasus (Grün et al. 1985; Naumann 1966). This "Grün flux" has served as a standard for the past three decades. Many meteoroid environment models are either an extension of the Grün flux or are normalized to it.

The Grün flux expresses the flux of meteoroids at 1 au as a function of particle size (see figure 13). It contains several built-in assumptions; for instance, in deriving particle sizes, Grün assumed a single meteoroid velocity of 20 km/s. It is important to keep these assumptions in mind when producing derivative models. Combining the Grün flux with a new velocity distribution, for instance, without considering the implications for cratering can lead to models that are inconsistent with observations.

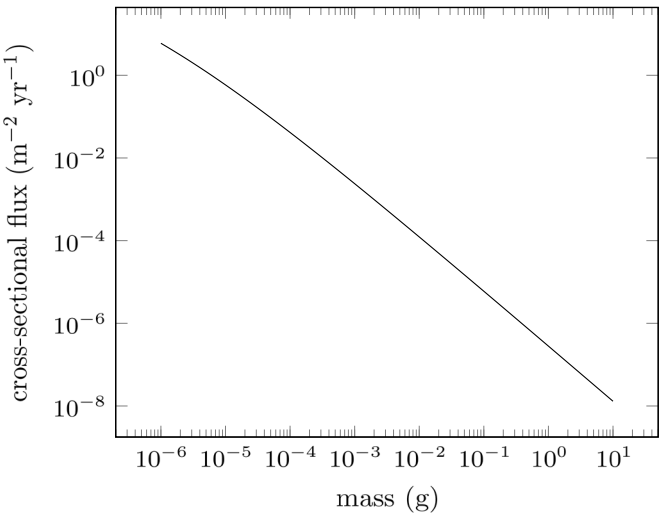

Figure 13. Meteoroid flux at 1 au as a function of limiting meteoroid mass (Grün et al. 1985).

3.2.2 Directionality

While sporadic meteors are present throughout the year, neither their speeds nor their radiants are random. Instead, sporadic meteor radiants are clustered into groups called "sources." These sources correspond to certain directions within the Sun-centered ecliptic coordinate system. This is a system in which coordinates are represented as latitude-longitude pairs, where ecliptic latitude is measured from the Earth's orbital plane and a Sun-centered ecliptic longitude of 0 corresponds to the Sun's location relative to the Earth (see figure 14).

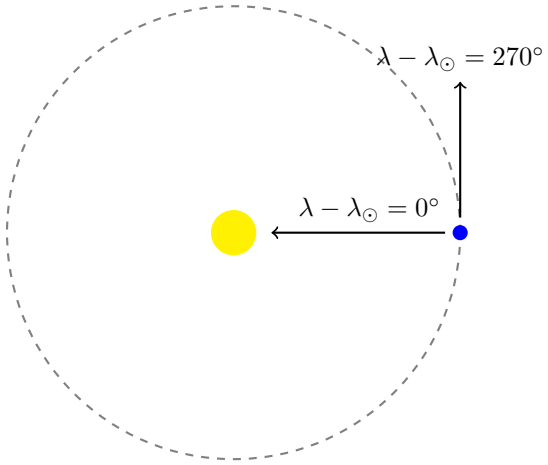

Figure 14. Diagram of Sun-Earth configuration and corresponding values of Sun-centered ecliptic longitude. The "apex" direction refers to the direction of the Earth's motion, at which $\lambda - \lambda_\odot = 270°$.

The first-discovered and most obvious sporadic sources are the helion and antihelion sources, so named because they appear to originate from points near the sunward and antisunward directions, respectively. Approximately half of sporadic radar meteors belong to these sources (Campbell-Brown 2008). The next most visible source is the apex source; apex refers to the direction of the Earth's motion. Many apex meteors have retrograde orbits and are therefore colliding "head-on" with the Earth at high speeds. The apex source can be divided into north and south components, which lie about 20° above and below the ecliptic plane. The final two sporadic sources are the north and south toroidal sources. They lie significantly (about 60°) above or below the apex and are the weakest of the sporadic sources.

The observed strengths of these sources are not representative of their meteoroid populations. The brightness of a meteor increases dramatically with velocity ($\propto v^4$), in contrast to its linear dependence on mass. As a result, the apex source, with its population of high-speed meteors, shows up strongly in meteor surveys, even though it contains relatively few meteors compared to the helion and antihelion sources (see figure 15). When we correct for this effect and consider the flux of meteors greater than a given mass (see figure 16), instead of the flux of meteors greater than a given brightness, the helion and antihelion sources constitute 68% of the sporadic background. The apex source makes up 22% and the toroidal source a mere 10% (Campbell-Brown 2008). Finally, the threat a meteoroid poses to a spacecraft is roughly proportional to the particle's kinetic energy ($\propto v^2$). The directionality of the sporadic flux greater than a given kinetic energy is intermediate to the prior two cases (see figure 17).

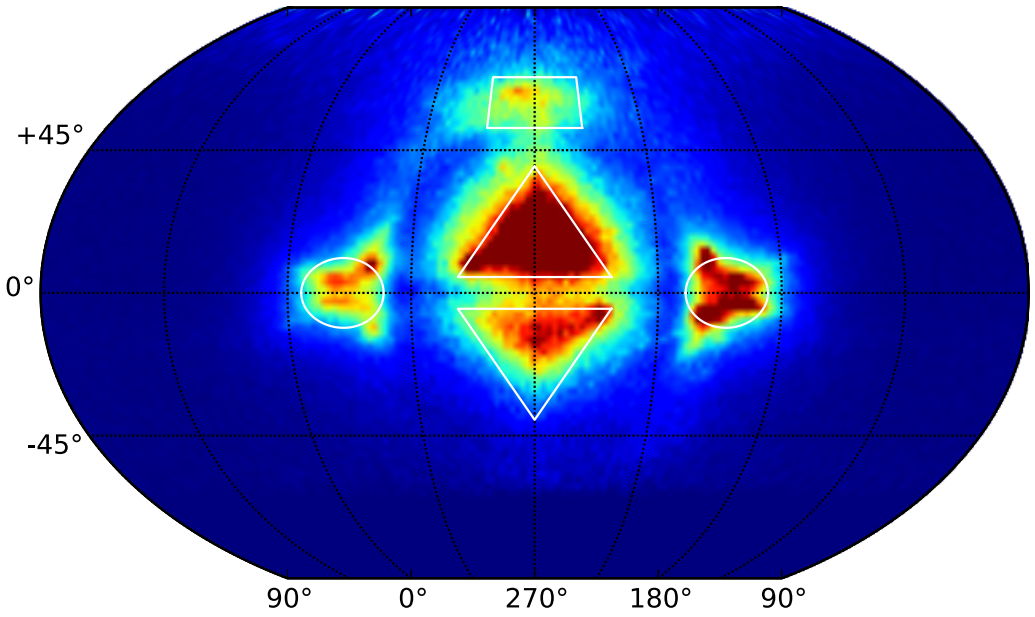

Figure 15. Meteor radiant distribution observed by CMOR; observational biases have been taken into account following Campbell-Brown (2008). Coordinates are Sun-centered ecliptic latitude and longitude. Dark red indicates regions of parameter space that are more highly populated with meteoroids. Triangles mark the north and south apex sources, circles mark the helion and antihelion sources, and a trapezoid marks the north toroidal source. The south toroidal source is not visible to CMOR, due to the detector's northern latitude. Data courtesy of the University of Western Ontario and the MEO.

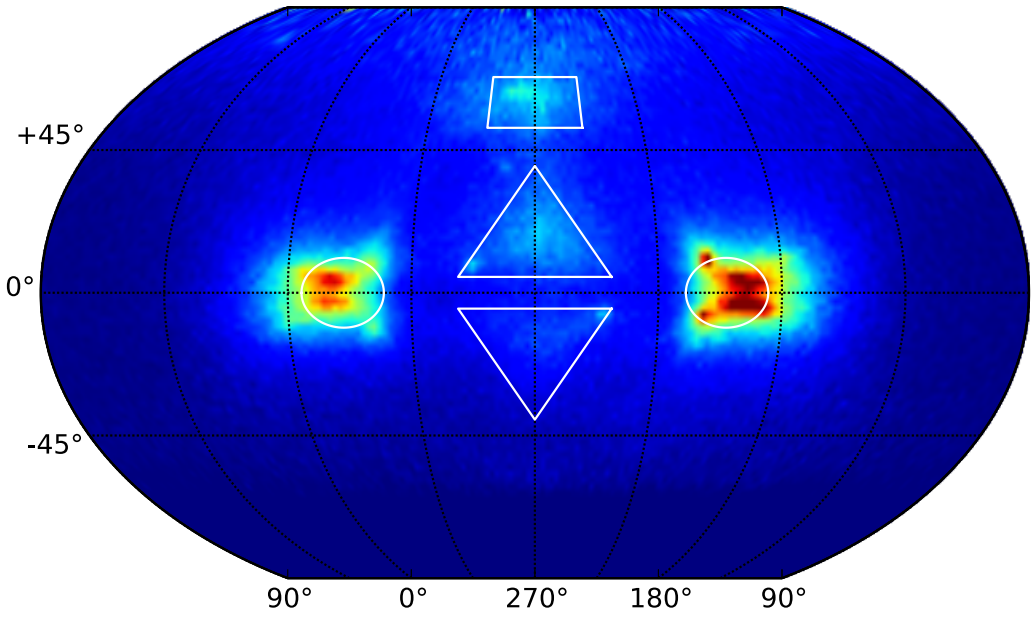

Figure 16. Meteor radiant distribution observed by CMOR. Observational biases have been taken into account and the results have been weighted to a constant limiting mass.

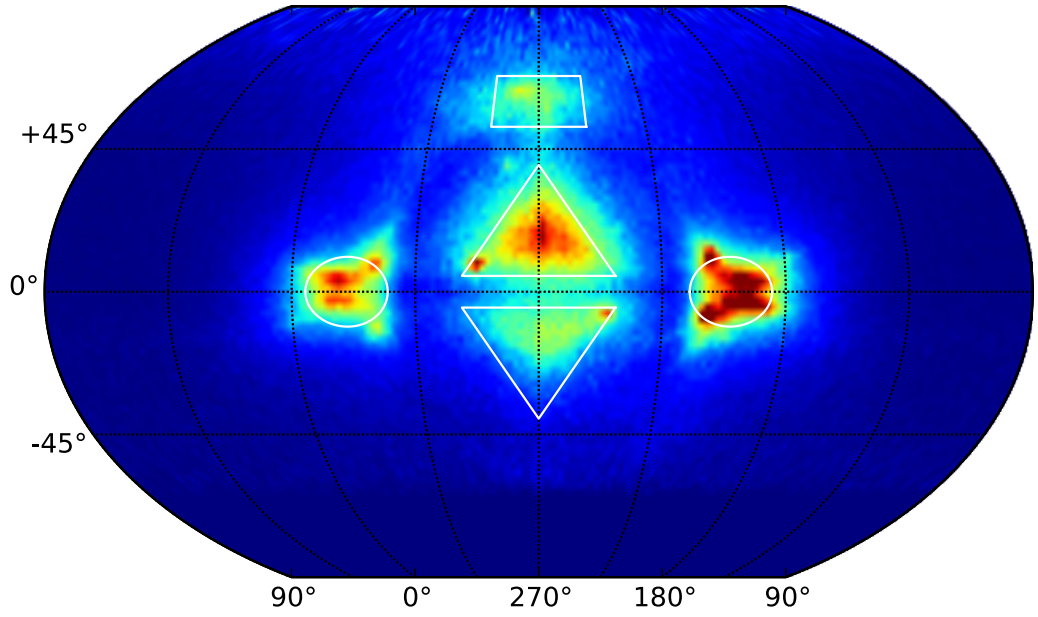

Figure 17. Meteor radiant distribution observed by CMOR. Observational biases have been taken into account and the results have been weighted to a constant limiting kinetic energy.

It is important to realize that this is the directionality of the meteoroid environment as observed at Earth, and Wiegert et al. (2009) demonstrated that the bulk of the sporadic meteoroid complex as seen at Earth can be produced by just a few comets. This suggests that the directionality of the sporadic complex elsewhere in the Solar System could differ significantly from that near Earth, depending on which comets contribute meteoroids to the local environments.

3.2.3 Velocity Distribution

The speed of a meteoroid as it hits the Earth's atmosphere can vary from 11 to 72 km/s. Meteoroid speeds are bounded on the low end by the Earth's escape velocity; objects traveling slower than 11 km/s at 100-km altitude are in orbit around the Earth. Similarly, the Solar System's escape velocity places an upper limit on meteoroid speeds. At 1 au, objects traveling faster than 42 km/s relative to the Sun will exit the Solar System. The Earth itself travels around the Sun at 30 km/s; thus, a meteoroid on a head-on collision course with the Earth will at most have an apparent speed of 72 km/s. Particles can exceed this limit in three ways: very small particles can be accelerated by radiation pressure until they exit the Solar System, particles of any size can be accelerated to high speeds by close encounters with planets (Wiegert 2014), and interstellar particles can pass through the Solar System at high speeds. However, none of these processes have been demonstrated to contribute significantly to the meteoroid population in the size range that threatens spacecraft, so we exclude them from further discussion.

The distribution of meteoroid speeds within the above limits is not well-determined. The velocity distribution of the meteoroid environment has been measured numerous times with various meteor observatories, but each survey yields a somewhat different result. This is due, at least in part, to the differing observational biases between surveys, but real velocity distribution differences may exist between different meteoroid size ranges (Wiegert et al. 2009, Nesvorný et al. 2010). Differences in assumed parameters, such as the exact dependence of a meteor's brightness on its speed, can lead to significantly different velocity distributions for a given set of data (see figure 18).

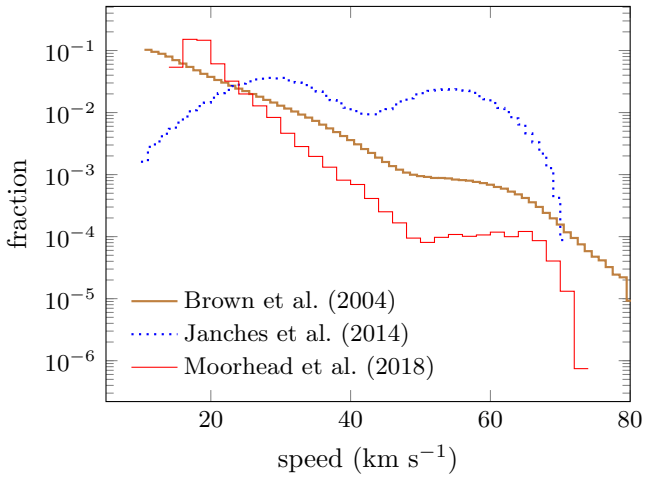

Figure 18. Distribution of meteoroid speeds at the top of the atmosphere as observed by meteor radars (Brown et al. 2004; Janches et al. 2014; Moorhead et al. 2018). These data have been weighted to a uniform limiting mass.

3.2.4 Densities

Meteoroid densities are particularly challenging to measure. Meteorite densities can be measured directly, but these rocks are the remnants of only the most durable meteoroids and have been substantially altered by their passage through the atmosphere. Few meteoroid parent bodies have measured densities, and the overall density of a parent body may differ significantly from that of an ejected particle. Densities have been measured for interplanetary dust particles (Love et al. 1994), but these densities vary by more than an order of magnitude and may differ from those of larger particles. It is sometimes possible to recover debris remnants from craters in returned spacecraft surfaces, but these remnants have also been altered in impact.

Because of these limitations, meteoroid densities are usually constrained through modeling. The rate at which a meteor decelerates in the atmosphere depends on both its size and its mass. In theory, one should therefore be able to use the in-atmosphere trajectory to measure the meteoroid's density. However, this is complicated in practice by the fact that meteoroids fragment, and that this fragmentation is difficult to model. One can exclude highly fragmentary meteors in an attempt to model only single-body meteoroids, but this approach yields a biased data set.

A crude measure of meteoroid density can be obtained using the observable properties of meteors, such as end-height and presence of flares. Meteors that terminate at high altitudes are presumed to be less dense, and multiple flares indicate that the meteoroid is weak. Comparisons between meteors and high-speed pellets indicated that meteoroids were likely porous, fragile, and with densities ranging from 0.2-1.0 g/cm^3 (Whipple 1952). Thus, a typical meteoroid density of 0.5 g/cm^3 was used in early NASA models (Cour-Palais 1969). In contrast, Grün used a density of 2.5 g/cm^3 in his analysis of the Helios micrometeoroid experiment (Grün et al. 1980).

Kikwaya et al. (2011) performed a recent analysis of meteoroid densities that attempted to take fragmentation into account. This 2011 study measured densities associated with different orbital classes: meteoroids associated with Halley-type and long-period comets had a peak in bulk densities around 1 g/cm^3, while those associated with Jupiter-family comets or asteroids had a peak in bulk density between 3.5 and 4 g/cm^3. Moorhead et al. (2017) derived a two-population meteoroid density distribution from these data; see figure 19.

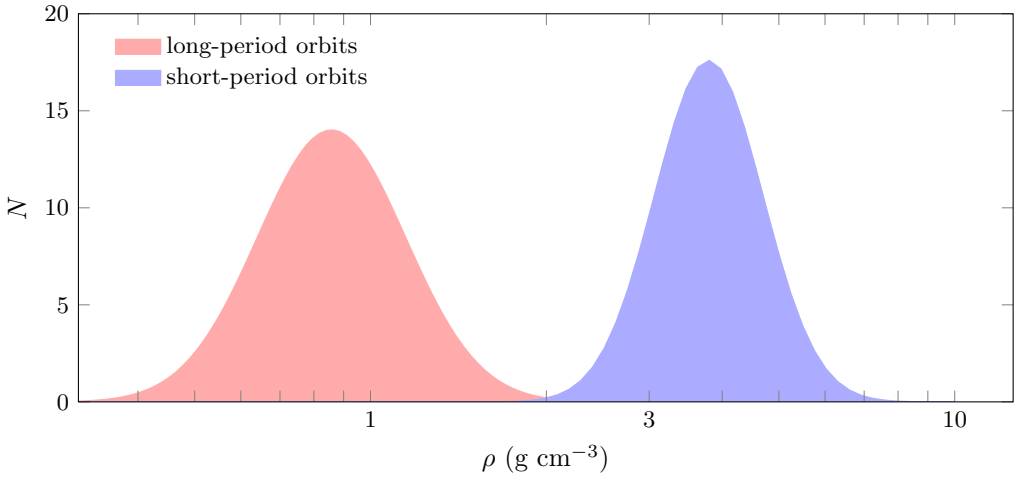

Figure 19. Density distribution for meteoroids on long-period and short-period orbits according to Moorhead et al. (2017), based on density measurements from Kikwaya et al. (2011).

3.2.5 Diurnal and Annual Variations

The sporadic meteor flux as measured at a particular location on the Earth's surface varies over the course of a day. This is simply the result of the Earth's rotation; when an observer's location faces in the direction of the Earth's motion (between local midnight and noon), it is on the Earth's "windshield" and is impacted by both prograde (orbiting in the same direction as the Earth) and retrograde (orbiting in the opposite direction) meteors. While on the leeward side of the Earth, only prograde meteors are observed, and the flux is less. Note that the diurnal variation is local; the sporadic meteoroid flux on the Earth as a whole does not vary significantly over the course of a day.

The sporadic flux incident on the entire Earth does, however, vary over the course of a year. Each sporadic source has a unique yearly activity pattern, varying in strength by up to a factor of 4-5 (Campbell-Brown & Jones 2006). The north apex source displays the least variability, while the helion and antihelion sources display the most variability (up to a factor of 3 over the course of a year). These variations cancel each other out to some extent: over the course of the year, the total sporadic flux can exceed or fall short of the average value by about 40%. Most current meteoroid models do not reproduce these fluctuations; their incorporation into environment models is an area of future work.

Aside from these annual variations, the sporadic environment is stable over timescales of decades, centuries, and even thousands of years. The meteoroid environment does evolve on timescales of hundreds of thousands of years and longer due to collisions and radiative forces (e.g., Wiegert et al. 2009), but these timescales are far too long to be of concern to space missions.

3.2.6 Differences at Other Planets/Moons

Section 3.2 describes what we know about the sporadic meteoroid environment. However, the vast majority of the data described here are derived from meteors. As a result, we have a great deal of information about the meteoroid environment near Earth and very little direct information about the meteoroid environment throughout the rest of the Solar System. We can predict and model some of these differences, while others must be measured.

We expect the sporadic environment to vary over large distances, such as the distance from the Earth to Mars. However, besides predictable local effects, such as gravitational focusing and shielding, the environment does not vary significantly between the Earth and the Moon. The lunar distance is small even compared to the width of meteoroid streams. Thus, the only differences in the meteoroid environment as seen at the Moon and that seen at Earth are due to the differences in the two bodies. The Earth's gravity attracts and accelerates meteoroids, enhancing the meteoroid flux and increasing their speed. The Moon's gravity attracts meteoroids as well, but the effect is much weaker. Both the Earth and the Moon will also physically block a portion of the meteoroid environment; this shielding effect is 50% close to the surface. Finally, the Moon has no atmosphere. Thus, meteoroids slam into the lunar surface instead of burning up as a meteor. These impacts produce ejecta that can pose their own hazards to spacecraft.

Interplanetary differences in the meteoroid environment are more extreme. For instance, meteoroids have a maximum speed of 72 km/s relative to the Earth, but these orbital speeds increase closer to the Sun. "Head-on" Mercury-meteoroid collisions can reach speeds of 116 km/s. The Parker Solar Probe is expected to encounter meteoroids with relative speeds of hundreds of km/s on its way to the Solar corona. Correspondingly, meteoroid speeds in the outer Solar System will typically decrease. Thus, Mars, with its greater distance from the Sun and smaller mass likely has a somewhat gentler meteoroid environment than the Earth.

The picture beyond Mars is more complicated. Asteroids can produce meteoroids and so the meteoroid flux likely increases near the asteroid belt. Our gas giant planets have such large masses (particularly Jupiter) that their gravitational effects on the environment will be rather extreme. All of the gas giants have rings, which contain additional hazardous particles. The gas giants also have moons, which can produce meteoroids in response to impacts.

On top of these predicted differences in the meteoroid environment near other planets, there can be unpredicted differences as well. As discussed in section 3.2, recent modeling of the meteoroid directionality near Earth has demonstrated that the sporadic environment could very well be produced primarily by just a couple of comets. Yet there are many comets with orbits approaching the Earth that could, yet do not, contribute to the sporadic background. Each planet has a different set of nearby comets, and we do not know which of these, if any, contribute to the sporadic complex as seen at other planets (or between planets). Without measurements of the meteoroid environment directionality throughout the Solar System—which do not currently exist—it is difficult-to-impossible to predict the meteoroid directionality and speed distribution near other planets.

3.3 Meteor Showers and Streams

The speeds at which meteoroids are ejected from their parent bodies are very small in comparison to the parent's orbital velocity. As a result, meteoroids initially deviate very little from the parent's orbit, and the ejecta are generally organized into a tail. Over time, the effects of radiation pressure and Poynting-Robertson drag will cause the tail to elongate and spread into a meteoroid stream. Eventually, meteoroids will be dispersed along the entire orbit. Over even longer time spans, the stream will be so dispersed that it will no longer be considered a stream but will instead constitute part of the sporadic complex. The duration of time needed for a tail to become a stream and for a stream to be subsumed into the sporadic background will vary from comet to comet and stream to stream.

Radiative forces have a greater effect on small particles, so the smallest meteoroids will stray the furthest from the stream. As a result, meteor showers tend to contain more large particles than the sporadic meteoroid complex. Because larger particles produce brighter meteors, meteor showers are particularly enjoyable to watch. However, for every bright fireball, there are orders of magnitude more tiny meteoroids capable of damaging a spacecraft. Through their sheer numbers, these tiny sporadic meteoroids pose far more risk to spacecraft than their larger counterparts.

When a meteoroid stream intersects the Earth's orbit, meteoroids will collide with the Earth and produce meteors. At this orbit intersection, the meteoroids have similar directions of motion and will appear to originate from a common direction. This common direction, or radiant, is one of the fundamental measurable characteristics of a meteor shower. If the stream is relatively new and meteoroids are more concentrated in one part of the stream orbit, the number of meteors may vary from year to year. For most established meteor showers, the activity level is fairly consistent from year to year.

3.3.1 Major Meteor Showers

In this section, we list some of the most significant meteor showers. Table 2 lists all meteor showers that are (1) included in the MEO's annual meteor shower forecast and (2) have a ZHR of 10 or higher. In addition to these major showers, the MEO also incorporates a number of more minor meteor showers into the annual forecast. Minor showers may combine to produce a moderate boost to the meteor flux, or they can blend in with a major shower. The set of showers included varies by year.

Table 2. Basic characteristics for major meteor showers. These characteristics include peak ZHR, date of activity (both peak date and time span), radiant, and geocentric velocity. The meteoroid flux can be derived from ZHR; in general, a high ZHR corresponds to a high meteoroid flux.

Shower	ZHR	Peak Date and Duration	Radiant	Speed
Quadrantids	120	Jan 3 (Dec 28–Jan 9)	230°, +49°	41 km/s
Geminids	120	Dec 13 (Dec 6–Dec 19)	113°, +32°	35 km/s
Perseids	100	Aug 12 (Jul 23–Aug 22)	48°, +57°	61 km/s
Daytime Arietids	60	Jun 8 (May 22–Jul 2)	45°, +24°	39 km/s
η Aquariids	60	May 6 (Apr 20–May 20)	337°, –1°	65 km/s
Daytime ζ Perseids	20	Jun 9 (May 20–Jul 5)	63°, +27°	29 km/s
South δ Aquariids	20	Jul 29 (Jul 14–Aug 23)	340°, –16°	42 km/s
Orionids	20	Oct 22 (Oct 11–Nov 9)	96°, +16°	66 km/s
Leonids	20	Nov 17 (Nov 6–Nov 30)	154°, +22°	71 km/s
Lyrids	18	Apr 22 (Apr 14–Apr 25)	96°, +33°	49 km/s
Daytime β Taurids	10	Jun 28 (Jun 5–Jul 17)	86°, 21°	29 km/s
Puppid-Velids	10	Dec 7 (Dec 1–Dec 15)	128°, –45°	40 km/s
Ursids	10	Dec 22 (Dec 17–Dec 26)	217°, +75°	33 km/s

For each shower we have given the ZHR at the shower's peak. However, the threat posed is related to not just the peak but also to the duration of the shower. The longer a shower lasts, the greater the integrated flux, or fluence, of meteoroid incidents on a spacecraft. Short-duration missions can benefit from short shower durations; if the shower is very limited in time scale, it is easier to avoid the threat window by delaying launch.

One further characteristic to take into account in determining risk is the mass index, which describes the relative number of small and large particles in a shower. The Geminids, for instance, have a "steep" mass index compared to the Perseids. As a result, while the Perseids produce more visible meteors (large particles), the Geminids produce a far larger number of small, yet still dangerous, 100-micron meteoroids.

3.3.2 Meteor Outbursts and Storms

While some meteor showers have a consistent level of activity, others can exhibit variable activity. This variation can be mild (Perseid activity often changes by 10–20% between years) to severe (Leonid activity varies by orders of magnitude). Some showers are only seen in "outburst," and some may only be seen once. Meteor shower variability can occur due to variability in the parent body's activity or the perturbation of the stream orbit by planets. Young showers may show variability simply because the meteoroids have not yet dispersed along the entire orbit. The Leonid meteor shower occurs annually and is one of the most active showers. It has also produced the most remarkable meteor outbursts (sometimes called meteor storms) in history; for instance, the 1833 Leonids produced hundreds of thousands of meteors per hour. The event sparked both public panic and scientific curiosity and is today considered to be one of the main precipitating events

behind modern meteoritics. The Leonids produced additional storms in 1866, 1966, and the early 2000s. These Leonid storms typically occur when Earth has a close approach to the parent body of the Leonids, comet 55P/Tempel-Tuttle.

While shower variability usually refers to variation in the number of meteors produced, meteor showers can also exhibit variability in timing, radiant, or size distribution. Often these variations are linked; i.e., a year with high activity can sometimes produce a higher proportion of large meteors.

Table 3 lists a selection of meteor shower outbursts. Much of this data summarizes Kronk's *Meteor Showers: An Annotated Catalog* (2014), which provides excellent historical summaries of meteor showers.

Table 3. Meteor shower outburst summary.

Shower	Typical ZHR	Outbursts: Year (ZHR or Hourly Rate)
Quadrantids	120	1909 (202), 1922 (79)
Lyrids	18	687 BC, 15 BC, 582 AD, 1863 (40), 1922, 1982 (75)
pi Puppids	NA	1982 (23)
June Boötids	NA	1916, 1998 (100)
Perseids	100	1991 (350), 1992 (220), 1993 (300), 1994 (250)
Aurigids	6	1986 (40), 1994 (37-55)
Draconids	NA	1933 (6000), 1946 (2000-3000), 1972 (10-15), 1998 (720)
Andromedids	NA	1940 (30), 2008, 2011
Leonids	20	1799, 1833 (10,000 - 60,000), 1898 (50-100), 1901 (300-400), 1903 (140), 1928 (50), 1932 (240), 1965 (120), 1966 (144,000), 1967-1969 (100-150), 1971 (170), 1972 (40), 1995 (35), 1996 (90), 1997 (100), 1998 (250), 1999 (3700), 2000 (480), 2001 (3430), 2002 (2940), 2003 (63), 2004 (37), 2006 (74), 2009 (56)
α Monocerotids	NA	1925, 1935 (2000), 1985, 1995 (EZHR=350)
Phoenicids	NA	956 (100), 1958 (30), 1972 (20)
Ursids	10	1979 (25-27), 1986 (64-122), 1993 (50-100), 2000 (90), 2007 (34)

3.3.3 Long-term Meteor Shower Variability

The variability and shower outbursts described in section 3.3.2 take place on a year-by-year basis. However, there are also showers whose activity has been observed to vary on time scales longer than a single year. For instance, the Geminids have no recorded activity before 1830 but have since grown to be the second strongest visual meteor shower (Plavec 1950). Additionally, Geminid activity in the 1990s and 2000s appears to be greater than it was in the 1980s (Miskotte et al. 2011). This growth in activity has been attributed to Jupiter-induced changed in the meteor stream orbit (Plavec 1950). Regardless of cause, it is clear that accurate long-term shower forecasting requires long-term shower monitoring.

3.3.4. New Meteor Showers

New meteor showers are frequently discovered; occasionally, these showers prove to be significant. These "new" showers are often previously unresolved showers that are marginally stronger than the sporadic shower flux (i.e., not actually "new" but newly discovered). However, sometimes truly new showers are predicted or reported; these showers tend to result from young meteoroid streams that had not previously encountered Earth.

An example of a recent meteor shower that arises from a new stream is the May Camelopardalids, which were first observed in 2014 and peaked in flux on the night of May 24, 2014. This new shower originates from the close approach of comet 209P/LINEAR, which was as close as 7.5 million km from Earth on May 28, 2014. This close approach was predicted to perhaps trigger a new and tremendous meteor storm (for a summary of early predictions, see Ye and Wiegert 2014). The dust production of comet 209P in the past was unknown, and the measured meteor fluxes from the May Camelopardalids were lower than predictions, indicating 209P was not as dusty in the past as guessed. However, the new May Camelopardalid meteor shower was successfully predicted and observed—a significant accomplishment.

Whether a new shower originates from a new physical stream of dust or is simply newly identified, its identification allows for more accurate meteor shower forecasting as well as the opportunity to identify its parent body.

3.4 Model Overviews

3.4.1 Historical Models

Early environment models consisted of analytic expressions that were constructed to fit meteoroid data. The models of Cour-Palais (1969), Kessler (1970), and Grün et al. (1985) all consisted of functions that gave the meteoroid flux as a function of particle size or mass. Each characterized the meteoroid speed distribution using a single average speed value (such as 20 km/s for Grün) and a single density (0.5 g/cm^3 for Cour-Palais and Kessler and 2.5 g/cm^3 for Grün). Mass, speed, and density distributions and values were all assumed to be independent, and meteoroid directionality was modeled as isotropic.

Smith (1994)—also known as TM 4527—attempted to remove several of the above simplifications using a patchwork combination of several models. The flux as a function of particle mass was derived from Grün et al. (1985), while the velocity distribution was derived from Kessler (1969). The directionality was assumed to be isotropic, and the density distribution took the form of a three-step function. This combination model stood for a decade and was used to assess meteoroid impact risk for the International Space Station (SSP 30425).

In addition to describing the interplanetary meteoroid flux at 1 au, TM 4527 describes how this flux is modified in near-Earth space. The Earth itself attracts meteoroids, increasing the meteoroid flux through a process called gravitational focusing. At the same time, the planet shields spacecraft from a portion of the meteoroid environment. TM 4527 takes both gravitational focusing and shielding into account, albeit in a crude manner.

TM 4527 was an early attempt at building a comprehensive model of the meteoroid environment. However, it combined models with inconsistent assumptions, and the result underrepresents the risk of meteoroid impacts in low Earth orbit; TM 4527 was shown to under-predict crater counts on LEO spacecraft (Scott et al. 2005). Several independent review boards recommended the development of a new model whose flux and speed distributions better matched observations.

3.4.2 Current Sporadic Environment Models

Current environment models use populations of meteoroids to model the flux, size, speed, and directionality of the meteoroid environment.

3.4.2.1 Divine/METEM. Divine (1993) developed one of the earliest non-isotropic models of the meteoroid environment. This model divides the meteoroid environment into five populations: the core, asteroidal, halo, inclined, and eccentric populations. The core population is the largest of these and comprises the bulk of the model. Each population is defined by its distributions of orbital eccentricity, inclination, and distance from the Sun. These distributions were derived from different data sets; for instance, the core population was extrapolated from Galileo data while the inclined population was invoked to explain Helios data (Garrett et al. 1999). Divine's initial populations have been revised several times; for instance, Staubach et al. (1997) describe a modified version of the Divine model that includes both interstellar particles and the effect of radiation pressure on the dust population.

Divine's populations were incorporated into a meteoroid model called METEM (Garrett et al. 1999). METEM described the meteoroid flux, speed, and directionality relative to a user-supplied spacecraft trajectory. METEM makes use of a revision of Divine's model provided in Matney (1995); this revision formulates descriptions of Divine's populations that correspond to textbook definitions of probability distributions and are easier to use.

Divine based his model on a number of data sets; of these, only the radar meteor data set provided information on meteoroids in the threat regime (i.e., larger than 10^{-6} g). A later reanalysis of these radar meteor data corrected several errors and concluded that Divine's model severely underpredicts the proportion of high velocity meteors (Taylor 1996). Furthermore, the Divine model as implemented in METEM does not reproduce the observed distribution of meteor radiants (McNamara et al. 2004).

3.4.2.2 Dikarev/IMEM. The European Space Agency's meteoroid model is the Interplanetary Meteoroid Model (IMEM), which was developed by Dikarev et al. (2005). The meteoroid distributions in this model are derived from populations of parent bodies, taking the effects of radiative forces and collisions into account. The end result is validated against several data sets, including the crater data used by Grün et al. (1985) and more recent observations of the zodiacal cloud by the Cosmic Background Explorer (COBE). Radar meteor observations from AMOR were considered for inclusion but ultimately discarded due to a discrepancy between the radar data and zodiacal cloud data.

IMEM is available as a computer tool; it computes impact fluxes and velocities relative to spacecraft trajectories. It is available with and without a GUI and is available for multiple platforms.

3.4.2.3. Jones/MEM. NASA's primary meteoroid model is the Meteoroid Engineering Model (MEM), which uses the sporadic source populations described by Jones (2004). This model ties meteoroid populations to parent body populations, primarily comets. In contrast to the Divine/METEM and IMEM models, which rely on *in situ* detection and zodiacal cloud data, MEM is calibrated primarily to meteor data from the CMOR. The total flux at 1 au is similar to that of Grün et al. (1985).

MEM improves on previous models by reproducing the directionality of the meteoroid environment using observations of meteoroids larger than 10^{-6} g. Meteoroid speed is not assumed to be independent of direction. Instead, the two are very much correlated; the more closely a meteoroid's radiant is aligned with the apex direction, the higher the speed can be (see figure 20).

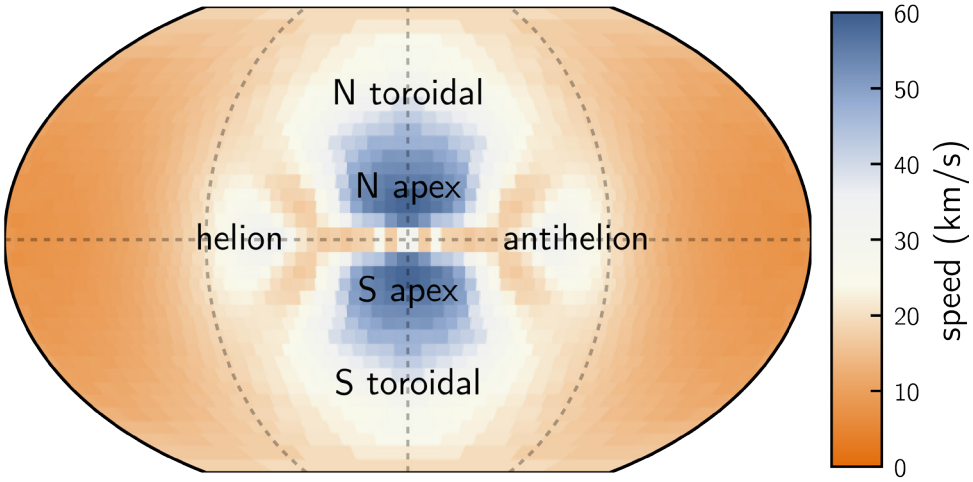

Figure 20. Average meteoroid speed as a function of direction (ecliptic latitude and longitude) at 1 au calculated using MEM 3.

The latest version of MEM, version 3 (Moorhead et al. 2019b), supplies the user with a graphical user interface (for Windows only) and a command-line executable (for Windows, Mac, or Linux). The user must supply a spacecraft trajectory; MEM then computes the meteoroid environment relative to this trajectory. MEM 3 models the meteoroid environment in the inner Solar System and is valid between heliocentric distances of 0.2 and 2 au. It can generate environments for spacecraft in orbit around the Earth, Moon, Mercury, Venus, and Mars, as well as in interplanetary space.

Drolshagen et al. (2008) conducted a comparison study of METEM, IMEM, and MEM in addition to older models such as Smith (1994). This study compares the flux and velocity distribution generated by these models for two different limiting masses and locations near the terrestrial

planets (Mercury, Venus, Earth, and Mars). Although these models are all calibrated to existing data, significant discrepancies exist between them. For instance, the models vary by a factor of 43 in flux near Mercury and by a factor of 1.8 in velocity near Mars (Drolshagen 2009). These differences highlight the gaps in our knowledge of the meteoroid environment at other locations in the Solar System.

3.4.3 Shower Models

In contrast to the sporadic background, meteor showers vary from year to year. A shower modeler must therefore make predictions rather than rely on typical shower rates.

3.4.3.1 MSFC Meteoroid Stream Model. The NASA MEO makes annual predictions of meteor shower activity. These predictions are based in part on the results of the MSFC Meteoroid Stream Model, described in Moser & Cooke (2008). The MEO models the evolution of meteoroid streams that produce major meteor showers at Earth with variable annual activity.

The stream model follows particles from their "ejection" from a comet to the present day. The simulated meteoroid's initial position and velocity reflects the known orbit of the parent comet and models of gas and dust emission from cometary nuclei. The gravitational effects of the Sun, planets, and the Moon are taken into account in computing the particle's trajectories. Radiative forces (radiation pressure and Poynting-Robertson drag) are also included. The gravitational interactions between planets are not computed. Instead, the stream model relies on the DE406 ephemeris, which describes the positions of the planets from 3000 BCE to 3000 CE (Standish 1998).

Close approaches between the Earth and meteoroids are tallied; groups of close encounters indicate a shower. An unusually large number of close encounters can indicate a higher meteoroid flux, which is then folded into the annual forecast. Finally, additional information, such as particle size, is extracted to further describe the shower.

3.4.3.2. Annual Shower Forecast. The MEO generates an annual meteor shower forecast to help spacecraft mitigate the increased risk of penetration during periods of elevated activity (see figure 21). These forecasts present the meteoroid flux near Earth due to showers over the course of the year for four different limiting particle masses. The shower flux is compared with the sporadic flux to illustrate the relative, as well as absolute, flux enhancement.

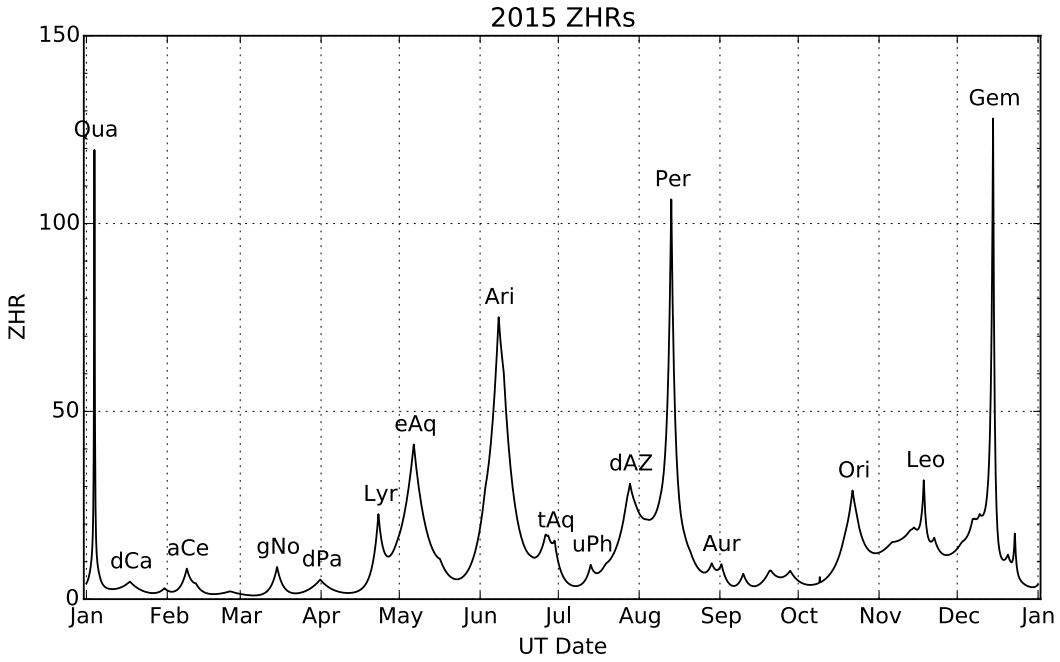

Figure 21. Annual meteor shower forecast for 2015. Activity is represented in terms of ZHR as a function of date over the course of the year. Activity peaks are labeled with a code representing the relevant meteor shower (for example, "Per" marks the Perseid meteor shower).

Five parameters are required for each shower: peak date, peak ZHR, size distribution exponent, the rate at which activity increases before the peak, and the rate at which activity decreases after the peak. We rely on both observations and predictions of individual meteor showers to obtain these parameters. For meteor showers with a consistent level of annual activity, such as the Geminids and the Lyrids, past performance is a reasonable indicator of future activity. For these reliable showers, the meteor forecast relies on measured values of peak ZHR, activity profile, and size distribution.

However, major showers with variable annual activity, including the Perseids, Leonids, and Taurids, are simulated using the stream model discussed in section 3.4.2. These stream model results are compared with any available predictions from independent researchers. Any variations from typical activity are folded into the meteor dataset, and a year-specific meteor forecast is generated from these data (Moorhead et al. 2017; Moorhead et al. 2019a)

3.5 References

Brown, P.G.; Jones, J.; Weryk, R.J.; and Campbell-Brown, M.D.: "The Velocity Distribution of Meteoroids at the Earth as Measured by the Canadian Meteor Orbit Radar (CMOR)," Earth, Moon, and Planets, Vol. 95, No. 1, pp. 617–626, 2004.

Burns, J.A.; Lamy, P.L.; and Soter, S.: "Radiation Forces on Small Particles in the Solar System," *Icarus*, Vol. 40, No. 1, pp. 1–48, 1979.

Campbell-Brown, M.D.; and Jones, J.: "Annual Variation of Sporadic Radar Meteor Rates," *Monthly Notices of the Royal Astronomical Society*, Vol. 367, No. 2, pp. 709–716, 2006.

Campbell-Brown, M.D.: "High Resolution Radiant Distribution and Orbits of Sporadic Radar Meteoroids," *Icarus*, Vol. 196, pp. 144–163, 2008.

Cour-Palais, B.G.: "Meteoroid Environment Model - 1969 (Near Earth to Lunar Surface)," NASA SP (Series), NASA, Washington, D.C., 1969.

Dikarev, V.V.; Grün, E.; Baggaley, W.J.; et al.: "The New ESA Meteoroid Model," *Advances in Space Research*, Vol. 35, No. 7, pp. 1282–1289, 2005.

Divine, N.: "Five Populations of Interplanetary Meteoroids," *Journal of Geophysical Research*, Vol. 98, No. E, pp. 17029–17048, 1993.

Drolshagen, G.: "Comparison of Meteoroid Models," Committee Report IADC AI 24.1, NASA, 2009.

Drolshagen, G.; Dikarev, V.V.; Landgraf, M.; et al.: "Comparison of Meteoroid Flux Models for Near Earth Space," *Earth, Moon, and Planets*, Vol. 102, No. 1, pp. 191–197, 2008.

Garrett, H.B.; Drouilhet, S.J.; Oliver, J.P.; and Evans, R.W.: "Interplanetary Meteoroid Environment Model Update," *Journal of Spacecraft and Rockets*, Vol. 36, No. 1, pp. 124–132, 1999.

Grün, E.; Pailer, N.; Fechtig, H.; and Kissel, J.: "Orbital and Physical Characteristics of Micrometeoroids in the Inner Solar System as Observed by HELIOS 1," *Planetary and Space Science*, Vol. 28, No. 3, pp. 333–349, 1980.

Grün, E.; Zook, H.A.; Fechtig, H.; and Giese, R.H.: "Collisional Balance of the Meteoritic Complex," *Icarus*, Vol. 62, No. 2, pp. 244–272, 1985.

Han, D.; Poppe, A.R.; Piquette, M.; et al.: "Constraints on Dust Production in the Edgeworth-Kuiper Belt from Pioneer 10 and New Horizons Measurements," *Geophysical Research Letters,* Vol. 38, No. 24, 2011.

Jewitt, D.; Agarwal, J.; Weaver, H.A.; et al.: "Episodic Ejection from Active Asteroid 311P/PANSTARRS," *The Astrophysical Journal,* Vol. 798, No. 2, pp. 109, 2015.

Jones, J.: "Meteoroid Engineering Model – Final Report," SEE/CR-2004-400, NASA Marshall Space Flight Center, Huntsville, AL, 2004.

Kessler, D.J.: "Average Relative Velocity of Sporadic Meteoroids in Interplanetary Space," *AIAAJ*, Vol. 7, No. 12, pp. 2337–2338, 1969.

Kessler, D.J.: "Meteoroid Environment Model - 1970 (Interplanetary and Planetary)," NASA/SP-8038, NASA Johnson Space Center, Houston, TX, 1970.

Kikwaya, J.B.; Campbell-Brown, M.D.; and Brown, P.G.,: "Bulk Density of Small Meteoroids," *Astronomy and Astrophysics*, Vol. 530, No. A113, 2011.

Kronk, G.W.: *Meteor Showers: An Annotated Catalog*, Springer, 2014.

Love, S.G.; Joswiak, D.J.; and Brownlee, D.E.: "Densities of Stratospheric Micrometeorites," *Icarus*, Vol. 111, No. 1, pp. 227–236, 1994.

Marvin, U. B.: "The Discovery and Initial Characterization of Allan Hills 81005 - The First Lunar Meteorite" *Geophysical Research Letters*, Vol. 10, No. 9, pp. 775–778, 1983.

Matney, M.: "A Revision of Divine's Interplanetary Model," in IAU Colloquium No. 150, 1–6.
McNamara, H., Jones, J., Kauffman, B., Suggs, R. M., Cooke, W. J., & Smith, S. (2004). *Meteoroid Engineering Model (MEM): A Meteoroid Model For The Inner Solar System. Earth, Moon, and Planets*, 95(1), pp. 123–139, 2004.

The Meteoritical Society: "Meteoritical Bulletin Database, " <https://www.lpi.usra.edu/meteor/>, October 06, 2019.

Moorhead, A.V.; Cooke, W.J.; and Campbell-Brown, M.D.: "Meteor Shower Forecasting for Spacecraft Operations," in *Proceedings of the 7th European Conference on Space Debris*, 2017.

Moorhead, A.V.; Egal, A.; Brown, P.G.; et al.: "Meteor Shower Forecasting in Near-Earth Space," *Journal of Spacecraft and Rockets*, Vol. 866, No. 1, pp. 1–15, 2019a.

Moorhead, A.V.; Kingery, A.; and Ehlert, S.: "NASA's Meteoroid Engineering Model 3 and its ability to replicate spacecraft impact rates," *Journal of Spacecraft and Rockets*, accepted, 2019b, <http://arc.aiaa.org/doi/abs/10.2514/1.A34561>.

Moser, D.E.; and Cooke, W.J.: "Updates to the MSFC Meteoroid Stream Model," *Earth, Moon, and Planets,* Vol. 102. No. 1, pp. 285–291, 2008.

Naumann, R.J.: "The Near-Earth Meteoroid Environment," NASA-TN-D-3717, NASA Marshall Space Flight Center, 1966.

Öpik, E. J.: "Collision probabilities with the planets and the distribution of interplanetary matter," Proceedings of the Royal Irish Academy, Vol. 54, pp. 165–199, 1951.

Schiaparelli, M.J.V.: "Sur la Relation qui Existe Entre les Comètes et les Étoiles Filantes," *Astronomische Nachrichten*, Vol. 68, No. 2, pp. 331–332, 1867.

Smith, R.E.: "Natural Orbital Environment Definition Guidelines for Use in Aerospace Vehicle Development," NASA-TM-4527, NASA Marshall Space Flight Center, Huntsville, AL, 1994.
Staubach, P.; Grün, E.; and Jehn, R.: "The Meteoroid Environment Near Earth," *Advances in Space Research*, Vol. 19, No. 2, pp. 301–308, 1997.

Suggs, R.M.; Cooke, W.J.; Brown, P.G.; et al.: "Meteor Properties Database - Final Report," NASA-TP-2004-400, NASA Marshall Space Flight Center, Huntsville, AL, 2004.

Taylor, A.D.: "Earth Encounter Velocities for Interplanetary Meteoroids," *Advances in Space Research*, Vol. 17, No. 1, pp. 205–209, 1996.

Whipple, F.L.: "On Meteor Masses and Densities," *Astronomical Journal*, Vol. 57, No. 28, 1952.

Wiegert, P.A.: "Hyperbolic Meteors: Interstellar or Generated Locally via the Gravitational Slingshot Effect," *Icarus*, Vol. 242, No. C, pp. 112–121, 2014.

Wiegert, P.A.; Vaubaillon, J.J.; and Campbell-Brown, M.D.: "A Dynamical Model of the Sporadic Meteoroid Complex," *Icarus*, Vol. 201, No. 1, pp. 295–310, 2009.

Ye, Q.; and Wiegert, P. A.: "Will comet 209P/LINEAR generate the next meteor storm?," Monthly Notices of the Royal Astronomical Society, Vol. 437, No. 4, pp. 3283–3287, 2014.

4. SPACECRAFT EFFECTS

Spacecraft engineers sometimes ask, "If the meteoroid flux is so high, why aren't spacecraft experiencing impacts?" The answer to this question is that spacecraft are indeed hit by meteoroids, and, as you will read in this chapter, many spacecraft anomalies have been attributed to or associated with meteoroids. Besides these known cases, there are likely many more cases in which meteoroids caused anomalies but did not leave a "smoking gun." Finally, there may be additional cases in which a meteoroid was known to have caused an anomaly, but the investigation team did not publish their findings. These scenarios can give the false impression that meteoroid strikes are rare or nonexistent.

Another common misconception is that meteoroids strike spacecraft only during or primarily during meteor showers. At least two guide documents imply that meteoroid risk is confined to meteor showers (Bedingfield et al. 1996; National Research Council 2011). However, the opposite is true: sporadic meteoroids, which can strike spacecraft at any time of year, produce at least 90% of meteoroid strikes (Moorhead et al. 2017). Sporadic meteoroids tend to dominate even during meteor showers; therefore, anomalies that occur during a meteor shower are often not associated with that shower. A study of spacecraft anomaly patterns found that the timing of these anomalies was more closely correlated with the sporadic meteoroid flux than it was with meteor showers (Goel and Close 2015). The annual forecast issued by the MEO provides spacecraft operators with shower-to-sporadic meteoroid flux ratios for several limiting kinetic energies (Moorhead et al. 2017); these flux ratios can be used to estimate the probability that a meteoroid anomaly is associated with an active shower. Additional information, when available, can be used to refine these assessments. For instance, one can determine whether the shower radiant was visible from the spacecraft at the time of the impact. If velocity information is available, this quantity can also be used as a determinant, as meteor showers intercept the Earth or spacecraft at a single speed.

Finally, a third misconception about the meteoroid environment is that it is negligible compared to the human-made orbital debris environment throughout near-Earth space. In fact, the damage-limited meteoroid flux exceeds that of orbital debris at most altitudes (Cooke et al. 2017). Meteoroid impacts can rival debris impacts even in low Earth orbit; some International Space Station surfaces see equal numbers of meteoroid and debris impacts (Hyde et al. 2017). Spacecraft in Sun-synchronous orbits are at more risk from orbital debris than from meteoroids, but those in geosynchronous orbits are in far more danger from meteoroids. The orbital debris environment is a strong function of altitude; thus, altitude plays an important role in determining the primary cause of impacts in Earth orbit (NASA 2008).

4.1 Types of Meteoroid-Induced Anomalies

Meteoroids can physically damage or puncture spacecraft; as a result, programs often calculate the "probability of no penetration" (PNP) for pressure tanks or habitats. However, meteoroids can induce other types of anomalies, such as attitude changes and electrical disturbances, and can

damage external surfaces such as thermal protection systems. All of these anomalies can potentially contribute to the risk of losing or reducing the functionality of a spacecraft. In this section, we describe these anomaly types further and give examples of real anomalies that fit into each category.

4.1.1 Physical Damage

Meteoroids can produce craters on external vehicle surfaces, degrade the optics of instruments, and produce pits and fractures on spacecraft windows that force a replacement (Hyde et al. 2009; see figure 22). The risk of damage can prompt the use of thicker materials or the attachment of shields; the International Space Station, for instance, has made use of over 100 different debris shields (National Research Council 1997). There have also been instances where meteoroids have damaged the CCD chips of cameras when a path is available between the mirror and the imaging array (such as in XMM-Newton). In these cases, meteoroid impacts must be considered when choosing the positions of the mirror and focal plane (Carpenter et al. 2006).

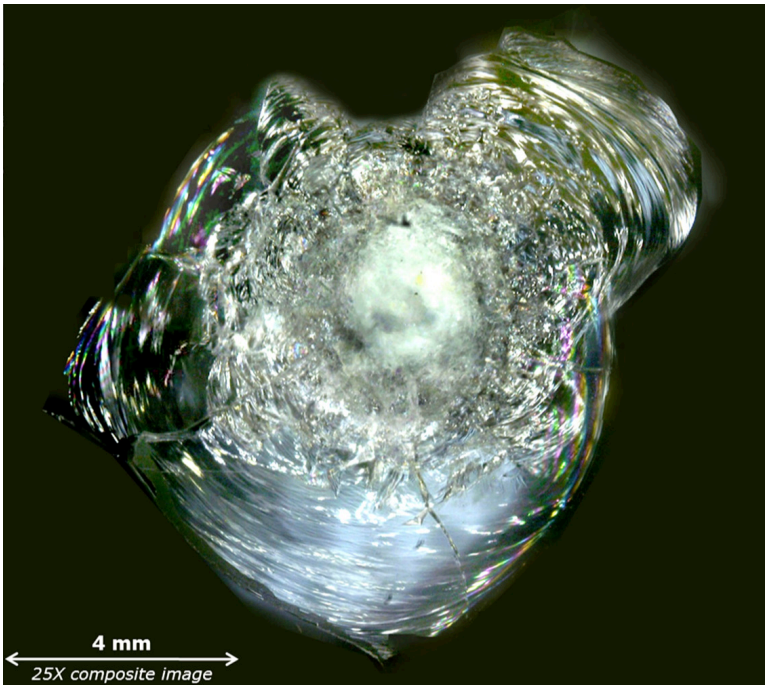

Figure 22. Meteoroid impact on window 6 of Endeavor, incurred during Space Shuttle mission STS-126 (Hyde et al. 2009). The crater was produced by a magnesium-rich meteoroid and has a depth of 0.68 mm. Image courtesy of the NASA/JSC Hypervelocity Impact Technology (HVIT) Team.

Larger (and faster and denser) meteoroids cause more extensive damage (Hayashida & Robinson 1991), but smaller meteoroids are much more common. Therefore, spacecraft programs should consider the smallest impact crater that could cause a failure. This often corresponds to the severing of a thin component such as an exposed wire, experiment or gravity gradient boom, or spacecraft tether. A particle as small as 100 μm in diameter can pose a threat to external wiring.

Thin but critical components can be protected by additional shielding; for instance, doublers were added to protect Shuttle radiator tubes (Scott et al. 2009), and a multi-layer insulation covering was considered as a protection mechanism for wire bundles on the Joint Polar Satellite System (Williamsen and Evans 2015; Squire et al. 2015).

In manned space programs, there is an appropriate emphasis on the safety of crew members when participating in extravehicular activities (EVAs). A spacesuit can be penetrated by a particle as small as 0.4 mm. This will produce a hole larger than 1 mm in diameter, which is big enough to cause a fatal loss of life support before the astronaut can reenter the vehicle and repressurize. At such a small size, the meteoroid risk is usually equal to, if not greater than, that of orbital debris. Experience acquired during the International Space Station program has also shown that handholds and other exposed surfaces can be damaged by meteoroid and debris impacts, creating sharp edges capable of ripping astronaut gloves (Christiansen and Lear 2013; see figure 23). Manned missions also have to assess the risk of meteoroid damage to thermal protection systems (TPS) critical during reentry. This includes the heat shield as well as the TPS on the rest of the vehicle, which also sees extremely high temperatures, especially on those vehicles returning from deep space missions with high velocity entry speeds.

Figure 23. Damage on an EVA glove caused by pitting of an International Space Station handrail by meteoroids or orbital debris. This damage was photographed after EVA #3 of STS-118. Image taken from figure 4 of Christiansen and Lear (2013).

In all scenarios, the extent of the damage caused by a meteoroid impact will generally depend on the meteoroid's mass or size, density, impact speed, and impact angle. The damage will also depend on the properties of the material being hit; so-called ballistic limit equations (BLEs) can help engineers calculate the depth or width of meteoroid impact craters. We refer readers to Hayashida and Robinson (1991) for examples of BLEs corresponding to single-wall penetrations.

In many cases, BLEs are nearly proportional to the kinetic energy of the meteoroid; for this reason, the MEO reports annual shower and sporadic fluxes to constant limiting kinetic energy (Moorhead et al. 2017).

4.1.2 Momentum Transfer

Adequate shielding or component redundancies can reduce the probability of a spacecraft failing due to physical damage. However, even when no critical damage occurs, meteoroid strikes can transfer momentum to the spacecraft. Meteoroids generally do not produce significant shifts in position, but a strike offset from the spacecraft's center of mass can impart a torque and cause a change in attitude. These torques can occasionally be large enough to disrupt science operations or exceed preprogrammed tolerances, throwing the vehicle into safe mode. If the torque is extremely large, the vehicle may not be able to recover. Thus, it is possible to lose a spacecraft to a meteoroid strike through means other than physical damage.

Smaller meteoroid strikes can cause minor disruptions in operations. In a recent example, a camera on the Lunar Reconnaissance Orbiter (LRO) was struck by a small meteoroid. The left Narrow Angle Camera, which scans the surface of the Moon one row of pixels at a time, showed a sudden disruption in one image. The oscillations in the image reflect the shaking of the camera induced by a meteoroid hit on its radiator and are apparent in figure 24. Thus, even when the spacecraft can recover from a meteoroid-induced attitude change, operations can be disrupted. Repeated attitude corrections can deplete fuel and shorten the spacecraft's lifetime. Such disruptions should be taken into account when calculating the lifetime of a mission.

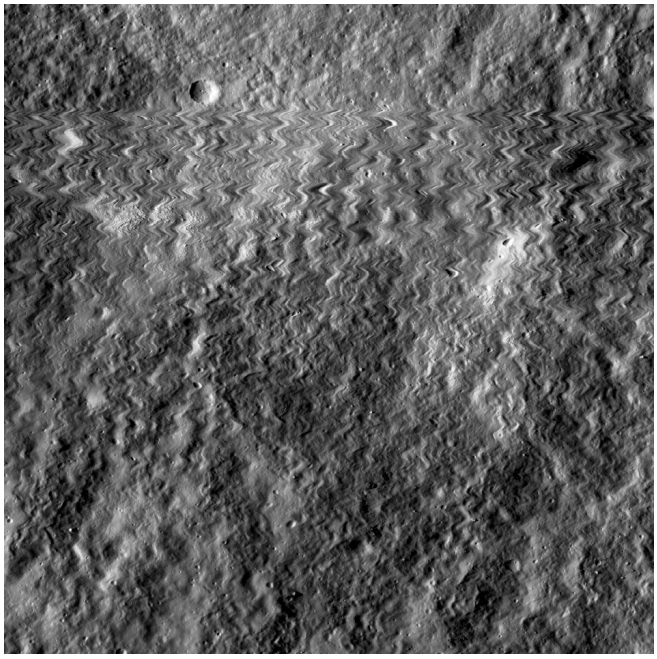

Figure 24. A visual scan of the Moon's surface by a Narrow Angle Camera on board LRO. A disruption is visible about one-sixth of the way from the top of the image—this disruption was caused by a meteoroid strike on the camera (NASA 2017). Image credit: NASA GSFC/Arizona State University.

The angular momentum imparted by a meteoroid depends on its mass, velocity, and location and angle of the strike. Attitude disturbances can also arise due to non-meteoroid causes, such as unexpected spacecraft behavior. In order to diagnose meteoroids as the cause of a disturbance, one must rule out other possible causes. In some cases, secondary effects can be used to identify the perturber as a meteoroid. For instance, the Gaia spacecraft has experienced large numbers of unexpected attitude disturbances (Gater 2014). It was later found that a fraction of these could be confirmed as meteoroids through local heating of the spacecraft structure (The Gaia Flight Control Team at the European Space Operations Center 2016).

4.1.3 Secondary Debris

When a meteoroid or orbital debris particle impacts the surface of a spacecraft, it can generate a spray of secondary debris particles (see figure 25 for an example). These ejected particles can contribute to the orbital debris environment and can even re-impact their parent spacecraft, increasing the area of the spacecraft that is affected. In fact, a recent study of two ISS surfaces found that secondary impacts were a significant cause of small craters (Hyde et al. 2017).

In cases where the meteoroid does not penetrate the surface, material may still detach from the opposite side in a process known as "spalling." In general, penetration of only one-third to one-half of a material's thickness is required for spalling (Drolshagen 2008). If spall is generated near sensitive components, it may produce anomalies or failures.

Another secondary impact effect should be considered for lunar surface operations. Large meteoroids in the kg size range impacting the Moon can excavate regolith which can in turn travel for tens of km from the impact site. The March 17, 2013, impact observed by the MEO's lunar impact monitoring program generated a crater later imaged by LRO with evidence of ejecta as far as 30 km away (Robinson et al. 2015). Although impacts of this size are relatively rare, they are more likely during meteor showers and lunar surface operations should consider shower forecasts in their planning.

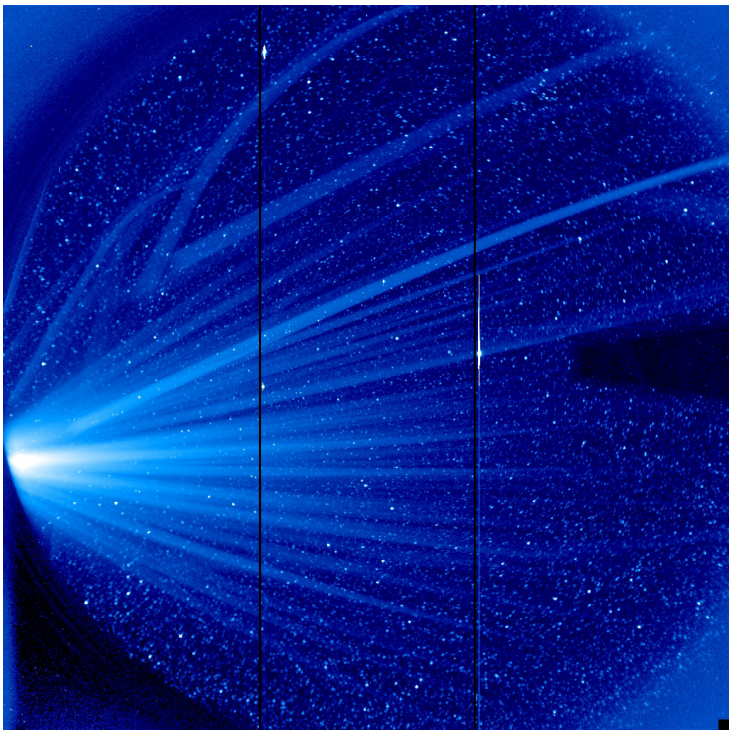

Figure 25. Secondary debris from a dust particle impacting the thermal blanket of the STEREO spacecraft. The impact occurred close to the SECCHI HI2 telescope, which was able to capture the event. Due to the long image exposure time (50 seconds), the secondary debris particles appear as long streaks rather than individual points. The impactor was estimated to be a micrometer in size and is thus too small to be considered hazardous, although even tiny impacts can degrade spacecraft surfaces over time (NASA 2018). Image credit: NASA GSFC.

4.1.4 Electrical disturbances

When a high-speed particle impacts the surface of a vehicle, it produces both an impact crater and plasma. The plasma is composed of material from the impacted surface and carries charge; in fact, the Galileo spacecraft's dust detector made use of this phenomenon to detect interplanetary dust particles (Grün et al. 2002).

The charge deposited by a meteoroid impact plasma can produce a brief pulse in current, particularly on exposed conductors such as solar array bus structures (McBride and McDonnell 1999). Alternatively, if a spacecraft has become differentially charged prior to impact, the plasma can trigger an electrostatic discharge that disturbs or damages on-board electronics (Landgraf et al. 2004). Hypervelocity gun tests conducted in the mid-1990s have shown that the magnitude of currents associated with an impact can be easily on the order of amperes (Crawford and Schultz 1993). McDonnell et al. (1994) proposed that a plasma-induced current resulting from a Perseid impact which created a conductive path between the solar array and sensitive hardware may have been responsible for the failure of the Olympus satellite in August 1993. Finally, Close et al. (2010) have

put forward the notion that high-speed meteoroid impacts can produce a localized electromagnetic pulse (EMP) capable of disrupting spacecraft attitude control electronics. Recent hypervelocity gun tests have demonstrated radio frequency (RF) production by an impact (Close et al. 2010); however, it is not certain that there is enough coherence for this to qualify as an EMP.

The total charge produced by a meteoroid impact plasma is proportional to $v^{3.5}$, where v is impactor speed (Dietzel et al. 1973; McBride and McDonnell 1999); in comparison, penetration depth is proportional to $v^{2/3}$. As a result, high-speed meteors will produce a disproportionate number of electrical disturbances. Showers like the Leonids (70 km/s) and Perseids (60 km/s) may therefore be more significant in terms of electrical disturbances than they are in terms of damage (McDonnell et al. 1994; McBride & McDonnell 1999).

While the high-speed meteoroid flux does not vary substantially with altitude, differential spacecraft charging is much more likely in certain locations. Spacecraft in geosynchronous orbit and those that pass through auroral latitudes can be particularly susceptible to charging (Davis & Duncan 1992). Programs managing such spacecraft should thus consider both the charging environment and variations in the high-speed meteoroid flux (any outbursts of high-speed showers are highlighted in the MEO's annual forecast).

4.1.5 Interaction with Other Environmental Hazards

As discussed in section 4.1.1, meteoroid impacts can directly damage spacecraft and cause anomalies. However, impacts may also interact with other environmental effects to produce other types of anomalies. Section 4.1.4 provides one such example of a "combination" effect, in which space plasmas produce differential spacecraft charging, and then the plasma generated by a meteoroid impact triggers a discharge of those charged surfaces.

Other examples can occur: for instance, coatings are used to protect solar panels from the erosion of their materials caused by atomic oxygen in low Earth orbit. To be effective, these coatings must be free of pinprick defects (Miller 2017). However, small meteoroid and orbital debris impacts can perforate an otherwise pristine coating, giving atomic oxygen access to vulnerable components.

4.2 Notable Meteoroid-Associated Anomalies

This section presents a few notable spacecraft anomalies that have either been attributed to or associated with meteoroids. In many cases, anomalies occur with no clear explanation and therefore it is impossible to know how many times meteoroid impacts have caused these anomalies. Nevertheless, the cases discussed here provide an idea of what effects meteoroid strikes can have and how their causes can be ascertained.

4.2.1 Mariner IV, 1967 (Physical Damage, Momentum Transfer)

Mariner IV was the first United States spacecraft to successfully visit Mars. Included amongst its instruments was an impact detector; this remains one of the few impact detectors sent

to Mars, despite the more than twenty successful subsequent missions to that planet. This impact detector—the Cosmic Dust Detector—consisted of a 22 cm by 22 cm square aluminum plate covered with a thin dielectric film and attached to an acoustical transducer (see figure 26). The transducer detected the vibrations caused by meteoroid strikes, while the film acted as a capacitor that would momentarily discharge when penetrated by a meteoroid impact.

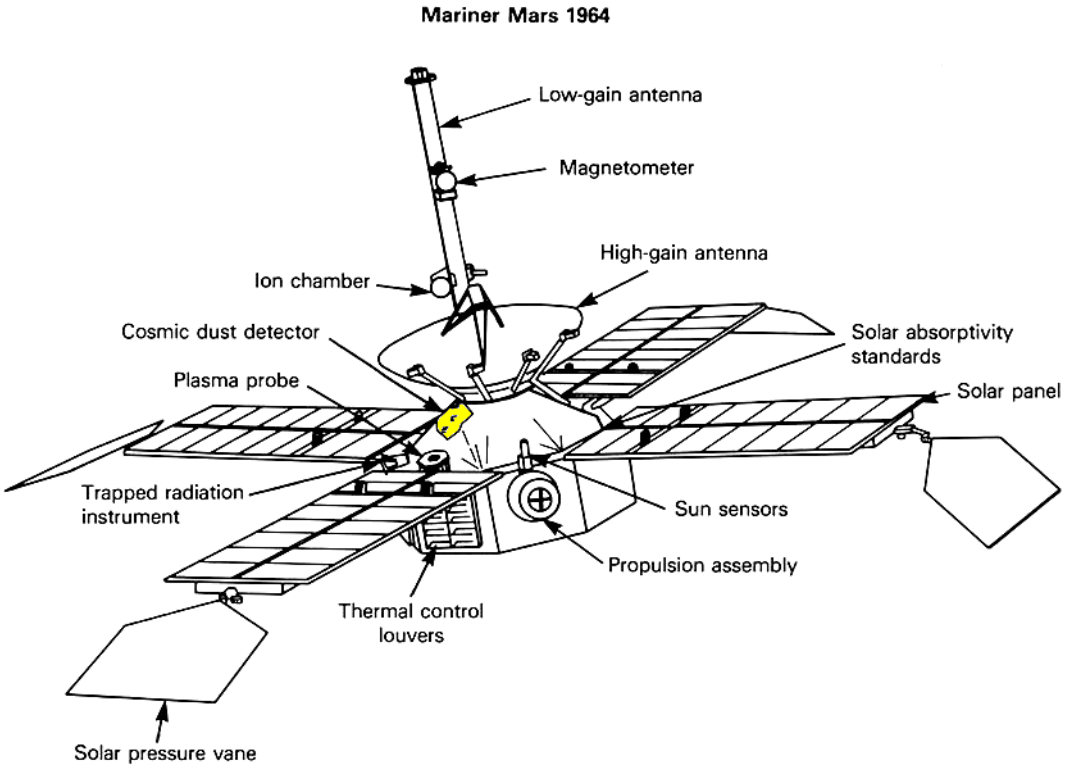

Figure 26. Diagram of the Mariner IV spacecraft. The Cosmic Dust Detector is highlighted in yellow and comprises a small portion of the spacecraft's total surface area.

The experiment registered the expected level of activity (i.e., occasional impacts) for almost three years. However, on September 14, 1967 (two years after Mariner's Mars encounter), the impact rate briefly jumped by a factor of 500-1500. The dust detector recorded 17 hits during either a 15-minute (Science and Technology Division 1968) or 45-minute (NASA 1971) time span; if this rate is extrapolated to include the entire spacecraft cross-section, the spacecraft was hit by thousands of particles. At the same time, the vehicle experienced a temporary change in attitude, and there was a 1° drop in the temperature of the spacecraft's interior. Fortunately, the spacecraft was operating normally again a week later (Science and Technology Division 1968).

Numerous attempts to identify the source of the meteoroid stream have failed. The 1960s investigators suggested particles from Comet Encke (NASA 1971), but modern calculations show that other comets are more likely. Paul Wiegert, an astronomer at the University of Western Ontario, has suggested "dark" comet D/1895 Q1 (Swift) as the most promising candidate (Phil-

lips 2006). The high impact rate experienced by Mariner IV has only one counterpart in spaceflight experience, which is that recorded by the Giotto spacecraft during its close approach to the nucleus of Comet Halley. This may indicate that Mariner unwittingly flew near a recently extinct comet nucleus. This should serve as a cautionary note for Mars-bound vehicles, because whatever its origin, it should be assumed that the meteoroid stream Mariner IV encountered still exists and remains a hazard.

4.2.2 ISEE-3, ca. 1978-1982 (Physical Damage)

The International Sun-Earth Explorer-3 (ISEE-3) spacecraft was the first to be placed in orbit around the Earth-Sun L1 Lagrangian point. While it initially studied the interaction between the solar wind and the Earth's magnetic field, it was renamed the International Cometary Explorer (ICE) and sent to visit comet Giacobini-Zinner in 1985.

The Lagrangian points are far removed from the near-Earth cloud of orbital debris and thus any impacting particles can be assumed to be meteoroids. Bloomquist and Graham (1983) reported that a window on a scientific instrument on board the spacecraft was punctured by a "micrometeorite" (this terminology is incorrect; only meteoroids can be found in space). The date of the anomaly was not specified. Bedingfield et al. (1996) added that the experiment in question was a low-energy cosmic ray experiment and that the impact caused a 25% data loss, although they identify the mission as ISEE-1, in seeming contradiction with Bloomquist and Graham (1983).

4.2.3 Solar A (Yohkoh)

Yohkoh ("Solar-A" prior to launch) was a Japanese Solar observatory spacecraft. Bedingfield et al. (1996) report that a small meteoroid punctured the membrane covering its optical system, resulting in the loss of the visual portion of the telescope (Yohkoh carried several telescopes and spectrometers). However, the mission continued operating until 2001.

4.2.4 Olympus 1, 1993 (Possible Electrical Anomaly)

The Olympus 1 technology demonstration satellite was an experimental European communications satellite launched in July 1989. It was larger than any other civilian communications satellite at that time but suffered a series of mishaps once in orbit. For example, less than two years after launch, in January 1991, the south solar array stopped tracking the Sun; it was thought that this may have been due to a mechanical blockage (Lenorovitz 1991). Four months later (May 29), there was an attitude control issue caused by a combination of problems with its RF sensors and the upload of recovery commands that were not yet fully validated (ibid). Control of the satellite was lost and the vehicle began to roll, rotating its solar array away from the Sun and entering a "deep freeze" (ibid). Nominally in a geostationary orbit (GEO), the out-of-control spacecraft drifted around the globe for 72 days before returning to its 19° W longitude slot and being recovered (Lenorovitz 1991; Caswell 1995). Two years later, during the Perseid meteor shower, Olympus 1 again went into an uncontrolled spin and could not be recovered; the last of the fuel was used to remove the spacecraft from geosynchronous orbit (Caswell 1995).

The 1993 Perseids were the most notable meteor shower outburst since the 1966 Leonids. The Perseid parent comet, 109P/Swift-Tuttle, was recovered in 1992 as it made its first pass through the Solar System in 130 years. Meteor shower forecasting techniques had not yet been developed, but many felt that this visit by the Perseid parent was cause for concern. Swift-Tuttle possesses the largest nucleus of any periodic comet and leaves a prodigious amount of material in its wake (Blaauw 2017). Historical data indicated that the Perseids could be exceptionally strong in the year following the comet's perihelion passage. Out of an abundance of caution, NASA delayed Discovery's launch in the STS-51 mission until after the meteor shower peak—the only time a Shuttle launch has been delayed due to a space environment concern (National Research Council 2011). The body and solar arrays of the Hubble Space Telescope were reoriented to minimize area exposed to the Perseid radiant during the peak (Beech et al. 1995), and The Solar Anomalous and Magnetospheric Particle Explorer (SAMPEX) closed the door to its Heavy Ion Large Telescope for a few hours during the peak of the Perseids (Bedingfield et al. 1996).

A strong outburst did occur on August 12, with ground observers reporting Perseid visual rates in excess of 250 per hour (Rendtel 1993). In space, the cosmonauts on board the Mir-1 Space Station allegedly reported hearing "pings" on the spacecraft exterior (reported by Beech et al. 1995, original source unknown) and cosmonauts discovered a 10-cm-diameter hole, as well as numerous smaller pits, in a solar panel on a later spacewalk (Lenorovitz 1993; Harland 2005). However, we note that this spacewalk did not occur until September 28, making it much more likely that it was caused by a sporadic meteoroid or piece of orbital debris. No other anomalies were reported, except for Olympus, whose roll gyro stops at 23:32 UTC on August 11 (about three hours before the peak of the shower). The spacecraft entered Emergency Sun Acquisition mode but failed to acquire the Sun. Attempts to recover the spacecraft exhausted the bulk of the remaining fuel, making it impossible to return the satellite to service. Late on August 12, the mission was terminated, and the spacecraft was moved into a disposal orbit 200 kilometers below GEO with the last of the fuel.

An exhaustive ESA investigation explored several possible causes of the failure. The timing of the failure during the Perseid outburst led the investigators to consider a meteoroid strike. Several factors pointed in favor of a Perseid strike (Caswell et al. 1995):

- Several parts of the spacecraft were exposed to the Perseid radiant. The south solar array in particular had 8.5 square meters exposed directly to the stream.
- A possible failure mechanism involved the conduction of charge from a meteoroid impact plasma to the gyro through the spacecraft umbilical.
- The probability of a Perseid impact was approximately equal to the probability of a sporadic impact. However, the probability of a Perseid-generated impact plasma was about five times more likely than a sporadic-generated impact plasma (Caswell et al. 1995).

Both McDonnell et al. (1994) and Caswell et al. (1995) noted, however, that the cause of the anomaly remains unknown and cannot be definitively linked to the Perseids.

It should be noted that during the next major Perseid outburst, on August 13, 2009, LandSat 5 suffered an unusual anomaly involving a temporary gyro failure which sent the spacecraft tumbling (Cooke 2009). Fortunately, normal operations were restored by August 17. This event enhanced the reputation of the Perseid shower as a potential threat to satellites, the risk not coming

from physical damage or penetration of a vital component but from electrical effects caused by the discharge and plasma produced by the very high-speed meteoroid impact.

4.2.5 Chandra, 2003 (Momentum Transfer)

Chandra is an operational NASA X-ray observatory launched on July 23, 1999. Its orbit has a perigee of approximately 16,000 km and an apogee near 133,000 km; at these altitudes, the risk posed by orbital debris is minimal and any particle impacts are overwhelmingly likely to be meteoroids (Cooke et al. 2017). Just before 4:00 UTC on November 15, 2003, the spacecraft experienced a sudden change in attitude of approximately 13 arcseconds (Bucher & Martin 2004).

Analyses performed by the program indicated that a disturbance torque of about 0.27 foot-pounds would be needed to change the vehicle attitude by the observed amount, and based on the fact that the impact occurred during the annual Leonid meteor shower, attributed the cause to the impact of a 1-mm-diameter Leonid (WKT 2004). However, subsequent analysis by other researchers showed that an impact by a north apex sporadic meteoroid was five times more likely than a Leonid impact, given that the event occurred a few days after the shower peak (Cooke, personal communication). The Leonid radiant is embedded in the north apex source, and north apex meteoroids have high speeds (average of 55 km/s), so the impact of such a particle would be difficult to distinguish from that of a Leonid. Consequently, the higher flux of the north apex favors a sporadic meteoroid hit as the cause of this anomaly.

4.2.6 GOES 13, 2013 (Momentum Transfer)

On May 22, 2013, during a tornado outbreak across the midwestern United States, the GOES-13 weather satellite experienced a sudden attitude displacement, resulting in a drift of 2° per hour from the nadir direction. This exceeded the allowed tolerances for the vehicle, which entered safe mode. Normal operations were restored seven days later, but NOAA had to switch to a backup GOES spacecraft to provide weather coverage during this interval (Leone 2013).

Analysis of the shift in the direction of the GOES camera field of view (McKnight and Mahmot, personal communication) suggests a strike by a helion sporadic meteoroid as the most likely explanation for the sudden torque on the spacecraft. The helion and antihelion sources dominate the sporadic complex and therefore are expected to be the leading cause of both impact and momentum-transfer meteoroid anomalies. It was hypothesized that the meteoroid struck the arm of the spacecraft (Smith 2013); long, protruding elements would increase the torque imparted by a strike.

4.3 Risk Evaluation and Mitigation

When conducting risk assessments, each mission will need to consider their dominant meteoroid-induced failure modes. As an example, it is critical to avoid punctures of the International Space Station to protect its human inhabitants and their air and water. Thus, the ISS uses meteoroid and debris models to ensure that the PNP is sufficiently high. Other manned missions may factor meteoroid anomalies into calculations of the probability of a loss of the mission (LOM)

such as an abort or the loss of crew (LOC). Unmanned spacecraft that must maintain precise attitudes may instead focus on managing meteoroid momentum transfers; the astrometry space observatory Gaia conducted such an analysis before launch (Risquez et al. 2012). Finally, while the risk of meteoroid-induced electrostatic discharges should be considered, the quantification of this risk is hampered by our lack of knowledge of the threshold for such events. Following standard design practices to mitigate spacecraft charging will minimize effects from meteoroid-induced plasmas as well as the usual charging environments. See NASA-HDBK-4002A for general guidelines.

4.3.1 Evaluation of Risk

In general, for a vehicle in low Earth orbit, the sporadic environment accounts for the bulk of the risk. For example, if we consider only meteoroids that carry a kinetic energy of at least 800 J (this is the kinetic energy of a 1 mm-diameter meteoroid traveling at 20 km/s, and is roughly equivalent to the energy of a medium-to-high-power pistol), sporadics constitute 98% of the meteoroid flux when averaged over long periods. For this reason, the MEO encourages missions to use a model like MEM, which models the sporadic complex, when designing a vehicle.

Table 4 lists flux percentages for a selection of limiting kinetic energies, which we quote to give readers a rough idea of the relative importance of shower meteoroids. However, while the damage produced by a meteoroid impact is close to being kinetic energy limited, in practice it depends on properties of the spacecraft surface in question. Depending on how a material's ballistic limit equations in turn depend on the mass and speed of the impactor, the relative importance of showers can be greater or less than listed in table 4.

Table 4. Particle diameter (first column) that corresponds to each listed kinetic energy (second column), assuming a density of 1 g/cc and a speed of 20 km/s. The third column lists a weapon or hazard that has a similar energy, while the fourth column lists the type of damage that may result from impact onto a spacecraft (Cooke 2009). The fifth column lists the percentage of the flux constituted by meteor showers.

Diameter	Energy	Destructive Equivalent	Expected Damage	Shower Fraction (%)
0.4 mm	54 J	Air gun	Wires severed, ESD, radiator or suit damage	1
1 mm	840 J	Pistol	Attitude disturbance, penetration of weaker materials	2
3 mm	23 kJ	Rifle	Significant material damage, possible TPS failure	4
1 cm	840 kJ	A vehicle at highway speeds	Catastrophic damage	15
2.7 cm	16 MJ	Armor-piercing rounds	Catastrophic damage	50

The total, long-term risk posed by meteoroid impacts is best evaluated through a BUMPER (Hyde et al. 2017a) analysis using the appropriate meteoroid environment model and the spacecraft's geometry (see figure 27); any high-cost, high-risk mission should perform such a risk analysis. It is important to note that BUMPER only produces PNP figures for specific components, such as fuel tanks, pressure walls, etc., and ignores potential electrical anomalies and momentum transfer.

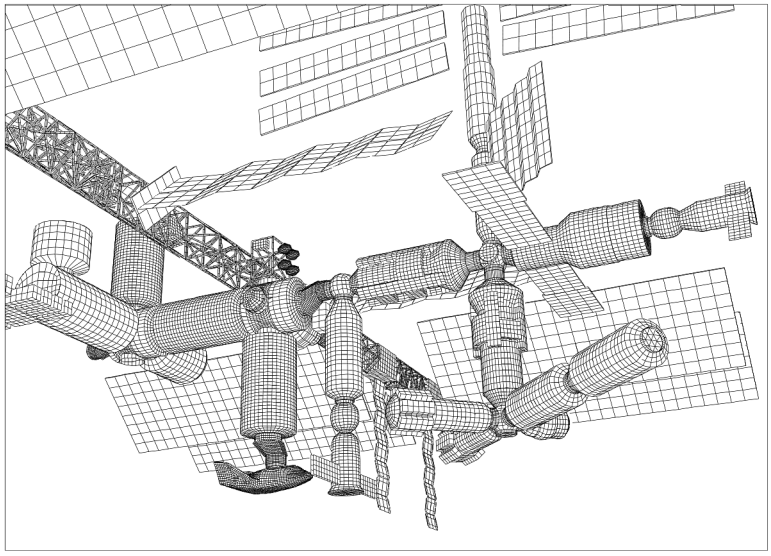

Figure 27. Finite element model of the International Space Station used for BUMPER meteoroid and orbital debris analysis (National Research Council 1997). Note that in many cases, a component may block a portion of the meteoroid environment from reaching another element of the spacecraft.

All NASA missions must submit an Orbital Debris Assessment Report (ODAR; see NASA Procedural Requirement 8715.6B or recent equivalent [NASA n.d.]). The software used in producing this report, DAS, contains a meteoroid model suitable for the evaluation of the vehicle's compliance with the NASA debris mitigation guidelines and US Government standard practices for limiting orbital debris. However, DAS is not and was not intended to be a design tool. That is the role of BUMPER and equivalent programs at other space agencies and commercial entities (such as ESABASE2 n.d.).

The risk posed by meteor showers can be assessed by combining an existing sporadic meteoroid risk assessment with the MEO's annual meteor shower forecast. These forecasts present each year's predictions for meteor shower activity, including any unusual activity such as storms or outbursts. The forecast includes so-called "enhancement factors" that roughly quantify the increase in risk due to meteor showers on a spacecraft element that is directly facing the shower radiant. These enhancement factors are for a worst-case orientation and do not take the spacecraft's geometry into account. Therefore, if the inclusion of shower activity places the risk above an acceptable level, an additional custom analysis is needed to determine the true risk level.

4.3.2 Mitigation

The sporadic meteoroid environment must be mitigated through proper design. A common way to protect a spacecraft against impacts is through the use of shields. The "Whipple shield," a simple sheet of metal that is offset from the surface of the spacecraft, is particularly effective against meteoroids. Due to the high speeds involved, a meteoroid impacting a sheet with a thickness comparable to its own diameter will tend to vaporize before striking the spacecraft itself

(Whipple 1947). The impact will also vaporize a portion of the shield, but generally the degradation of the shield due to impacts over the lifetime of a spacecraft is minimal. The simple, single-layer Whipple shield, while effective for meteoroids, can be less effective for lower-velocity orbital debris impacts (Christiansen et al. 1995). There are many variations of the Whipple shield that use different materials (such as mesh, Nextel, aluminum, or Kevlar) and multiple layers. The International Space Station uses a stuffed Whipple shield consisting of an outer sheet of aluminum and 12 intermediate layers of Nextel or Kevlar (National Research Council 1997).

Another means of mitigating the risk of impacts through design is to include redundancies. As mentioned in section 4.2.1, thin components such as wires can be easily severed by small impacts. However, as long as the risk of severing a particular wire is unlikely, then making that wire fully redundant will cause the risk of failure to be very unlikely.

In contrast, meteor shower outbursts and storms are typically mitigated through operational means rather than by spacecraft design. These are naturally vehicle-dependent, but common measures include orienting solar arrays so they are edge-on to the shower radiant, shutting down high-voltage components in the case of outbursts of fast meteor showers like the Leonids and Perseids, turning a less vulnerable side of the vehicle towards the shower radiant to protect sensitive surfaces such as telescope mirrors (for example, the Hubble Space Telescope during the 1993 Perseids; Beech et al. 1995), and delaying launches (National Research Council 2011) or space walks until after the outburst.

One recent scenario in which the meteoroid risk was temporarily elevated was the fly-by of Mars by Comet C/2013 A1 (Siding Spring). The comet missed Mars by about 140,000 km; for comparison, the distance between the Earth and the Moon is 384,000 km. Since cometary comae can exceed 100,000 km in radius, this potentially put Mars and its human-made satellites in the path of a massive meteoroid onslaught. Later observations revealed that the coma would miss Mars, but some of the orbiters fired thrusters to phase their orbits such that they would be shielded from the coma by the planet during the time of the fly-by. Mars Express also considered reorienting the spacecraft during the close encounter as a contingency plan (Scuka 2014).

In some cases, missions may determine that the meteoroid impact risk is within acceptable levels and take no mitigation measures. The *New Horizons* mission provides us with such a case study. Between the spacecraft's 2006 launch and its 2015 flyby of the Kuiper belt object Pluto, two additional moons were discovered around Pluto. Impacts onto these moons could potentially generate rings of debris near Pluto, raising concerns that *New Horizons* might encounter a harsher meteoroid environment than planned for. However, the spacecraft's trajectory was originally chosen to pass through a point where particle orbits would not be stable, and additional analyses estimated that the impact risk was acceptable. Although alternative trajectories were designed, in the end the mission opted to maintain their nominal trajectory (Johns Hopkins University APL New Horizons Mission 2013).

Spacecraft programs are encouraged to give some thought to a threshold or thresholds that will trigger mitigation activity during a meteor outburst. This threshold should be high enough that it is not set in motion by an annual shower such as the Geminids, but at a level commensurate with protecting the vehicle during a time of unusually elevated risk. Again, the risk posed by meteor

showers or even meteor storms is low for a specific vehicle, but, when integrated over the entire set of active satellites, it can be quite significant. Luck is very much a factor, as one cannot determine which satellite may be struck, and prudence dictates that programs should be prepared in case they are unfortunate like Olympus in 1993.

Finally, one may take a hybrid approach to risk mitigation that involves both designing to the meteoroid environment and reducing risk operationally. The inspection and replacement of parts can fall into this category: the original parts must be designed to withstand meteoroid bombardment for some minimum period, after which they can be examined for impacts and, if necessary, replaced. Shuttle windows, for example, needed to last through a mission but would be replaced before the next mission if they incurred a large impact. The shuttle program replaced at least 46 windshields for this reason before the end of 1994 (Bedingfield et al. 1996).

4.4 References

Bedingfield, K.L.; Leach, R.D.; and Alexander, M.B.: "Spacecraft System Failures and Anomalies Attributed to the Natural Space Environment," TR-NASA-RP-1390, NASA Marshall Space Flight Center, Huntsville, AL, 1996.

Beech, M.; Brown, P.: and Jones, J.: "The Potential danger to Space Platforms from Meteor Storm Activity," *Quarterly Journal of the Royal Astronomical Society*, Vol. 36, pp. 127–152, 1995.

Blaauw, R.C.: "The Mass Index and Mass of the Geminid Meteoroid Stream as Determined with Radar, Optical and Lunar Impact Data," *Planetary and Space Science*, Vol. 143, No. 1, pp. 83–88, 2017.

Bloomquist, C.; and Graham, W.: "Analysis of Spacecraft On–orbit Anomalies and Lifetimes," TR-NASA-CR-170565, NASA Goddard Space Flight Center, Greenbelt, MD, 1983.

Bucher, S.; and Martin, E.: "Chandra Flight Note 439: 2003:319 Attitude Disturbance," Astrophysics Data System (ADS), 2004.

Abbey, A.F.; Ambrosi, R.M.; and Wells, A.: "Effects of Micrometeoroid and Space Debris Impacts in Grazing Incidence Telescopes," *Space Telescopes and Instrumentation II: Ultraviolet to Gamma Ray*, Vol. 6266, SPIE Astronomical Telescopes + Instrumentation, Orlando, FL, 2006.

Caswell, R.D.; McBride, N.; and Taylor, A.: "OLYMPUS End of Life Anomaly – a Perseid Impact Event?" *International Journal of Impact Engineering*, Vol. 17, pp. 139–150, 1995.

Christiansen, E.L.; Crews, J.L.; Kerr, J.H.; et al.: "Testing the Validity of Cadmium Scaling," *International Journal of Impact Engineering*, Vol. 17, pp. 205–215, 1995.

Christiansen, E.L.: "Meteoroid/Debris Shielding," NASA-TP-2003-210788, NASA Johnson Space Center, Houston, TX, 2003.

Christiansen, E.L.; and Lear, D.M.: "Solving Problems Caused by Small Micrometeoroid and Orbital Debris Impacts for Space-walking astronauts," JSC-CN-30442.

Close, S.; Colestock, P.; Cox, L.; et al.; "Electromagnetic Pulses Generated by Meteoroid Impacts on Spacecraft," *Journal of Geophysical Research: Space Physics*, Vol. 115, No. A12, pp. A12328, 2010.

Cooke, W.J.: "The 2009 Perseid meteoroid environment and Landsat 5," NASA MEO Internal Report, NASA Marshall Space Flight Center, Huntsville, AL, 2009.

Cooke, W.; Matney, M.; Moorhead, A.V.; and Vavrin, A.: "A Comparison of Damaging Meteoroid and Orbital Debris Fluxes in Earth Orbit," in Proceedings of the 7th European Conference on Space Debris, 2017.

Davis, V.A.; and Duncan, L.W.: Spacecraft Surface Charging Handbook, PL-TR-92-2232, Maxwell Laboratories, Inc., La Jolla, CA, 1992.

Dietzel, H.; Eichhorn, G.; Fechtig, H.; et al.: "The HEOS and HELIOS Micrometeoroid Experiments," *Journal of Physics E Scientific Instruments*, Vol. 6, pp. 209–217, 1973.

Drolshagen, G.: "Impact Effects from Small Size Meteoroids and Space Debris," *Advances in Space Research*, Vol. 41, No. 7, pp. 1123–1131, 2008.

ESABASE2: "Welcome to the ESABASE2 Homepage," < https://esabase2.net/>, n.d.

Gaia Flight Control Team: "Meteoroid Impact Detection by the Gaia Spacecraft at L2," Presented at the European Space Operations Center, Germany, 2016.

Gater, W.: "Galaxy Mapper's First Discovery: Surprise Space Debris," <https://www.newscientist.com/article/dn25925-galaxy-mappers-first-discovery-surprise-space-debris/>, 2014.

Goel, A.; and Close, S.: "Electrical Anomalies on Spacecraft Due to Hypervelocity Impacts," in 2015 IEEE Aerospace Conference, Big Sky, MT, 2015.

Grün, E.; Brown, P.G.; Graps, A.L.; et al.: "Dust Astronomy: New Venues in Interplanetary and Interstellar Dust Research," in *ASP Conference Series: The Future of Solar System Exploration*, 2003–2013, M.V. Sykes (ed.), Vol. 272, Astronomical Society of the Pacific, pp. 283–296, 2002.

Harland, D.M.; and Lorenz, R.D.: *The Story of Space Station Mir*, Springer Praxis Books, 2005.

Hayashida, K.B.; and Robinson, J.H.: "Single Wall Penetration Equations," NASA-TM-103565, NASA Marshall Space Flight Center, Huntsville, AL, 1991.

Hyde, J. L., Lear, D. M., and Christiansen, E. L. (2009). STS-126 OV-105 Flight 22 Post Flight MMOD Inspection Results. JSC-64921.

Hyde, J.; Bjorkman, M.; Christiansen, E.; and Lear, D.: "Micrometeoroid and Orbital Debris Risk Assessment with Bumper 3," in *Proc. 7th European Conference on Space Debris,* Darmstadt, Germany, JSC-CN-38422, NASA Johnson Space Center, Houston, TX, 2017.

Hyde, J.; Christiansen, E.; Lear, D.; and Nagy, N.: "Surveys of ISS Returned Hardware for MMOD Impacts," in *Proceedings of the 7th European Conference on Space Debris*, Darmstadt, Germany, JSC-CN-39201, NASA Johnson Space Center, 2017.

Johns Hopkins University APL New Horizons Mission: "New Horizons Team Sticking to Original Flight Plan at Pluto," < http://spaceref.com/news/viewsr.html?pid=44206>, June 14, 2013.

Landgraf, M.; Jehn, R.; Flury, W.; and Dikarev, V.: "Hazards by Meteoroid Impacts onto Operational Spacecraft," *Advances in Space Research*, Vol. 33, No. 9, pp. 1507–1510, 2004.

Lenorovitz, J.M.: "Emergency Recovery Effort Bringing Olympus 1 Satellite Under Control," *Aviation Week & Space Technology*, Vol. 135, No. 4, pp. 60–61, 1991.

Lenorovitz, J.M.: "Russia May Hold Space Station Key," A*viation Week & Space Technology*, Vol. 139, pp. 22–24, 1993.

Leone, D.: "GOES – 13 Back in Action after Meteoroid Strike," <http://spacenews.com/35715goes-13-back-in-action-after-meteoroid-strike/>, June 10, 2013.

McBride, N.; and McDonnell, J.A.M.: "Meteoroid Impacts on Spacecraft: Sporadics, Streams, and the 1999 Leonids," *Planetary and Space Science*, Vol. 47, No. 8, pp. 1005–1013, 1999.

McDonnell, J.A.M.; McBride, N.; Green, S.F.; et al.: "The Olympus Satellite Anomaly: Hypervelocity Impact Effects and Meteoroid Collision Assessment," Contract study report to ESA and British Aerospace.

Miller, S.: "Tutorial: Atomic Oxygen Effects and Contamination," in Presentation at the Applied Space Environments Conference (ASEC) 2017, NASA Glenn Research Center, Cleveland, OH, 2017.

Moorhead, A.V.; Cooke, W.J.; and Campbell-Brown, M.D.: "Meteor Shower Forecasting for Spacecraft Operations," in *Proceedings of the 7th European Conference on Space Debris*, Dermstandt, Germany, NASA Marshall Space Flight Center, Huntsville, AL, 2017.

NASA: "Camera on NASA's Lunar Orbiter Survived 2014 Meteoroid Hit," <https://www.nasa.gov/feature/goddard/2017/camera-on-nasas-lunar-orbiter-survived-2014-meteoroid-hit>, 2017.

NASA: Handbook for Limiting Orbital Debris, NASA-HDBK-8719.14, 2008.

NASA: "Mariner-Venus 1967," NASA-SP-190, NASA Headquarters, Washington, D.C., 1971.

NASA: “Micrometer Impact on STEREO Spacecraft,” <https://stereo.gsfc.nasa.gov/gallery/item.php?id=selects&iid=202>, 2018.

NASA: Mitigating In-Space Charging Effects – A Guideline, NASA-HDBK-4002A, 2011.

NASA: “Welcome to the NODIS Library,” <https://nodis3.gsfc.nasa.gov>, n.d.

National Research Council: *Limiting Future Collision Risk to Spacecraft: an Assessment of NASA’s Meteoroid and Orbital Debris Programs*, The National Academies Press, Washington, D.C., 2011, doi:https://doi.org/10.17226/13244.

National Research Council: *Protecting the Space Station from Meteoroids and Orbital Debris*, The National Academies Press, Washington, D.C., doi:https://doi.org/10.17226/5532.

Phillips, T.: “Mariner Meteor Mystery, Solved?” <https://science.nasa.gov/science-news/science-at-nasa/2006/23aug_mariner4>, 2006.

Rendtel, J.: “Perseids 1993: A First Analysis of Global Data,” *WGN, the Journal of the IMO*, Vol. 21, No. 5, pp. 235–239, 1993.

Risquez, D.; Van Leeuwen, F.; and Brown, A.G.A.: “Dynamical Attitude Model for Gaia,” *Experimental Astronomy*, Vol. 34, No. 3, pp. 669–703, 2013.

Robinson, M.S.; Boyd, A.K.; Denevi, B.W.; et al.: “New Crater on the Moon and a Swarm of Secondaries,” *Icarus*, Vol. 252, pp. 229–235, 2015.

Science and Technology Division, Library of Congress: Astronautics and Aeronautics, 1967: *Chronology on Science, Technology, and Policy*, 1968.

Scott, S. S., Fisher, M., Evans, H., Schonberg, W., Compton, L, Williamsen, J., Peterson, G., and Pandya, S. A. (2009). Independent technical inspection of the BUMPER II micrometeoroid and orbital debris risk assessment. NASA-TM-2009-215731.

Scuka, D.: “One Plan Becomes Two Plans,” <http://blogs.esa.int/mex/2014/09/10/one-plan-becomes-two-plans>, September 10, 2014.

Smith, M.: “Micrometeoroid Collision to Blame for GOES-13 Anomaly,” <https://spacepolicyonline.com/news/micrometeoroid-collision-to-blame-for-goes-13-anomaly/>, June 10, 2013.

Squire, M.D.; Cooke, W.J.; Williamsen, J.; et al.: “Joint Polar Satellite System (JPSS) Micrometeoroid and Orbital Debris (MMOD) Assessment,” NASA-TM-2015-218780, NASA Langley Research Center, Hampton, VA, 2015.

Whipple, F.L.: “Meteorites and Space Travel,” Astronomical Journal, Vol. 52, p. 131, 1947.

Williamsen, J.E.; and Evans, S.E.: “Orbital Debris Wire Harness Failure Assessment for the Joint Polar Satellite System,” *Procedia Engineering*, Vol. 103, pp. 650–656, 2015.

WKT: “Chandra Experiences a Bump in the Night,” <https://chandra.cfa.harvard.edu/ chronicle/0104/leonidhit/>, 2004.

5. EFFECTS ON THE GROUND

Small meteoroids pose a far greater threat to vehicles and astronauts in space than they do to people on the Earth's surface, as the Earth's atmosphere tends to destroy meteoroids through ablation and fragmentation. A few meteoroids survive atmospheric entry and become meteorites, which hit the ground but generally with drastically reduced speeds. Occasionally, very large meteoroids or small asteroids can produce airbursts, shock waves, and even craters.

This section discusses the variety of effects that meteoroids and asteroids produce on or close to the ground. We discuss the frequency at which meteorite falls occur and present notable meteoroid or asteroid impact events in recent history. Our discussion focuses primarily on effects seen at Earth, but we also briefly discuss meteoroid effects on the Moon and Mars.

5.1 Types of Effects

Particles ranging in size from tiny dust grains to asteroids impact the Earth's atmosphere. All of these particles impact the Earth at very high speeds; at a minimum, their relative speed is about 11 km s^{-1} (or about 25,000 mi per hour) at an altitude of 100 km. However, the effects produced by a micron-sized dust particle are different from those produced by a mm-sized meteoroid, which are in turn drastically different from those produced by a 100-m asteroid. This section describes these effects, starting with those caused by the smallest particles and working up to those caused by the rare asteroid impact. Although neither dust particles nor asteroids are meteoroids, we include some discussion of the effects produced by these objects.

5.1.1 Accumulation of Dust Particles

Smaller particles are more easily decelerated by the atmosphere—interplanetary dust particles (IDPs; see chapter 2) typically slow down rapidly instead of "burning up" and producing a visible meteor. In general, particles smaller than 10^{-12} g do not produce meteors, although the exact limit depends on speed and density (Ceplecha et al. 1998). These cosmic dust particles then drift downward through the atmosphere and collect on the Earth's surface. Cosmic dust particles have been captured in the stratosphere (Zolensky & Warren 1994) and on the ground; particles have been recovered from roof gutters in European cities (New Scientist Staff and Press Association 2016), as well as in Antarctica.

5.1.2 Meteors

Particles larger than 10^{-12} g generally have too much momentum to be slowed to sub-ablation speeds by the upper atmosphere. Instead, they plow into lower layers of the atmosphere at high speeds, heating up and creating the visible light phenomenon known as a meteor (see chapter 2). At the low end of this range, the resulting meteors are extremely faint and may only be detected using radars or telescopes. Larger meteoroids (those weighing closer to 10^{-3} g)

produce brighter meteors that can be seen by the naked eye. At about 20 cm in diameter, meteoroids create fireballs and superbolides whose visually impressive displays and occasional sonic booms can attract the attention of the public. These large events terminate in one of several ways: (1) the object may ablate away entirely in the atmosphere, (2) the object may partially ablate and drop the remainder on the ground as a meteorite, or (3) the object may disintegrate explosively. Meteorites and airbursts are discussed in sections 5.1.3 and 5.1.4.

As meteoroids ablate and fragment, they also deposit material in the atmosphere. For instance, the constant influx of meteoroids produces a permanent layer of sodium atoms in the atmosphere (see figure 28). This sodium layer can be used to study the mesosphere (see, for example, Xu and Smith 2004) or to create artificial laser guide stars for adaptive telescope optics (Humphreys et al. 1992). Besides sodium, meteoroids also deposit iron, potassium, silicon, and other elements in the atmosphere (Plane 1991; Carillo-Sánchez et al. 2016).

Figure 28. An image of the atmosphere taken from the International Space Station. The yellow sodium layer can clearly be seen. Image credit: NASA.

5.1.3 Meteorites

Meteorites are produced when part of a meteoroid survives passage through the atmosphere. The meteorite never represents the original meteoroid's mass or shape: some part of the original object is always lost to ablation in the atmosphere. Ablation can end either when the original meteoroid is completely ablated away, when the object impacts the Earth's surface, or when the remaining mass has been decelerated to a speed of 3–4 km s^{-1}. In the latter scenario, ablation ends but the object continues to move; it follows a free fall trajectory called *dark flight*, so named because the luminous part of the trajectory has ended and the body has "gone dark."

To produce a meteorite, the meteoroid must be large, composed of a mechanically strong material, and have a low entry speed. The odds of a fireball producing a meteorite increase when (a) the fireball was visible at a final height of less than 35 km, (b) its terminal velocity was less than 10 km/s, and (c) its estimated terminal mass is greater than 0.1 kg (Brown et al. 2013b). Meteor scientists also use the final height, initial speed, initial mass, and entry angle of a meteor to generate a crude estimate of its material strength termed the PE (not an acronym) criterion. A larger PE criterion is associated with greater material strength and less atmospheric ablation (Ceplecha and McCrosky 1976). Table 5 presents a classification scheme for PE values. However, while fireballs may be classified as type IIIa or IIIb, there are no known meteorites that fall into these categories. Cometary material is simply too fragile to survive passing through the atmosphere.

Table 5. PE classification scheme for fireballs.

Type	PE Range	Probable Material Association
I	–4.6 < PE	Ordinary chondrite-like
II	–5.25 < PE ≤ –4.6	Carbonaceous chondrite
IIIa	–5.7 < PE ≤ –5.25	Short period cometary
IIIb	PE ≤ –5.7	Weak cometary material

Table 5 mentions two categories—ordinary chondrites and carbonaceous chondrites—to which meteorites may belong. Meteorites may also be classified as "iron," "stony-iron," or "stony" (examples are presented in figure 29), but meteorite classification is substantially more complex than this and there are an immense number of subdivisions of and exceptions to these simple categories.

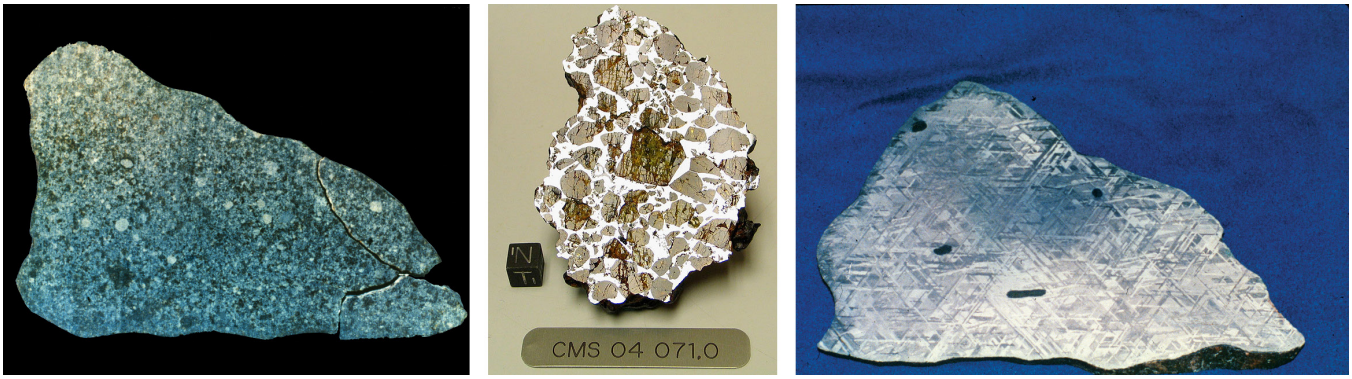

Figure 29. Three meteorites illustrating meteorite categories. At left is a stony meteorite found in Antarctica, in the center is a stony-iron meteorite (more specifically a pallasite) also found in Antarctica, and at right is an iron meteorite from Barringer Crater. Each meteorite has been sliced and polished to reveal the object's internal structure. Image credit: NASA.

Meteorite discoveries are divided into finds and falls. Meteorite *finds* are those events in which the meteorite was first noticed as an object lying on the ground, and for which there is no record of the associated meteoric phenomenon. In contrast, meteorite *falls* occur when a meteorite is linked to an observed meteor. In some cases, the meteor's trajectory can be used to identify the likely location of a meteorite. In all cases, the meteorites themselves are named after the location where the meteorite is found, although that may be the name of a lake (Tagish Lake), a town (Grimsby), or even a farm (Dingle Dell), to give a few examples. Micrometeorites (50 μm – 2 mm) and dust particles are not named.

It is estimated that, within an area of a million square km, 9 meteorite-producing events occur each year that produce at least 1 kg of meteorites (Halliday et al. 1989). If we combine this rate with the Earth's total surface area of 510.1 million square km, we expect that 4600 kg-or-larger meteorites fall onto the Earth each year. However, 71% of the Earth's surface is covered by water, and 50 million square km are covered by forest and woodlands. As a result, the number of new meteorites that are recoverable is, at most, 900 per year. Perhaps 1% of those are actually found; around 40,000 meteorites of any age have been found to date (Planetary Science Institute 2019).

The number of meteorite falls is even smaller. To be categorized as a fall, the meteor must be observed; thus, the event must take place in either a populated area or near a meteor camera or radar network. Most detections are optical and therefore much more likely to occur at night. Due to these restrictions, there are only around 1000 observed meteorite falls. Instrumentally-detected meteorite falls are even rarer; as of 2015, there were 22 (Borovička et al. 2015).

5.1.3.1 Meteorite Finds. Most known meteorites are discovered well after landing on the ground, often by accident. For example, the world's largest single meteorite, the Hoba or Hoba West meteorite, caught the attention of farmer Jacobus Brits as he sat upon it (Spargo 2008). In rare cases, "fossil" meteorites are found embedded in geological layers that are hundreds of millions of years old (see Schmitz 2013, for example).

While meteorites fall all over the Earth, they are more likely to be found in certain locations, particularly deserts. The lack of water reduces meteorite erosion, and the lack of vegetation makes meteorites easier to find, particularly on sandy or icy surfaces. The Antarctic Search for Meteorites (ANSMET) is a program that sends teams to locate meteorites in the Transantarctic Mountains and preserves them for scientific study. Antarctica is an ideal collection site because its glaciers collect meteorites over tens of thousands or even millions of years (Case Western Reserve University 2019). In most cases, these meteorites are carried into the ocean along with the glacier, but a fraction are trapped and concentrated at the base of the Transantarctic mountain range. ANSMET has collected over 23,000 meteorites from Antarctica since 1976. The Sahara Desert has also proved to be a prime location for meteorite finds, and many commercial ventures have collected meteorites in northwest Africa.

It is difficult to determine much about the trajectory associated with a meteorite find. At most, the presence or lack of a crater can be used to estimate the object's final trajectory. However, certain individual meteorite finds have provided evidence of astronomical events. For instance, the

discovery of Martian meteorites (by which we mean those originating from Mars rather than those falling onto Mars) confirmed that rocks could be transferred efficiently from Mars to the Earth (Gladman & Burns 1996).

5.1.3.2 Meteorite Falls. These events can be recorded using a variety of techniques and under different circumstances (time of day or night, viewing range, etc.), and some observations are more reliable than others. Almost all instrumentally-observed falls are imaged from the ground, though the Tagish Lake and Almahata Sitta fireballs were not imaged at all; instead, satellite data and images of the dust trail were used in their analyses. While some of these falls were fully characterized by professional photographic or video networks, others were caught in "casual" video or photography (i.e., images captured on the fly by members of the public). The Almahata Sitta event was the only meteorite fall to be predicted in advance: the associated asteroid 2008 TC_3 was discovered and observed 19 hours before it entered the atmosphere. The Chelyabinsk fall is the most well-known and thoroughly observed, although primarily through casual video and photographic recordings, and is by far the most destructive in terms of property damage (see section 5.3.4).

Even when a meteor is observed and thought to land in a promising area, meteorites may not be recovered. This is because the final stage of the trajectory, called "dark flight," is not luminous and cannot be observed. Furthermore, the meteorite's path during dark flight is much more affected by air density and winds than it is during the ablation stage. It can therefore be difficult to pinpoint the final landing spot of a meteorite, especially when only visual (rather than instrumental) observations are available. Doppler weather radar observations have been used to help narrow the range of possible landing sites (Fries & Fries 2010), but meteorite recovery remains challenging and labor-intensive.

The type of instrument that observed the meteorite fall determines the type of information that can be gleaned from it; an in-depth description of the methods used to observe meteoric phenomena is presented in chapter 2. In addition to typical meteor detectors— i.e., calibrated video, photography, radar, infrasound, seismic, and satellite observations—members of the public often witness and occasionally record bright meteor events. These casual observations are often recorded with low quality cameras, and provide only coarse measurements of the trajectory and mass if the image can be calibrated at all.

Although the MEO tracks bright meteors, including fireballs and occasionally meteorite-producing events, meteorite recovery is not the main focus of the office. However, scientists and commercial meteorite hunters may track meteors with the specific goal of recovering meteorites. Instrumentally observed falls are particularly prized: the combination of a known meteoroid orbit with a known meteorite composition provides a link between the parent body or parent body population and a material record of the formation of our Solar System. In all cases, meteorites can provide information about the composition and, to an extent, history of natural space debris. In fact, the only samples of Martian rock we have on Earth are meteorites. For these reasons, meteorite recovery partly or wholly motivated the establishment of several meteor networks, including the Prairie Meteorite Network (United States, 1964–1975), the European Fireball Network (continental Europe, 1963-), and the Desert Fireball Network (Australia, ca. 2008–). Despite these efforts, meteorite falls remain rare.

5.1.4 Meteorite Pits

A meteorite undergoing dark flight is falling at terminal velocity. While this is much slower than its original speed relative to the Earth, the meteorite may still produce a pit or dent in the surface on which it lands. In many cases, these pits are only slightly larger than the meteorite itself. These impacts are not explosive and are similar to what might result from throwing a rock (see figure 30). Meteorites landing in deep snow have been found to create funnels called "snow carrots" (Luther et al. 2017). In many cases, meteorites create no visible dents in the ground at all.

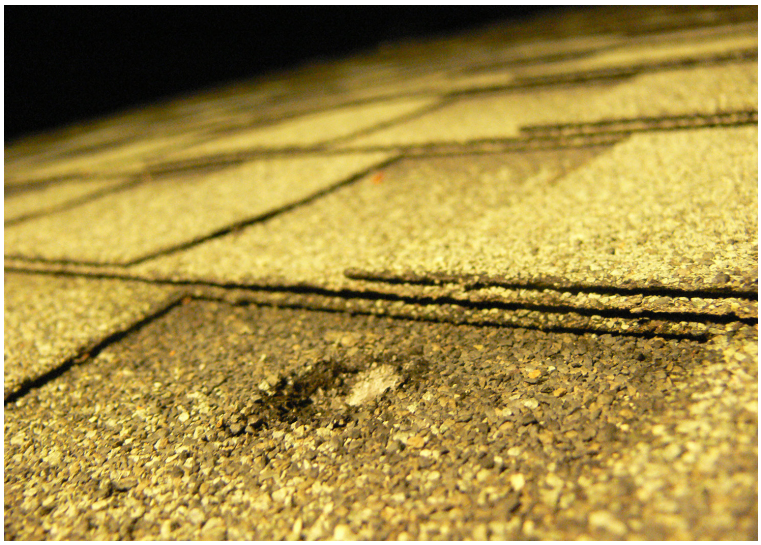

Figure 30. A small dent in the roof of a house caused by a falling meteorite, specifically fragment N01 of the Novato meteorite which fell on October 17, 2012. Image credit: SETI/CAMS (NASA Ames Research Center).

We follow the example of French (1998) in distinguishing between impact pits, which are produced by a meteorite hitting the ground at dark-flight speed, and impact craters, which are produced by asteroids hitting the ground at close to their original speed. We discuss the latter in section 5.1.6.

5.1.5 Airbursts

An airburst occurs when an incoming body breaks up in the atmosphere. Large objects do not easily decelerate; therefore, as they descend deeper into the atmosphere and ram through denser layers of air, they experience increasingly high pressures. If the aerodynamic pressure the object experiences exceeds the internal strength of the meteoritic material, the meteoroid will disintegrate. This deposits the object's kinetic energy into a small volume of air in the atmosphere and produces an explosion or airburst. The airburst in turn generates a blast wave that can potentially harm and damage people and property on the ground.

Early models of airbursts assumed these events were similar to atmospheric nuclear explosions. However, while nuclear bomb tests explode from a single point in the atmosphere—the bomb's location—an incoming natural object ablates and explodes while traveling along a trajectory. Chyba et al. (1993) modeled the Tunguska airburst as originating from a cylindrical object that was compressed into a pancake by the ram pressure. Boslough et al. (2015) modeled airbursts as originating from a tapered cylinder of material expanding behind the object and a supersonic bow shock in front of the object. Boslough et al. also argue that objects with steep trajectories may result in a "backfire plume" that carries some material backward along the wake; this material shoots out of, then falls back onto, the atmosphere. This backfire effect can make the risk of damage *greater* than that caused by an atmospheric nuclear explosion of the same energy (Boslough et al. 2015). In contrast, shallow trajectories like that of the Chelyabinsk fireball can make the damage *less* than that of a nuclear explosion (Brown et al. 2013a).

Most airbursts, however, are significantly weaker than the Chelyabinsk and Tunguska events (both of which are discussed further in section 5.3). Figure 31 shows the location and energies of airbursts occurring between 2000 and 2013 that were equivalent to at least 1 kt of TNT. The Chelyabinsk airburst, labeled "X," is significantly stronger than all other airbursts during this period.

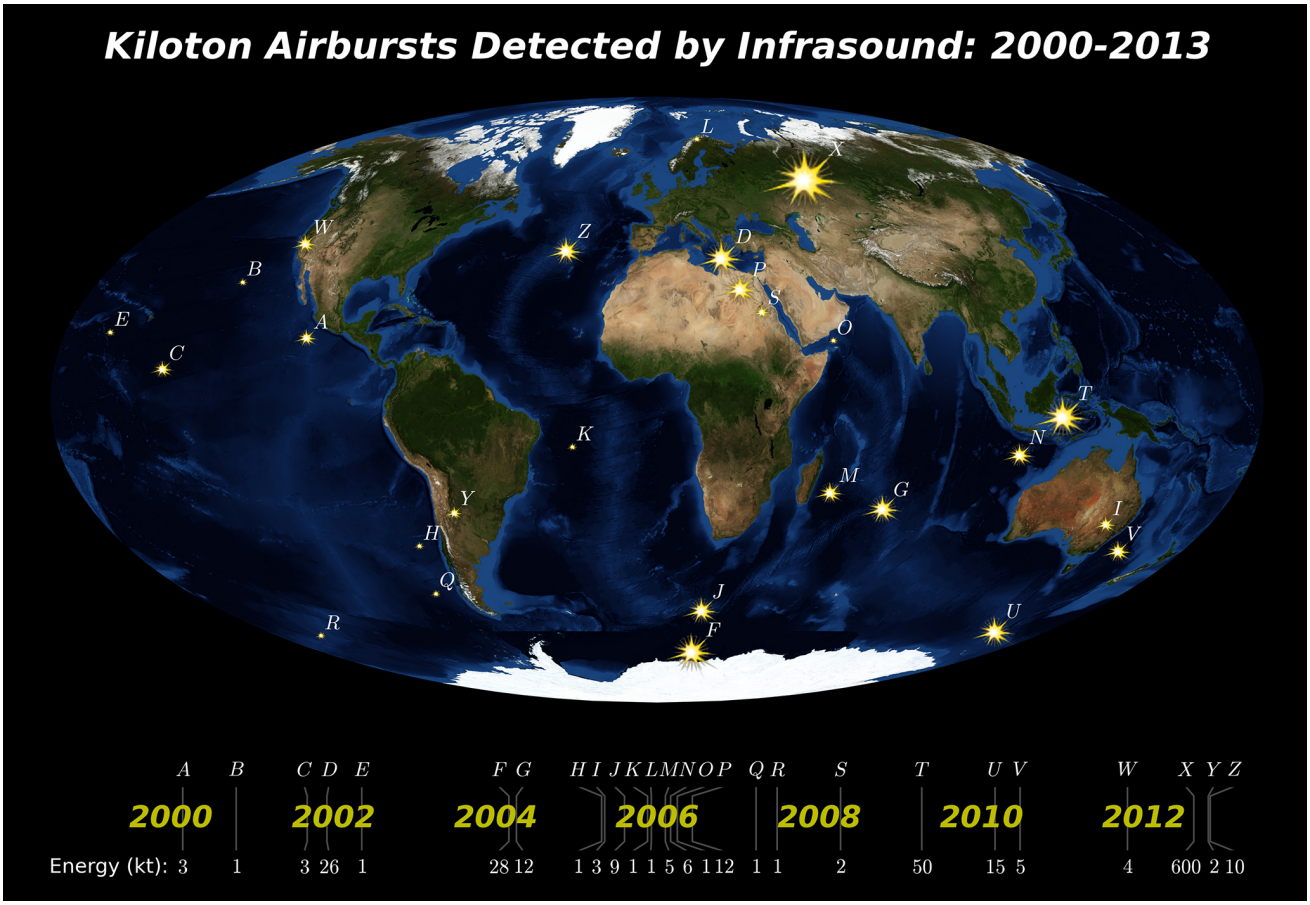

Figure 31. Airbursts occurring between 2000 and 2013 that were equivalent to one kiloton of TNT or greater. The Chelyabinsk airburst is marked "X" and, with an energy of 600 kiloton TNT equivalent, is by far the most energetic event shown here.

Airbursts can cause a variety of ground effects. The blast wave from unusually large events can knock down trees or break windows. More commonly, airbursts create acoustic or infrasonic pressure waves in the air and vibrations in the ground. Boslough & Crawford (2008) theorize that airbursts could even have melted sand to form the Muong-Nong tektites (which are unusually large and layered for tektites) and Libyan desert glass.

You may note that we use the term "object" in this section rather than "meteoroid"—this is because airbursts are produced by objects that are about 1 meter in diameter or larger. According to the International Astronomical Union, this is also the dividing line between a meteoroid and an asteroid. Thus, airbursts are an asteroidal phenomenon, although particularly large and fast meteoroids close to the meter boundary may also be capable of producing airbursts.

5.1.6 Impact Craters

When an asteroid or comet enters the atmosphere, it is subject to the same ablative and fragmentary processes as a meteoroid. However, because of the asteroid's size and strength, the atmosphere may not be able to break it up entirely before it reaches the ground. The incoming asteroid may create a brilliant superbolide and fireball fragments, explode in mid-air, and/or impact the ground.

If a large or sturdy asteroid or comet is not destroyed in the atmosphere in an airburst, it can hit the Earth's surface at hypersonic speed and create an impact crater. Unlike the creation of meteorite pits, this type of event is explosive and can create shock waves both before (as an airburst) and after impact. These impacts can create long-lasting craters on the Earth's surface; the 1.2 km Barringer Crater (also known as Meteor Crater) in Arizona was created by a 30 m iron asteroid (French 1998) and is 50,000 years old (see figure 32) .

Figure 32. Barringer crater (also known as Meteor Crater). Image credit: APoD.

Although we differentiate between meteorite pits and impact craters, impact craters may also be accompanied by meteoroid remnants that are also termed "meteorites." In this case, the meteorites have survived not only atmospheric ablation but also an energetic impact with the ground. Large impacts are so energetic that they may melt or vaporize the ground where they strike and can produce distinctive blobs of natural glass called tektites. Rocks near the impact site may be shocked by the energy of the impact and form shatter cones. The presence of meteorites, shatter cones, and/or tektites can be used to confirm that a crater is meteoritic in origin. For instance, Chesapeake Bay lies on top of an ancient (35 million years old) impact crater, but, due to geologic processes such as erosion, the crater is no longer obvious to the human eye. However, tektites were found in the process of drilling deep into the bay, revealing its impact crater origin.

A discussion of the hazards posed by large impact events is beyond the scope of this document; we refer the reader to the NASA Near Earth Object Program for further information.

5.2 Impact Frequency as a Function of Size/Energy

While larger bodies are more hazardous individually, as a population they are far less common. The vast majority of natural objects that enter the Earth's atmosphere are dust particles and small meteoroids, which pose no threat to people on the ground. Occasionally, meter-class meteoroids will generate fireballs and superbolides that produce airbursts and meteorites. Very rarely, a meteoroid of this size will create a small impact crater, as was the case in the Carancas meteorite fall (Tancredi et al. 2009). Large meteoroids represent a small risk to those on the ground. Asteroids, which are even less numerous, pose a larger risk, as the combination of their larger size and higher material strength can produce airbursts and shock waves, large meteorites, and, in rare cases, high speed impacts directly onto the Earth's surface.

The number of meter-sized objects colliding with the Earth as a function of energy has been estimated using several independent techniques; a selection of these estimates is presented in figure 33. Note that we expect thousands of meteorite-producing events per year and hundreds of airbursts, but explosive impacts are spaced hundreds of years apart.

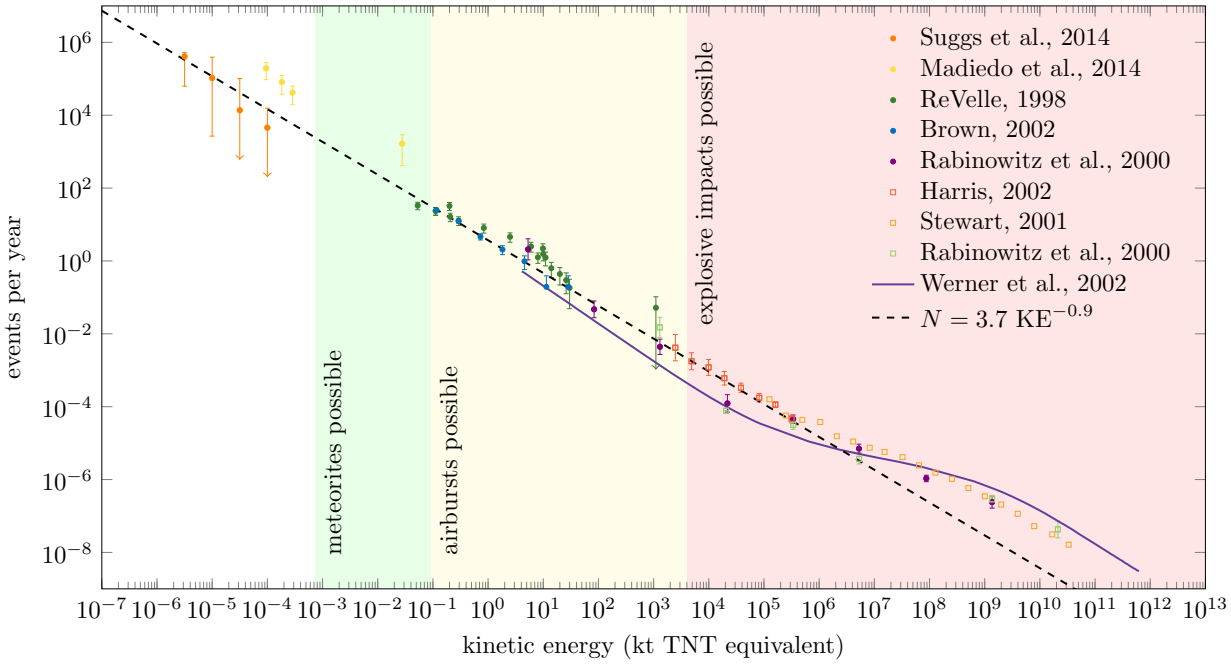

Figure 33. The frequency at which meteoroids and asteroids hit the Earth's atmosphere as a function of kinetic energy, following Brown et al. (2002) and Suggs et al. (2014); the best fit line of $N = 3.7\ KE^{-0.9}$ is from Brown et al. (2002). This is a cumulative distribution and reflects the frequency of events of a given kinetic energy or greater. This plot also includes the approximate kinetic energy ranges at which meteorites, airbursts, and explosive impacts become possible. However, not all objects above these limits will produce such events; high-speed meteoroids are less likely to produce meteorites, for instance.

5.2.1 Property Damage and Injury

Meteorite falls and airbursts do occasionally cause damage to the landscape and human property and may even cause injuries. Table 6 summarizes 68 known meteorite falls and finds (see section 5.1.3 for definitions) and the corresponding observations and damage from 1950 to 2015. The data was taken from the Meteoritical Bulletin Database (MBD), which has over 60,000 entries, and was compiled by searching for terms such as "damage," "home," "house," "building," "roof," "vehicle," "car," "automobile," "person," and "crater." In 43 cases, building components such as roofs, ceilings, floors, or windows were damaged. Nine cases reported damage to automobiles or boats. Either a crater, pit, or depression was listed in 17 cases. There were only two reports of injury to a person (Sylacauga and Mbale) and one animal fatality report (Valera).

Table 6. List of meteorite falls/finds that caused damage or produced a crater from 1950 to 2014. In many cases, the parent fireball was observed visually or aurally; explosions (possible airbursts) were also witnessed frequently. This data was found using the Meteoritical Bulletin Database (The Meteoritical Society 2019). This list is not exhaustive.

Meteorite Name	Date	Location	Observation	Damage
St. Louis	12/10/1950	USA	Fireball, explosions	Vehicle
Sylacauga	11/30/1954	USA	Fireball, explosions	Roof, person injured
Sinnai	02/19/1956	Italy	Fireball	Roof, floor
Centerville (McMurchie)	02/29/1956	USA	–	Roof, planter
Hamlet	10/13/1959	USA	–	Gutter
Chernyi Bor	1960s	USSR	Explosion	Trees
Kiel	04/26/1962	W. Germany	None	Roof
Bogou	12/14/1962	Africa	Sounds	Small crater
Denver	07/17/1967	USA	None	Roof
Schenectady	04/12/1968	USA	–	Roof
Andreevka	08/07/1969	USSR	–	Roof
Murchison	09/28/1969	Australia	Fireball, tremor	Roof
Wethersfield (1971)	04/08/1971	USA	–	Roof, ceiling
Havero	08/02/1971	Finland	Sonic booms	Roof, floor
Valera	10/15/1972	Venezuela	Bright light	Cow fatality
San Juan Capistrano	03/15/1973	USA	–	Roof
Canon City	10/27/1973	USA	Meteor	Roof
Naragh	08/18/1974	Iran	–	Roof
Acapulco	08/11/1976	Mexico	Fireball	Small crater
Louisville	01/31/1977	USA	Fireball, sonic booms	Buildings and a vehicle
Walnut Hill	10/1978	USA	–	Roof
Wethersfield (1982)	11/08/1982	USA	Fireball, sonic booms	Roof
Aomori	06/30/1984	Japan	None	Roof
Claxton	12/10/1984	USA	Whistling sound	Mailbox, depression in dirt
Uchkuduk	06/21/1989	Uzbekistan	Sonic boom	Small crater
Burnwell	09/04/1990	USA	–	Porch
Tahara	03/26/1991	Japan	–	Sea vessel decking
Mbale	08/14/1992	Uganda	Explosion, rumbling, smoke trail	Person injured
Peekskill	10/09/1992	USA	Fireball	Vehicle, pit in ground
Mihonoseki	12/10/1992	Japan	Fireball	Roof, two floors
Coleman	10/20/1994	USA	Fireball, sonic boom	Roof
Lohawat	10/30/1994	India	–	Small crater
Devri-Khera	10/30/1994	India	Fireball	Small crater
Neagari	02/18/1995	Japan	Fireball	Vehicle
Tsukuba	01/07/1996	Japan	Fireball, explosions	Roof
Turtle Lake	10/21/1996	USA	–	Vehicle
Guangmingshan	12/30/1996	China	Sounds	Small crater
Juancheng	02/15/1997	China	Fireball, explosion	Roof
Portales Valley	06/13/1998	USA	Explosions, meteor trail	Roof, wall

Table 6. List of meteorite falls/finds that caused damage or produced a crater from 1950 to 2014. In many cases, the parent fireball was observed visually or aurally; explosions (possible airbursts) were also witnessed frequently. This data was found using the Meteoritical Bulletin Database (The Meteoritical Society 2019). This list is not exhaustive (Continued).

Meteorite Name	Date	Location	Observation	Damage
Kunya-Urgench	06/20/1998	Turkmenistan	Fireball	Large crater
Dashoguz	09/05/1998	Turkmenistan	Meteor trail	Small crater
Ourique	12/28/1998	Portugal	Fireball, sounds	Small crater
Kobe	09/26/1999	Japan	Fireball, explosion	Roof
Dunbogan	12/14/1999	Australia	–	Roof, ceiling
Dergaon	03/02/2001	India	Fireball, explosions	Crater
Alby sur Cheran	02/2002	France	–	Roof, insulation
San Michele	02/20/2002	Italy	–	Roof
Dongyang	07/2002	China	Explosion	Roof
Kilabo	07/21/2002	Nigeria	Fireball, explosions	Small crater
Hiroshima	02/01-03/2003	Japan	Fireball	Roof, plasterboard
Park Forest	03/26/2003	USA	Fireball	Several roofs, ceilings, window, furnishings, several vehicles
New Orleans	09/23/2003	USA	Fireball	Roof, two floors, crawlspace
Kasauli	11/02/2003	India	Sound	Crater
Werdama	05/21/2006	Libya	Explosion	Small crater
Moss	07/14/2006	Norway	Fireball, rumbling	Roof, trees, fence
Mahadevpur	02/21/2007	India	Fireball, fragmentation	Roof
Cali	07/06/2007	Colombia	Fireball, explosions	Several roofs, windows shattered
Carancas	09/15/2007	Peru	Fireball	Large crater
Grimsby	09/26/2009	Canada	Fireball, radar, infrasound	Vehicle
Cartersville	03/01/2009	USA	Sonic boom, doppler radar	Roof, ceiling
Lorton	01/18/2010	USA	Fireball, explosion	Roof, ceiling, carpet, floor
Soltmany	04/30/2011	Poland	–	Roof
Draveil	07/13/2011	France	–	Multiple roofs, vehicle windshield
Thika	07/16/2011	Kenya	Fireball, explosions	Greenhouse, roof
Ladkee	05/04/2012	Pakistan	Fireball	Small crater
Wolcott	04/19/2013	USA	Sonic boom	Roof, ceiling, pipe
Jinju	03/09/2014	South Korea	Fireball	Plastic roof

5.3 Notable Events

In this section, we present several notable individual events. The first four events—Peekskill, Park Forest, Carancas, and Chelyabinsk—are meteorite falls. The last two events—Chelyabinsk and Tunguska—are superbolides that are notable for both their size and damaging effects (both produced airbursts, for instance). Though they both occurred over Russia over 100 years apart, these events are so well-known in meteor science and even in mainstream public consciousness that they go by mononyms like Madonna or Prince.

5.3.1 Peekskill

The Peekskill meteorite fall in New York on October 9, 1992, was observed by a large number of eyewitnesses. It was the first meteorite fall to be video recorded by casual observers—over 15 videos from several states were documented. Witnesses observed a green, fragmenting fireball brighter than the full moon that lasted over 40 seconds (Beech et al. 1995, Brown et al. 1994). A 12.4 kg fragment impacted a vehicle in Peekskill, NY, creating a sizeable hole in the rear end of the car and small crater beneath it. It's likely that other meteorites were produced, but none have yet been found.

A trajectory was reconstructed using casual video and photography of the fireball. The meteor likely had an initial speed of about 15 km/s (Brown et al. 1994) and an initial size of 1.7 by 1.7 by 1 m (Ceplecha 1996). The angle of entry was very shallow (such events are sometimes described as "earth-grazers"), making the duration quite long.

5.3.2 Park Forest

This meteorite fall occurred on March 26, 2003, and is famous due to its location. The area in and near Park Forest, a suburb of Chicago, was "the most densely populated region to be hit by a meteorite shower in modern times" (Simon et al. 2004). Note that the term "meteorite shower" does *not* carry the same meaning as "meteor shower"; instead, it refers to a cluster of meteorites falling from the same event. These falling meteorites damaged several houses and vehicles, and multiple meteorites were recovered. The accompanying large fireball was witnessed by observers in Illinois, Indiana, Michigan, and Missouri and recorded by casual videographers. Loud detonations were heard by residents (Simon et al. 2004) and recorded by acoustic instruments.

Data from both optical and acoustic sensors, as well as from satellite and seismic detectors, allowed this bright fireball to be characterized. The initial meteoroid diameter was estimated to be 1.8 m, corresponding to an energy of about 0.5 kt of TNT (Brown et al. 2004). Combining both ground-based video recordings and satellite data yields an initial velocity of about 20 km/s (Brown et al. 2004). This speed is relatively high for a meteorite fall and may explain why the total mass of all recovered meteorites is comparatively low.

5.3.3 Carancas

An unusual meteorite fall was observed on September 15, 2007, in Carancas, Peru (Tancredi et al. 2009). Startled residents witnessed a bright daytime fireball, then heard an explosion and saw a rapidly expanding dust cloud. The impact created a 13.5 m crater, and stony meteorite fragments were found close to the impact site. The Carancas fall produced a seismic surface wave that was detected 47–125 km from the impact site; this was the first unambiguous seismic detection of crater formation via meteoroid impact on the Earth's surface (Tancredi et al. 2009). Infrasound instruments also recorded the shock waves from the fireball and allowed scientists to estimate an initial meteoroid size between 0.6 m and 4 m (Brown et al. 2008; Borovicka and Spurny 2008; Le Pichon et al. 2008). Trajectory reconstruction estimated an initial speed of 12 km/s and an impact speed of a few km/s (Brown et al. 2008; Le Pichon et al. 2008). The energy that went into making the crater was estimated to be the equivalent of 1–3 tons of TNT (Tancredi et al. 2009).

The 2007 Carancas meteorite fall in Peru blurs the line between meteorite pits and impact craters. The size estimate of 0.6 to 4 m in diameter spans the meteoroid-asteroid boundary. It produced a crater that, unlike typical meteorite pits, was significantly larger than the object, with a diameter of 13.5 m (Brown et al. 2008; Borovička and Spurný 2008; Le Pichon 2008). Yet the object was slowed to a small fraction of its initial speed and must have entered dark flight before impacting the ground. Furthermore, the object, while stony in composition, produced an impact crater significantly larger than itself. This behavior is typically seen only from iron impactors, and so it was posited that the object may have had unusual strength for a stony impactor (Brown et al. 2008).

5.3.4 Chelyabinsk

On February 15, 2013, at approximately 9:20 a.m. local time, an unusually bright superbolide streaked across the pre-dawn sky over the Ural region of Russia (figure 34). The fireball lit up the sky "like it was day" and exploded to form an airburst. This airburst produced a powerful blast wave that damaged more than 4000 buildings in the city of Chelyabinsk and its surroundings, mostly in the form of broken windows and doors. One building in Chelyabinsk—a zinc plant—suffered major structural damage, as seen in figure 35. More than 1500 people were injured by glass and debris (Popova et al. 2013).

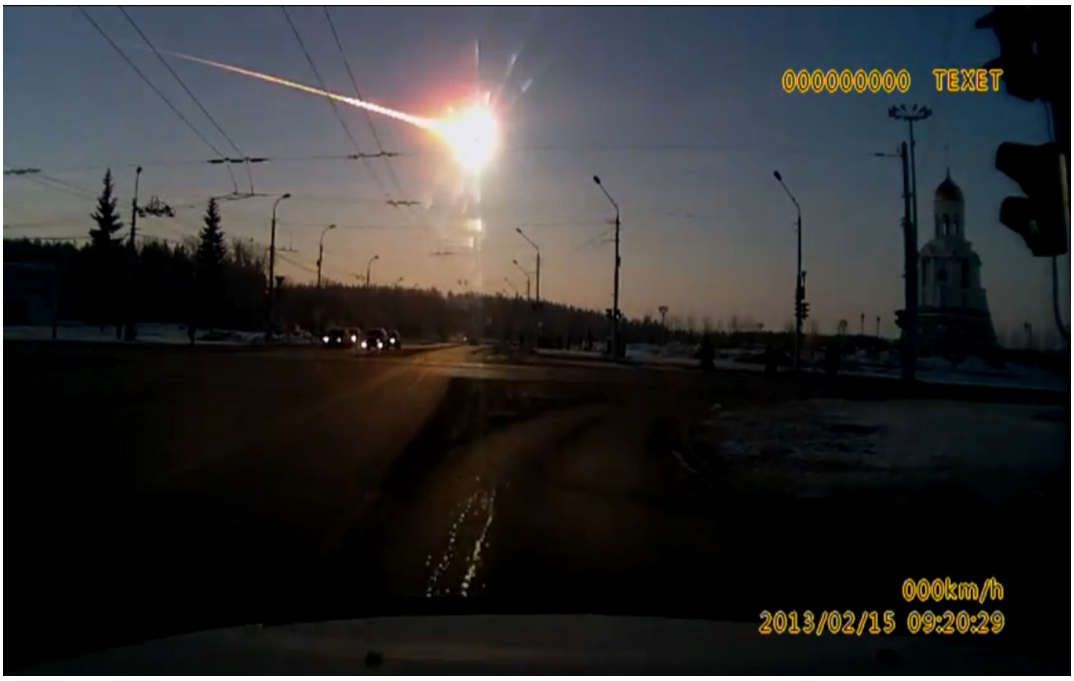

Figure 34. A Chelyabinsk superbolide seen from Kamensk-Uralsky in Sverdlovsk Oblast, Russia. Image credit: Aleksandr Ivanov (Isanov 2013).

Figure 35. Damage to the zinc plant in the city of Chelyabinsk. Image credit: Oleg Kargopolov/AFP/Getty Images.

The Chelyabinsk event was recorded by security cameras and by hundreds of members of the public equipped with car-mounted dashcams and hand-held phone cameras. The airburst was observed globally by multiple instruments such as seismic and infrasound stations, some as far away as Antarctica (15,000 km distant). The event was the largest ever recorded by the Comprehensive Nuclear-Test-Ban Treaty Organization (CTBTO), an organization with a global network of infrasound stations established to detect illicit above-ground nuclear tests. Finally, a 6–8 m hole was found in the ice of Lake Chebarkul, about 70 km west of the city of Chelyabinsk. Hundreds of small meteorites were found in the area south-southwest of Chelyabinsk, and a large meteorite of approximately 600 kg was later recovered from the bottom of Lake Chebarkul (Popova et al. 2013).

Videos of the superbolide in flight were painstakingly calibrated and used to obtain the trajectory, speed, and orbit of the body. When combined with data from seismic, infrasound, and U.S. government sensors (NASA Jet Propulsion Laboratory), the video-derived light curve yields an energy of 500 ± 100 kilotons of TNT for the airburst (Brown et al. 2013a). The asteroid that caused the Chelyabinsk superbolide and airburst was estimated to be 19 m in diameter with a mass of 12,000 metric tons (Borovička et al. 2015). Chelyabinsk serves as a demonstration of the potential damage caused by a small asteroid.

5.3.5 Tunguska

On June 30, 1908 at 7:17 a.m. local time, an explosion in the Tunguska region of Russia flattened 2150 ± 50 km^2 of trees (Longo 2007). Hundreds of reindeer were killed but there is no evidence that any person died in the blast. A trader named Semenov, located more than 40 miles away from "ground zero," saw fire in the sky, heard the explosion, and was knocked off his chair by the blast (Yeomans 2013). The resulting heat made him feel as if his shirt was "on fire." Other firsthand accounts describe trees first being set on fire, then extinguished by the blast wave; glass windows breaking; and the ground shaking. Seismic stations around the world registered the tremors, which reached 5.0 on the Richter scale in Eurasia. Clouds of dust in the atmosphere reflected sunlight from beyond the horizon, lighting up the night skies in Eurasia in the evenings following the explosion, so much so that it was possible to read the newspaper at midnight.

The first expedition to make it to the remote impact site in 1927 found an estimated 80 million trees laying on their sides (figure 36) in a radial pattern, pointing to an epicenter near the Podkamennaya Tunguska River in central Siberia. Trees at ground zero remained standing, though their branches had been stripped away by the fast-moving shock wave. No crater was found at the blast site, and no meteorites have ever been recovered.

The observational information derived from historic barograms, seismic records, and forest conditions (such as fallen tree orientations, displacements, tree trauma, and fire damage), combined with constraints from nuclear testing, laboratory experiments, and computer models, allows for the estimation of the energy of the Tunguska explosion. The generally agreed-upon theory is that a small asteroid or comet exploded in the atmosphere; recent modeling work indicates that the airburst released an energy of 3–5 megatons (Boslough and Crawford 2008). The physical size of the asteroid or comet depends on its composition, density, shape, and speed, but the object was probably at least tens of meters in diameter.

Figure 36. Trees toppled by the Tunguska explosion. Image credit: Leonid Kulik Expedition.

5.4 Impacts on the Moon and Mars

The effects discussed in section 5.1 are not confined to the Earth. Other bodies with thick atmospheres, like Mars, Venus, Titan, and Triton, also experience meteoric phenomena. If a body has no atmosphere, the meteoroids instead impact the surface at full speed. This section describes meteoroid and meteor observations on the Moon and Mars; however, meteoroid impacts occur on all bodies in the Solar System.

5.4.1 The Moon

The majority of meteoroids entering the Earth's atmosphere are completely ablated. The Moon, with little-to-no atmosphere, has no such protection and meteoroids impact the lunar surface without slowing down. Upon impact, the meteoroid's kinetic energy is partitioned into crater excavation, seismic wave production, light production, and debris plume generation.

Before-and-after images taken by NASA's Lunar Reconnaissance Orbiter (LRO) revealed 599 changes on the surface within 4 years of operation (Robinson et al. 2013). These changes were measured by repeatedly scanning a mere 1% of the lunar surface at high resolution. A subsequent analysis reported 222 new impact craters (Speyerer et al. 2016). The impact flash for one new crater identified by LRO was observed by the NASA Meteoroid Environment Office (Robinson et al. 2015).

Seismic signals from meteoroid impacts on the Moon were detected by seismometers placed on the lunar surface by Apollo astronauts. Meteoroid impacts are associated with the most powerful seismic sources recorded by the Apollo seismic network; they also contribute significantly to the lunar micro-seismic background noise (Gudkova et al. 2011). Many seismic events have been attributed to meteoroid impacts on the Moon, as evidenced by the results of the Apollo Passive Seismic Experiment (Oberst and Nakamura 1991).

The flash of light produced by larger meteoroids is detectable by instruments on Earth. Unambiguous detections of lunar impact flashes began during the Leonid meteor storm in 1999 (e.g., Ortiz et al. 2000). Over the years, successful video observations of Geminid, Lyrid, Perseid, Taurid, and sporadic impacts have been reported. As discussed in section 2.4.1, the NASA MEO began a routine monitoring program to observe the Moon for meteoroid impact flashes in early 2006. This has resulted in the observation of 437 impacts by the MEO as of December 31, 2018, and these impacts are used to measure the flux of centimeter-sized meteoroids (Suggs et al. 2014).

Lunar impacts also generate plumes of secondary debris. At very small sizes (nanogram or smaller), secondary debris is the primary cause of microscopic lunar impact craters (Grün et al. 1985). Such tiny impacts are of course not visible from the Earth or orbiting satellites, but can be found on returned lunar samples.

5.4.2 Mars

Unlike the Moon, Mars has an atmosphere capable of ablating meteoroids. The density of the Martian atmosphere at 120 km is similar to that of the Earth (Adolfsson et al. 1996); meteors are observed at this height on Earth and would therefore presumably also be visible on Mars. Numerical integrations performed by Adolfsson et al. (1996) indicate that high-speed meteoroids—i.e., those traveling 30 km/s or more—would be as bright in the Martian atmosphere as they are in the Earth's, although slow meteors would be dimmer.

A few attempts have been made to observe Martian meteors. In 2005, a dedicated meteor observation campaign using the NASA Mars Exploration Rover (MER) Spirit began and had the goal of observationally constraining the meteoroid flux at Mars (Domokos et al. 2007). Spirit's Panoramic Camera (Pancam) was employed to observe the Martian skies for 2.7 hours. Unfortunately, there were no conclusive meteor detections. However, this nondetection allowed scientists to place an upper limit on the background meteoroid flux at Mars of 4.4×10^{-6} km^{-2} hr^{-1} for a minimum meteoroid mass of 4 g. The popular Grün model (Grün et al. 1985) predicts a flux of 10^{-6} km^{-2} hr^{-1} at this size and thus falls within the constraint derived from Spirit.

Although watching the Martian sky has not yet resulted in a meteor detection, meteorites have been discovered on the Martian surface. The Curiosity, Spirit, and Opportunity rovers have discovered several iron meteorites. One of the iron meteorites found by Curiosity—an oblong metallic rock approximately 2 m across—is shown in figure 37.

Figure 37. Iron meteorite "Lebanon" on Mars imaged by MER Curiosity. A series of high-resolution circular images (outlined in white) are superimposed upon a lower resolution view. Image credit: NASA/JPL-Caltech/LANL/CNES/IRAP/ LPGNantes/CNRS/IAS/ MSSS.

Finally, the remnants of a recent Martian meteor shower have been detected from space. On October 19, 2014, Comet C/2013 A1 (Siding Spring) passed within a very small distance of Mars (in fact, it was the closest known flyby of a planet by a comet). Once again, no direct meteor observations were made, as neither the rovers nor the orbiting spacecraft were positioned to observe the shower. However, the NASA Mars Atmosphere and Volatile Evolution Mission (MAVEN) satellite subsequently detected a glowing layer of ionized magnesium and iron deposited in the atmosphere by the ablating meteoroids (Schneider et al. 2015). NASA's Mars Reconnaissance Orbiter and ESA's Mars Express spacecraft detected a temporary layer of ions in the ionosphere (Gurnett et al 2015; Restano et al. 2015). MAVEN also sampled dust from Siding Spring directly using a neutral gas and ion mass spectrometer, finding sodium, magnesium, and iron in the first direct measurements of dust composition from an Oort cloud comet.

5.5 References

Adolfsson, L.G.; Gustafson, B.A.S.; and Murray, C.D.: "The Martian Atmosphere as a Meteoroid Detector," Icarus, Vol. 119, pp. 144−152, 1996.

Beech, M.; Brown, P.; Hawkes, R.L.; et al.: "The Fall of the Peekskill Meteorite: Video Observations, Atmospheric Path, Fragmentation Record and Orbit," *Earth, Moon, and Planets*, Vol. 68, No. 1–3, pp. 189–197, 1995.

Brown, P.; Ceplecha, Z.; Hawkes, R.L.; et al.: "The Orbit and Atmospheric Trajectory of the Peekskill Meteorite from Video Records," *Nature*, Vol. 367, pp. 624–626, 1994.

Brown, P.; Pack, D.; Edwards, W.N.; et al.: "The Orbit, Atmospheric Dynamics, and Initial Mass of the Park Forest Meteorite," *Meteoritics & Planetary Science*, Vol. 39, No. 11, pp. 1781–1796, 2004.

Brown, P.G.; Assink, J.D.; Astiz, L.; et al.: "A 500-Kiloton Airburst over Chelyabinsk and an Enhanced Hazard from Small Impactors," *Nature*, Vol. 503, pp. 238–241, 2013a.

Brown, P.G.; Marchenko, V.; Moser, D.E.; et al.: "Meteorites from Meteor Showers: A Case Study of the Taurids," *Meteoritics and Planetary Science*, Vol. 48, No. 2, pp. 270–288, 2013b.

Brown, P.G.; ReVelle, D.O.; Silber, E.A.; et al.: "Analysis of a Crater-Forming Meteorite Impact in Peru," *Journal of Geophysical Research*, Vol. 113, No. 9, pp. E09007, 2008.

Brown, P.G.; Spalding, R.E.; ReVelle, D.O.; et al.: "The Flux of Small Near-Earth Objects Colliding with the Earth," *Nature*, Vol. 420, pp. 294–296, 2002.

Borovička, J.; and Spurný, P.: "The Carancas Meteorite Impact – Encounter with a Monolithic Meteoroid," *Astronomy & Astrophysics,* Vol. 485, No. 2, pp. L1–L4, 2008.

Boslough, M.; Brown, P.; and Harris, A.: "Updated Population and Risk Assessment for Airbursts from Near-Earth Objects (NEOs)," IEEE Aerospace Conference, pp. 1–12, 2015.

Boslough, M.B.E.; and Crawford, D.A.: "Low-Altitude Airbursts and the Impact Threat," *International Journal of Impact Engineerin*g, Vol. 35, No. 12, pp. 1441–1448, 2008.

Carrillo-Sánchez, J.D.; Nesvorný, D.; Pokorný, P.; et al.: "Sources of Cosmic Dust in the Earth's Atmosphere," *Geophysical Research Letters*, Vol. 43, No. 23, pp. 979–986, 2016.

Case Western Reserve University: "FAQs," < http://caslabs.case.edu/ansmet/faqs/>, 2019.

Ceplecha, Z.; Brown, P.; Hawkes, R.L.; et al.: "Video Observations, Atmospheric Path, Orbit and Fragmentation Record of the Fall of the Peekskill Meteorite," *Earth, Moon, and Planets*, Vol. 72, No. 1–3, pp. 395–404, 1996.

Ceplecha, Z.: "Earth's Influx of Different Populations of Sporadic Meteoroids from Photographic and Television Data," Bulletin of the Astronomical Institutes of Czechoslovakia, Vol. 39, pp. 221–236, 1988.

Ceplecha, Z.; Borovička, J.; Elford W.G.; et al.: "Meteor Phenomena and Bodies," Space Science Reviews, Vol. 84, pp. 327, 1998.

Ceplecha, Z.; and McCrosky, R.E.: "Fireball End Heights: A Diagnostic for the Structure of Meteoric Material," *Journal of Geophysical Research*, Vol. 81, pp. 6257–6275, 1976.

Chyba, C.F.; Thomas, P.J.; and Zahnle, K.J.: "The 1908 Tunguska Explosion: Atmospheric Disruption of a Stony Asteroid," *Nature*, Vol. 361, pp. 40–44, 1993.

Domokos, A.; Bell, J.F.; Brown, P.; et al.: "Measurement of the Meteoroid Flux at Mars," *Icarus*, Vol. 191, pp. 141–150, 2007.

French, B.M.: Traces of Catastrophe: A Handbook of Shock-Metamorphic Effects in Terrestrial Meteorite Impact Structures, Lunar and Planetary Institute, Houston, TX, pp. 120, 1998.

Fries, M.; and Fries, J.: "Doppler Weather Radar as a Meteorite Recovery Tool," *Meteoritics and Planetary Scienc*e, Vol. 45, pp. 1476–1487, 2010.

Gladman, B.J.; and Burns, J.A.: "Mars Meteorite Transfer: Simulation," *Science*, Vol. 274, pp. 161–162, 1996.

Gudkova, T.V.; Lognonné, P.; and Gagnepain-Beyneix, J.: "Large Impacts Detected by The Apollo Seismometers: Impactor Mass and Source Cutoff Frequency Estimations," *Icarus*, Vol. 211, No. 2, pp. 1049–1065, 2011.

Gurnett, D.A.; Morgan, D.D.; Persom, A.M.; et al.: "An Ionized Layer in the Upper Atmosphere of Mars Caused by Dust Impacts from Comet Siding Spring," *Geophysical Research Letters*, Vol. 42, pp. 4745–4751, 2015, doi: 10.1002/2015GL063726.

Grün, E.; Zook, H.A.; Fechtig, H.; et al.: "Collisional Balance of the Meteoritic Complex," *Icarus*, Vol. 62, pp. 244–272, 1985.

Halliday, I.; Blackwell, A.T.; and Griffin, A.A.: "The Flux of Meteorites on the Earth's Surface," *Meteoritics*, Vol. 24, pp. 173–178, 1989.

Humphreys, R.A.; Bradley, L.C.; and Herrmann, J.: "Sodium-layer Synthetic Beacons for Adaptive Optics," *The Lincoln Laboratory Journal*, Vol. 5, pp. 45–66, 1992.

Isanov, A., YouTube: "Взрыв метеорита над Челябинском 15.02.2013.avi," <https://www.youtube.com/watch?v=iCawTYPtehk>, February 14, 2013.

Le Pichon, A.; Antier, K.; Cansi, Y.; et al.: "Evidence for a Meteoritic Origin of The September 15, 2007, Carancas Crater," *Meteoritics & Planetary Science*, Vol. 43, No. 11, pp. 1797–1809, 2008.

Longo, G.: "The Tunguska Event," in *Comet/Asteroid Impacts and Human Society: an Interdisciplinary Approach*, P. T. Bobrowsky and H. Rickman (eds.), Springer-Verlag, pp. 303–330, 2007.

Luther, R.; Artemieva, N.; Ivanova, M.; et al.: "Snow Carrots after the Chelyabinsk Event and Model Implications for Highly Porous Solar System Objects," *Meteoritics & Planetary Science*, Vol. 52, pp. 979-999, 2017.

Meteoritical Bulletin Database, <http://www.lpi.usra.edu/meteor/metbull.php>.

Michel, P.; DeMeo, F.E.; and Bottke, W.F.: *Small Near-Earth Asteroids as a Source of Meteorites*, The University of Arizona Press, pp. 785, 2015.

NASA Ames Research Center: “CAMS,” < http://cams.seti.org/index-N.html>.

NASA Jet Propulsion Laboratory: “Fireballs,” <https://cneos.jpl.nasa.gov/fireballs/>.

NASA Press Release 14-311: “Mars Spacecraft Reveal Comet Flyby Effects On Martian Atmosphere,” <http://www.nasa.gov/press/2014/november/mars-spacecraft-reveal-comet-flyby-effects-on-martian-atmosphere/#.Vbu5M_n48-W>, 2014.

New Scientist Staff and Press Association: “Cosmic Dist Grains Found on City Rooftops for the Fist Time,” < https://www.newscientist.com/article/2115336-cosmic-dust-grains-found-on-city-rooftops-for-the-first-time/>, 2016.

Oberst, J.; and Nakamura, Y.: “A Search for Clustering Among the Meteoroid Impacts Detected by the Apollo Lunar Seismic Network,” *Icarus*, Vol. 91, pp. 315–325, 1991.

Ortiz, J.L.; Sada, P.V.; Bellot Rubio, L.R.; et al.: “Optical Detection of Meteoroidal Impacts on The Moon,” *Nature*, Vol. 405, pp. 921–923, 2000.

Rabinowitz, D.; Helin, E.; Lawrence, K.; et al.: “A Reduced Estimate of The Number of Kilometre-Sized Near-Earth Asteroids,” *Nature*, Vol. 403, pp. 165–166, 2000, doi:10.1038/35003128.

Revelle, D.O.: “Meteoroids,” Conference Proceedings, 2001.

Plane, J.M.C.: “The Chemistry of Meteoric Metals in the Earth’s Upper Atmosphere,” *International Reviews in Physical Chemistry*, Vol. 10, pp. 55–106, 1991.

Planetary Science Institute: “FAQ – Meteoroids/Meteorites,” <https://www.psi.edu/epo/faq/meteor.html>, 2019.

Popova, O.P.; Jenniskens, P.; Emel’yanenko, V.; et al.: “Chelyabinsk Airburst, Damage Assessment, Meteorite Recover, and Characterization,” *Science*, Vol. 342, pp. 1069–1073, 2013.

Restano, M.; Plaut, J.J.; Campbell, B.A.; et al.: “Effects of the Passage of Comet C/2013 A1 (Siding Spring) Observed by the Shallow Radar (SHARAD) on Mars Reconnaissance Orbiter,” Geophysical Research Letters, Vol. 42, pp. 4663–4669, 2015, doi:10.1002/2015GL064150.

Robinson, M.S.; Bowles, Z.R.; Daubar, I.; et al.: “Recent Impacts on the Moon,” American Geophysical Union Fall Meeting 2013, #P13B-1752, 2013.

Robinson, M.S.; Boyd, A.K.; Denevi, B.W.; et al.: “New Crater on the Moon and a Swarm of Secondaries,” Icarus, Vol. 252, pp. 229–235, 2015.

Schmitz, B.: “Extraterrestrial Spinels and the Astronomical Perspective on Earth’s Geological Record and Evolution of Life,” *Chemie der Erde – Geochemistry*, Vol. 73, pp. 117–145, 2013.

Schneider, N.M.; Deighan, J.I.; Stewart, A.I.F.; et al.: "MAVEN IUVS Observations of the Aftermath of the Comet Siding Spring Meteor Shower on Mars," *Geophysical Research Letters*, Vol. 42, pp. 4755–4761.

Simon, S.B.; Grossman, L.; Clayton, R.N.; et al.: "The Fall, Recovery, and Classification of the Park Forest Meteorite," *Meteoritics and Planetary Science*, Vol. 39, pp. 625–634, 2004.

Spargo, P.E.: "The History of the Hoba Meteorite - Part 1: Nature and Discovery," *Monthly Notes of the Astronomical Society of South Africa*, Vol. 67, No. 5-6, pp. 85–94, 2008.

Speyerer, E.J.; Povilaitis, R.Z.; Robinson, M.S.; et al.: "Quantifying Crater Production and Regolith Overturn on the Moon with Temporal Imaging," *Nature*, Vol. 538, pp. 215-218, 2016.

Stewart, J.S.; "A Near-Earth Asteroid Population Estimate from the LINEAR Survey," *Science*, Vol. 294, pp. 1691–1693, 2001.

Suggs, R.M.; Moser, D.E.; Cooke, W.J.; and Suggs, R.J.: "The Flux of Kilogram-Sized Meteoroids from Lunar Impact Monitoring," *Icarus*, Vol. 238, pp. 23–36, 2014.

Tancredi, G.; Ishitsuka, J.K.; Schultz, P.H.; et al.: "A Meteorite Crater on Earth Formed on September 15, 2007: the Carancas Hypervelocity Impact," *Meteoritics & Planetary Science*, Vol. 44, pp. 1967–1984, 2009.

The Meteoritical Society: "Meteoritical Bulletin Database," <http://www.lpi.usra.edu/meteor/metbull.php>, November 16, 2019.

Xu, J.; and Smith, A. K.: "Studies of Gravity Wave–induced Fluctuations of the Sodium Layer Using Linear and Nonlinear Models," *Geophysical Research Letters*, Vol. 109, pp. D02306, 2004, doi:10.1029/2003JD004038.

Yeomans, D.K.: *Near-Earth Objects – Finding Them Before They Find Us*, Princeton University Press, Princeton, New Jersey, pp. 172, 2013.

Zolensky, M.E.; and Warren, J.L.: "Collection and Curation of Interplanetary Dust Particles Recovered from the Stratosphere," in *Lunar and Planetary Inst., Workshop on the Analysis of Interplanetary Dust Particles*, pp. 56–57, 1994.

6. CURRENT AND FUTURE WORK

The final chapter in this handbook is dedicated to discussing the largest questions that need to be addressed with regards to our understanding of the meteoroid environment. More specifically, this chapter discusses: the limitations of current meteor data, the key uncertainties that need to be addressed to make further progress on understanding the meteoroid environment, future observational facilities the MEO is planning to deploy, and planned improvements to the MEO's engineering models.

6.1 The Luminous and Ionization Efficiency of Meteors

Meteoroids are never directly detected; instead we measure their effects on spacecraft surfaces, *in situ* detectors, and planetary surfaces and atmospheres. A certain degree of modeling is required to derive the mass of the original meteoroid from the effect it produces. For instance, the brightness of a meteor is determined by the luminous efficiency, or the percentage of the meteor's kinetic energy that is converted into photons. Similarly, the radar detectability of a meteor is governed by the ionization efficiency, or the relationship between kinetic energy and the number of ions produced. All meteoroid masses, sizes, and fluxes derived from optical data rely on the assumed luminous efficiency, and all meteoroid masses, sizes, and fluxes derived from radar data rely on the assumed ionization efficiency.

The ionization and luminous efficiencies do not take the form of a single value; instead, they are thought to be functions of meteor velocity. However, the precise form of the dependence on velocity is unknown. Wildly disparate functions have been proposed for luminous efficiency; figure 38 displays a few such functions. Note that there are approximately 1-2 orders of magnitude difference in luminous efficiency between these profiles. Furthermore, some of these profiles are for specific materials, such as iron, yet even the two iron curves shown (Ayers et al. 1970; Hill et al. 2005) are noticeably different. When we consider the fact that the composition of a given meteoroid is not necessarily known, the uncertainty in its luminous efficiency becomes even greater.

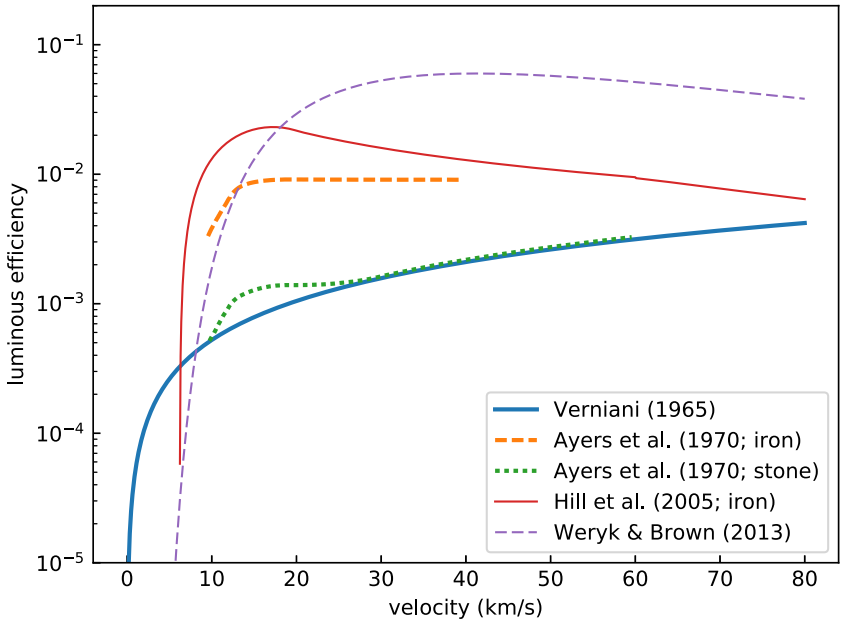

Figure 38. Five sample luminous efficiency profiles.

The luminous and ionization efficiencies relate the light or ionization produced by a meteor to its kinetic energy; the former is critical to optical observations, while the latter is critical for radar observations. The interpretation of meteor head echoes detected by high-power, large-aperture radars, however, is also dependent on our understanding of the plasma surrounding the head of the meteor. As a result, the masses of meteoroids detected via head echoes may be less certain than those detected via trail echoes.

6.1.1 Recent Work

At present, the ionization efficiency of a meteor appears to be better constrained than the luminous efficiency. Recent laboratory measurements (Thomas et al. 2016; DeLuca et al. 2018) of the amount of ionization produced by small particles moving at meteoric speeds show rough, but not exact, agreement with the theory of Jones (1997). The radar cross-section of the meteor head is less well-known, but is the subject of ongoing research (see, for example, Marshall et al. 2017).

Because the ionization efficiency is comparatively well-known, some meteor scientists have attempted to leverage this as a way to measure luminous efficiency. For instance, Weryk & Brown (2013) used simultaneous radar and optical observations of meteors to relate brightness to ionization and thus extrapolate a luminous efficiency relation from an assumed ionization efficiency relation. Their end result is a luminous efficiency that is higher than all other models for most meteor speeds; it has not gained widespread acceptance.

Many attempts have been made to measure luminous efficiency directly from optical meteor detections. In theory, the deceleration and brightness of a meteor can be used to model its mass and thus obtain an estimate of the luminous efficiency (see, e.g., Verniani 1965). In practice, unknown quantities such as the degree of fragmentation, shape factor of the meteoroid, and lack of detectable deceleration obscure the meteoroid's mass. One recent attempt to measure luminosity efficiency used a carefully curated sample of high-precision, non-fragmenting meteors observed with the Canadian Automated Meteor Observatory; however; even this special set of meteors produced luminous efficiency estimates that are highly scattered and cannot be used to distinguish between existing models (Subasinghe & Campbell-Brown 2018). As a result, the luminous efficiency remains a large source of uncertainty in meteor astronomy.

6.1.2 Future Work

Luminous efficiency research continues in two primary veins: (1) detailed modeling of natural meteors and (2) laboratory measurements of manmade meteors. The latter shows more immediate promise for constraining the luminous efficiency.

Thomas et al. (2017) describe an experimental setup that includes four optical ports that enable brightness measurements of an ablating particle. However, the ability of this instrument to measure the luminous efficiency was limited by low photon statistics. At the 2019 Meteoroids conference in Bratislava, R. Marshall reported that the group is adding a more advanced optical detection system to their laboratory apparatus; the result is a ten-fold improvement in light measurements over Thomas et al. (2017). Furthermore, Marshall reported that the group plans to make measurements for meteoritic minerals, such as olivine, in addition to iron and aluminum.

These laboratory experiments measure the ablation of very small particles of a known composition, shape, and density. Yet even if the ionization and luminous efficiency for these materials were measured perfectly, the challenge of applying it to meteoroids of unknown composition and physical structure would remain. One tool that can assist in determining the composition of meteoroids is the collection of detailed meteor spectra; high precision spectra can reveal the relative abundance of different materials. It is extremely difficult to obtain a detailed spectrum of a moving object; two approaches are to use a grating that separates an entire image into separate colors (see, e.g., Rudawska et al. 2016) or to use radiometers to measure the brightness as a function of wavelength for the entire sky (an approach used by part of the European Fireball Network; Spurný et al. 2007).

6.2 Ballistic Effects of Meteoric Material

In situ experiments provide some of the best constraints on the meteoroid flux; for instance, the famous Grün model (Grün et al. 1985) relies on three such experiments (Pioneer 8 and 9, HEOS, and Pegasus) to constrain the overall interplanetary meteoroid flux. *In situ* observations of large meteoroids are essentially measurements of the cratering rate; damage equations are needed to convert crater counts to meteoroid fluxes. However, these damage equations are generally derived from gun tests of spherical aluminum projectiles onto spacecraft-like surfaces (see, for example, figure 39) and may not accurately describe meteoroid-induced damage.

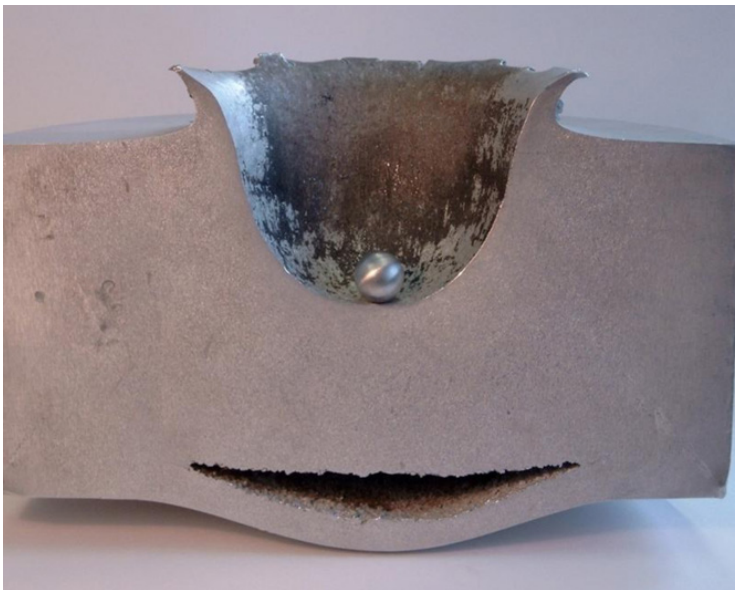

Figure 39. The result of a hypervelocity impact test using a metal projectile and metal target. Image credit: ESA.

Gun tests using meteoritic projectiles (perhaps milled or otherwise crafted from meteorites) could start to probe how meteoroid damage equations differ from orbital debris damage equations and, if a sufficient number of such tests are done, could be used to construct meteoroid-specific ballistic limit equations. Gun tests using porous or "fluffy" projectiles would be particularly valuable, but are likely not possible with current technology.

Until we develop the capability to accelerate mm-sized, meteoroid-like particles to speeds of at least 11–20 km/s in a laboratory setting, it will not be possible to empirically derive damage equations for meteoroids as we do for humanmade debris particles. However, in the meantime, one approach is to analytically or numerically simulate these impacts. For instance, Watts & Atkinson (1995) developed a set of ballistic limit equations for the Long Duration Exposure Facility using analytical methods that, at least in the case of aluminum, exhibited good agreement with empirical equations.

6.2.1 Recent Work

There is little recent work in hypervelocity impact testing using natural projectiles or meteoroid analogs. There are a number of studies of impacts using ice spheres or organic materials, but these tests are intended to study the effects of airplanes flying into hailstones and thus take place at very low speeds (see, e.g., the Kim et al. 2003 study of simulated hail ice accelerated to speeds of 0.03–0.2 km/s, or the Hou & Ruiz 2007 study of the impact of simulated bird flesh at similar speeds). Mihaly (2013) attempted to use nylon spheres as a meteoroid analog but abandoned these projectiles due to their propensity to disintegrate during acceleration.

The few existing impact tests that use meteorites are designed to simulate the impact of these objects not on spacecraft but on asteroids. The purpose is to either study weathering processes or the feasibility of asteroid deflection by impacts. For instance, Flynn et al. (2017) present results from meteoroid-on-asteroid-analog tests taking place at roughly 5 km/s. These speeds are far lower than most meteoroid impacts speeds and thus it would be difficult to extrapolate the results to typical spacecraft impacts. However, they do demonstrate that low-velocity impact testing using meteorite projectiles is currently possible.

Meanwhile, numerical simulations of hypervelocity impacts have advanced over the decades as computers have improved and are sometimes used to simulate meteoroid impacts. For instance, Evans et al. (2008) present a single simulation of a meteoroid analog (a 375-micron-diameter "bumpy sphere" of silica glass) striking a woven Kevlar target at a meteoric speed of 24.5 km/s. The most common approach to simulating hypervelocity impact effects is to use smoothed-particle hydrodynamics (SPH) codes, in which matter is not simulated within a grid but rather using a set of particles that are smeared or smoothed in position. The main advantages of SPH simulations are that they can be easily parallelized and that they can handle large fluctuations in material density much more easily than grid-based codes. The disadvantages are that they continue to have issues with numerical correctness and convergence, especially at boundaries, and thus do not yet produce completely reliable results (see Dai et al. 2017 for a discussion).

6.2.2 Future Work

We know of no planned activities to conduct hypervelocity impact tests with meteorites or meteoroid analogs, to perform numerical simulations of such impacts, or to develop new ballistic limit equations for meteoroid material. Some of these activities (such as conducting impact tests with meteoritic material, particularly fluffy aggregates of meteoritic material, at meteor speeds) do not appear to be possible with current technology. However, a sustained effort to conduct and improve numerical simulations of meteoroid impacts, perhaps testing them against low-velocity impacts of meteoritic projectiles, would likely be a useful step towards a better understanding of meteoroid impact effects.

6.3 Material Properties

The damage done by a meteoroid when it strikes a spacecraft surface depends not just on its mass and size but also on its material properties. For instance, even the simplest ballistic limit equations are a function of impactor density as well as diameter or mass (Hayashida & Robinson 1991). The damage equations of Watts & Atkinson (1995) also depend on the speed of sound within the meteoroid. The shape of the projectile can also be important; rod- and cone-shaped projectiles tend to be more damaging than spherical particles (Hu & Schonberg 2003; Williamsen & Evans 2006).

Ideally, one would collect meteoroids from space and study their material properties directly, but, due to the extreme speeds at which meteoroids encounter the Earth, it is difficult to non-destructively capture anything larger than a tiny dust particle. (The lower spatial density of large particles adds to this challenge.) One can attempt to collect meteoroids at their sources where

the numbers are high and the speeds are much lower. A number of missions have visited comets and obtained measurements of coma particles, or "baby" meteoroids. For instance, the *Giotto* spacecraft flew through the coma of comet 1P/Halley (the parent of the Orionid and eta Aquariid meteor showers) and obtained measurements of the particle flux and size distribution (e.g., Fulle et al. 2000). The drawbacks of using comet missions to obtain meteoroid data are that it is expensive, large meteoroids comprise a small portion of the data, the material properties are typically not measured, and they probe only pristine meteoroids that have not been subjected to any weathering effects and thus may not closely resemble the aged meteoroids that encounter the Earth.

Thus, we have typically used meteor observations to constrain meteoroid physical properties. Given the difficulty in determining even the mass of a meteoroid (see section 6.1), obtaining its material properties is a particularly daunting task. In principle, it is possible to use a combination of the meteor's brightness and deceleration to determine its size and density. However, many meteor observations show no measurable signs of deceleration; precise, high-resolution position measurements are needed to measure the deceleration of fast meteors in particular. Furthermore, the deceleration of a meteor depends on a combination of the meteoroid's bulk density and its shape factor, and so density determinations depend to a degree on the correctness of our assumptions about the shape of a meteoroid. Fragmentation can further obscure any constraints on density.

The equations of meteor ablation also include terms such as the heat of ablation, thermal conductivity, molar mass, and specific heat of the meteoroid. Ablation models must also include some treatment of meteoroid fragmentation (Campbell-Brown & Koschny 2004; Borovička et al. 2007). As a result, the number of unknown parameters can be lengthy and requires fairly detailed observations and modeling to have any hope of constraining them via meteor observations.

6.3.1 Recent Work

In the past, any "measurements" of meteoroid densities were qualitative ones based on the behavior of a meteor; i.e., if a meteor began to ablate at a high altitude, it was thought to be less dense than those that began to ablate at low altitudes. More recently, detailed ablation modeling has begun to effectively constrain density (Kikwaya et al. 2011), although some parameters must be assumed, and, in some cases, there are multiple possible density solutions for a single meteor. These results indicated that meteoroid density is more closely linked to the type of orbit (or "dynamical type") than it is to the height at which the meteor starts to ablate; Moorhead et al. (2017a) used this linkage to construct a density distribution for version 3 of MEM.

The GIADA instrument aboard *Rosetta* collected over 300 dust particles escaping from the surface of comet 67P/Churyumov-Gerasimenko (Fulle et al. 2015). It was found that these particles could be either compact or fluffy, and that densities ranged from 0.8 to 3 g/cc; this is broadly consistent with the density range reported by Kikwaya et al. (2011), although the latter did not obtain any low densities for meteoroids on JFC-like orbits like that of comet 67P. However, if the fluffy particles were preferentially destroyed over time, the remaining compact particles would have densities consistent with Kikwaya et al. (2011, and thus also with Moorhead et al. 2017a).

6.3.2 Future Work

The density distribution of MEM is based on less than 100 density measurements obtained from ablation modeling. The MEO has therefore begun an effort to substantially expand the number of density measurements using the same model. These additional measurements will allow us to better assess whether there are exceptions to the density-dynamical type correlation noted by Kikwaya et al. (2011). They will also permit us to build a more detailed and robust density model.

Simultaneously, the meteor physics group at the University of Western Ontario is in the process of updating their ablation model to incorporate additional constraints; the length of the meteor wake, for instance, may probe the grain distribution (Armitage & Campbell-Brown 2019). Earlier models struggled to reproduce the brightness of meteor wakes (Campbell-Brown et al. 2013).

There are currently no planned missions to visit any known meteor shower parent body. However, the Origins, Spectral Interpretation, Resource Identification, Security, Regolith Explorer (OSIRIS-Rex) spacecraft has recently reached 101955 Bennu, a near-Earth asteroid, and has begun studying its regolith. OSIRIS-Rex will collect a sample of the asteroid's regolith and return that sample to Earth in 2023. Although asteroidal meteoroids are a small component of the meteoroid environment, OSIRIS-Rex will provide a close look at material that may feed into that population.

ESA is also planning the Comet Interceptor mission, which is planned to launch in 2028 and visit an unknown target. Comet Interceptor will be designed to intercept a pristine comet on its first visit to the inner Solar System; it will remain at the Sun-Earth L2 point for up to three years, waiting for a suitable long-period comet to appear. Long-period comets are not the primary contributor to the near-Earth meteoroid environment (e.g., Heisler et al. 1987), but the mission will provide additional data on cometary dust in general.

6.4 Uncertainties in the Near-Earth Sporadic Meteoroid Environment

The MEO has developed a model of sporadic meteoroids in near-Earth space that is extrapolated to other locations in the inner Solar System: MEM (McNamara et al. 2004; Moorhead et al. 2019b). This model consists of a single environment description, with no uncertainties. The reason for this is that most meteor studies rely on a number of assumptions (such as luminous efficiency) whose validity is poorly understood, and thus the degree of uncertainty is simply unknown. For example, we interpret impact data using ballistic limit equations that were derived from tests of man-made particles striking targets at speeds far slower than those of meteoroids; the degree to which meteoroid impact crater sizes may differ from these predictions is unknown.

While the uncertainty in the meteoroid flux in near-Earth space is not well-characterized, it is sometimes estimated as about a factor of 3 (Drolshagen & Moorhead 2019). This factor of 3 is supported by the work of Moorhead et al. (2019b), who demonstrated that the same model—MEM 3—overpredicts the number of impacts on LDEF by about a factor of 2, underpredicts the number of impacts on the Pegasus satellites by a factor of 2-3, and correctly reproduces the flux observed by CMOR. This analysis was performed using only satellites in low Earth orbit and observations of meteors within the Earth's atmosphere; the uncertainty will be more significant at larger geocentric distances.

The uncertainty associated with components of the meteoroid environment can be greater than the uncertainty in the overall flux. For instance, the meteoroid speed distribution obtained from different instruments and using different methods can differ significantly. Most recent studies of the speed distribution agree that, once properly debiased, the meteoroid distribution peaks at low speeds—generally, a few km/s faster than the escape velocity at the top of the Earth's atmosphere (11.1 km/s). The exact location of this peak and the degree to which the distribution is skewed toward low velocities varies between studies and may in fact be a function of meteoroid size (Wiegert et al. 2009; Nesvorný et al. 2011). Uncertainty in the speed distribution feeds into the uncertainty in the flux; faster meteoroids have a higher kinetic energy and will produce larger craters and brighter meteors. Any flux measurement is therefore dependent on the assumed speed distribution.

The overall flux and speed distribution of sporadic meteors, fortunately, is not thought to vary from year to year. It does, however, vary from season to season (Campbell-Brown & Jones 2006; Campbell-Brown & Wiegert 2009). These variations are of order 20% and are not currently reflected in meteoroid environment models.

6.4.1 Recent Work

Sporadic meteor flux measurements do not appear to be an area of active research. A search of the literature yielded no peer-reviewed publications of sporadic meteoroid flux measurements in the past ten years. However, the University of Western Ontario provides daily measurements of the sporadic meteoroid flux to the MEO using the algorithms presented in Campbell-Brown & Jones (2006).

Although there are few recent measurements of the sporadic flux, several recent studies have tested models of the sporadic environment against observations (e.g., Szalay & Horányi 2015; Janches et al. 2017; Pokorný et al. 2018; Moorhead et al. 2019b). These studies have taken meteoroid environment models, convolved them with estimates of meteoroid composition, ionization efficiency, and/or secondary ejecta production, and compared the results with observations ranging from radar meteors to *in situ* impact measurements. In some cases, the flux cannot be constrained due to gaps in our understanding of the data (Szalay & Horányi 2015), while in others, the comparison can be made but discrepancies of a factor of 2–3 remain (Moorhead et al. 2019b).

Several recent attempts have also been made to refine the meteoroid velocity distribution by applying the Jones (1997) treatment of ionization efficiency to radar meteor observations (Moorhead et al. 2017b; Moorhead 2018); the resulting velocity distributions have tended to skew slower than the distributions in the models. Unlike in the case of luminous efficiency, there is growing support behind a single model for the ionization efficiency of a meteor (Jones 1997; Thomas et al. 2016; DeLuca et al. 2018). Experimental results (Thomas et al. 2016; DeLuca et al. 2018) support a slightly different formulation of ionization efficiency than the theory of Jones (1997), but overall the magnitude and velocity dependence of the ionization efficiency is fairly consistent between theory and experiment.

6.4.2 Future Work

Ultimately, characterizing the uncertainty in the meteoroid flux is dependent on characterizing the uncertainty in the luminous and ionization efficiencies (see section 6.1) and ballistic limit equations (see section 6.2). However, there are steps we can take in parallel with those efforts to improve our models. For instance, several studies have measured the mass index of sporadic sources and the sporadic complex as a whole (Blaauw et al. 2011; Pokorný & Brown 2016); these indices could be incorporated into MEM to capture limiting-mass-dependent variations in relative source strength (and thus also velocity). Seasonal variations in the sporadic complex could also be included (Campbell-Brown & Jones 2006).

Furthermore, competing dynamical models of sporadic meteoroids (Wiegert et al. 2009; Nesvorný et al. 2011; Pokorný et al. 2018) could be incorporated into MEM and tested against *in situ* data in the same manner as Moorhead et al. (2019b). It may be that one of these models provides a closer match to the Pegasus and LDEF crater data while still matching meteor flux observations at the top of the Earth's atmosphere.

Simultaneously, efforts to characterize and de-bias meteoroid velocity and directionality must continue. One possible avenue towards improved velocity and radiant distributions is to revisit the methodology of Moorhead et al. (2017b) and Moorhead (2018) using the ionization efficiency of DeLuca et al. (2018), simultaneously reassessing the relative strengths of the sporadic sources reported by Campbell-Brown (2008). Such a study would generate mutually consistent velocity and radiant distributions that could potentially be incorporated into models such as MEM (see Moorhead et al. 2019b).

We should also look for opportunities to incorporate impact and anomaly data from spacecraft. NASA's proposed Lunar Gateway in particular may provide an opportunity to both obtain new and better measurements of the meteoroid flux, uncontaminated by orbital debris. The ratio of the meteoroid flux near the Moon to that near the Earth depends on the speed distribution, so even simple flux measurements near the Moon place constraints on the meteoroid speed distribution (this is also true for other locations at large geocentric distances; Love & Allton 2006). If flux measurements are available for multiple surfaces of a spacecraft, it may be possible to further constrain the local speed distribution (Zook 1991).

6.5 Uncertainties in the Near-Earth Shower Meteoroid Environment

While sporadic meteoroids pose the most significant risk to spacecraft, meteor showers can produce short-term elevations in risk that spacecraft operators may wish to mitigate. Thus, we also maintain a meteor shower model for near-Earth space that is used to generate meteor shower forecasts (Moorhead et al. 2017c; Moorhead et al. 2019a). Unlike MEM, the shower forecast model is *not* extrapolated to other locations in the inner Solar System; instead, it is restricted to near-Earth space (including the Moon). The reason for this restriction is that meteor showers are more localized and thus a single shower/orbital population is less likely to encounter multiple planets.

Showers are much more variable than the sporadic complex. Within a given year, they are much more short-lived; the strength of a shower may also vary from year to year. Certain showers, such as the Leonids and Draconids, exhibit outbursts that are many orders of magnitude more intense than they are in a "standard" year. Predicting these outbursts is critical, and thus the MEO spends a fair amount of time both monitoring meteor shower activity and simulating meteoroid streams to predict their future behavior.

A number of parameters are needed to successfully predict the behavior of a meteor shower and translate that behavior into damaging flux values. Describing the activity of a shower in a typical year requires knowledge of its peak activity (or ZHR), the rate at which activity increases and decreases near the peak, its mass index, and its speed relative to the Earth. Predicting future outbursts requires knowledge of the parent body of the stream and either its past behavior or a long enough baseline of meteor shower observations that the past behavior of the parent body can be constrained. Deducing the behavior of a comet in centuries past from the pattern of activity of its child meteor shower is a particularly difficult task (see, e.g., Egal et al. 2019).

6.5.1 Recent Work

The MEO and its collaborators at the University of Western Ontario regularly engage in observational studies of individual meteor showers; recent examples include studies of the Draconids (Ye et al. 2013), the Andromedids (Wiegert et al. 2013), the Kappa Cygnids (Moorhead et al. 2015), the eta Aquariids (Campbell-Brown & Brown 2015), and the Camelopardalids (Campbell-Brown et al. 2016). The MEO also regularly compares observations of major showers to our forecast predictions; these results are summarized in internal memos and have in some cases motivated changes to the forecast parameters. For instance, observations of the 2019 Daytime Arietids indicated that the shower is less skewed toward small particles than we previously assumed.

Finally, we recently used 15 years of meteor shower fluxes from the CMOR to improve our shower modeling parameters (Moorhead et al. 2017c). These CMOR data are valuable and unusual in that they provide almost two decades of consistently measured meteor shower fluxes. This long baseline allows us to compare the year-to-year activity of variable showers, such as the Draconids. It also allows us to stack many years of data to better characterize weaker showers that might otherwise be difficult to detect.

In addition to these observational efforts, the MEO regularly performs numerical simulations of meteor showers in an effort to better predict their future activity (Moser & Cooke 2004; Moser & Cooke 2008). For instance, we produced two parallel simulations of the 2018 Draconids (Egal et al. 2018; Egal et al. 2019); the predictions from these simulations were folded into a special advisory issued in advance of the shower. We also compare our results, when possible, with those of other modelers such as Vaubaillon, Maslov, Asher, and Jenniskens.

6.5.2 Future Work

The MEO plans to continue its collaboration with the University of Western Ontario to monitor meteoroid fluxes with CMOR. As mentioned above, this consistent long-term monitoring will allow us to characterize shower variability in a way that few other networks are capable of.

Our collaborators are also working to characterize the uncertainties associated with these fluxes, taking the influence of the solar cycle and other periodic effects into account. The longer that CMOR can generate consistent observations of the meteor environment, the more unique and useful these observations become, especially for periodically or infrequently outbursting showers.

The MEO is also working to develop an all-sky flux algorithm. The anticipated results are crude flux measurements for only the strongest meteor showers, but these flux measurements would provide a useful "lever arm" for measuring the steepness of the mass distribution of these showers (see, e.g., Campbell-Brown et al. 2016; Blaauw 2017). The mass or population index is an important input into our meteor shower forecasts and can strongly affect our flux predictions at the smallest sizes.

On the modeling side, we plan to implement several improvements in the MSFC stream model. It is increasingly clear that simulations must generate more information than simply the time at which a particle passes near the Earth—radiant and velocity information are also needed to verify that the shower has been correctly reproduced (Moorhead et al. 2015; Abedin et al. 2017). Evidence is also mounting that particle counts are a better tool for measuring activity than the "impact parameter" the MSFC stream model currently uses. The MEO has therefore modified its stream model to output radiant and velocity information and to develop tools to better convert the stream model results to quantitative shower activity predictions.

Using both our existing tools and these planned improvements, we will produce regular, incremental improvements in our ability to characterize and forecast individual showers. For example, the Geminid meteor shower is noticeably longer-lasting when observed by CMOR than when it is observed with video cameras or visual observers (Moorhead et al. 2017c). Thus, we plan to develop a mass-dependent Geminid profile that captures this behavior and can correctly predict off-peak fluxes for all limiting sizes.

6.6 The Interplanetary Meteoroid Environment

The overwhelming majority of meteoroid detections take the form of meteor observations. Many millions of meteors have been detected and measured during their passage through the Earth's atmosphere using the methods discussed in chapter 2; in contrast, no meteors have been detected in the atmospheres of other planets, except arguably a few large impacts on Jupiter's atmosphere. Additionally, most *in situ* detectors, including Pegasus, LDEF, and EURECA, operated in near-Earth space. As a result, the body of existing meteor and meteoroid observations are almost entirely limited to probing the meteoroid environment at Earth.

Meteoroids have, on occasion, been detected outside of Earth orbit; for instance, lunar impact monitoring has yielded a few hundred meteoroid impact detections on the surface of the Moon, and Pioneer 10 and 11 measured meteoroid impacts near Jupiter and Saturn. These data are valuable, yet limited; lunar impact measurements yield no velocity information and almost no directional information, and Pioneer 10 and 11 measured the flux of particles that are far too small to be hazardous.

Measurements of the interplanetary meteoroid environment are critical for building accurate interplanetary environment models. One can extrapolate from the meteoroid environment encountered at the Earth, but the uncertainty grows with geocentric distance. For example, the ratio of the flux at high altitudes to that in low Earth orbit depends on the meteoroid speed distribution (Love & Allton 2006). Uncertainties in the flux and in the speed distribution of meteoroids at low geocentric altitudes combine to produce larger uncertainties in the flux at high altitudes.

Even if the near-Earth meteoroid environment were perfectly characterized, it could not be used to extrapolate a fully accurate interplanetary environment. This is because it is possible, if unlikely, for meteoroid streams to intersect the orbits of other planets but not that of Earth. For example, Comet C/2013 A1 (Siding Spring) approached Mars extremely closely on October 19, 2014, but, because it never comes closer to the Sun than about 1.4 au, the comet never approaches the Earth. Similarly, the meteoroids and dust it produces are unlikely to ever produce noticeable activity at the Earth (certainly not within our lifetime). Mariner IV may have encountered another such shower; in 1965, Mariner's dust detector recorded a burst of activity (NASA 1971) indicating that the spacecraft was probably struck by thousands of particles in a short period of time. It's been hypothesized that the spacecraft passed through an unknown meteoroid stream or near the nucleus of a dead comet. Thus, these unknown streams are a critical source of uncertainty in our models of the meteoroid environment.

6.6.1 Recent Work

There have been no recent *in situ* measurements of the hazardous meteoroid flux in interplanetary space or even at large geocentric altitudes. In fact, all *in situ* measurements of particle fluxes have probed the environment at sizes that are too small to damage spacecraft. For instance, the Pioneer 10 and 11 spacecraft measured the flux of 1-10 ng meteoroids in the asteroid belt and near Jupiter (Humes et al. 1975); the minimum meteoroid mass that is typically considered damaging is 1 μg.

There are, however, limited and indirect measurements of the meteoroid flux outside of low Earth orbit. As mentioned previously in this handbook, the MEO monitors the rate of large impacts on the lunar surface via the flashes of light they produce. Furthermore, it was reported in 2015 that the Messenger spacecraft had detected variations in Mercury's calcium exosphere that are believed to be produced by meteoroid impacts (Killen & Hahn 2015); subsequent modeling supports Killen & Hahn's hypothesis that this is largely produced by debris from comet 2P/Encke (Christou et al. 2015; Pokorný et al. 2017). Separately, MAVEN observed the aftereffects of particles from Comet Siding Spring impacting the Martian atmosphere (Schneider et al. 2015). No showers have been detected subsequently, although Crismani et al. (2017) reported on the presence of a persistent meteoric metal layer in the Martian atmosphere and have derived a (large) upper limit on the meteoroid flux on Mars. The Lunar Dust Experiment (LDEX) instrument measured secondary ejecta around the Moon that are believed to be primarily produced by meteoroid impacts; recent modeling has attempted to constrain the relative strength of sporadic sources (Janches et al. 2018).

In each of these cases, interpretation of these results is hampered by some lack of information. For instance, lunar impacts are kinetic-energy-limited and do not probe the directionality or speed of the impactors. In the case of the MESSENGER, MAVEN, and LADEE/LDEX observations, the limiting observable and its dependence on quantities such as velocity are unknown. Thus, correctly interpreting these results will likely require substantial additional work and, where possible, additional observations.

6.6.2 Future Work

While these indirect measurements are promising, additional constraints on the meteoroid environment at other locations in the Solar System are needed. This could take the form of dedicated impact detectors on interplanetary missions, remote inspection of impact damage on interplanetary spacecraft, or the observation of meteors in the atmospheres of other planets by orbiting spacecraft. A large-area impact detector on Gateway would be particularly valuable for constraining the cislunar and interplanetary environment.

Spacecraft anomaly data could partially compensate for the absence of a dedicated meteoroid impact detector. Certain spacecraft are either sensitive to impacts or on orbits that are well-positioned to probe the meteoroid flux. For instance, the *Gaia* spacecraft must maintain a stable orientation to complete its mission of compiling the largest and most precise star catalog; it is therefore able to detect tiny attitude disturbances and thus fairly small meteoroid impacts. *Gaia* orbits near the Sun-Earth L2 Lagrange point and therefore would probe the interplanetary flux at 1 au. To give another example, the Magnetospheric Multiscale Mission (MMS) orbits the Earth with a high eccentricity and a fairly large minimum altitude (2,550 km); thus, at most points in its orbit, meteoroids dominate over orbital debris in producing impacts. MMS has experienced many anomalies, including a major impact on February 2, 2016. The rate of meteoroid-induced anomalies on MMS as a function of orbital altitude could be used to constrain not only the flux but potentially the speed distribution of meteoroids in near-Earth space. Understanding the speed distribution of meteoroids is a key component of accurately extrapolating our meteoroid model to other points in the Solar System. However, in both cases, the MEO has been unsuccessful in obtaining further information from these programs. Better collection and sharing of spacecraft anomaly data is needed to fold this information into our models.

6.7 References

Abedin, A.; Wiegart, P.; Brown, P.; et al.: "The Age and the Probable Parent Body of the Daytime Arietid Meteor Shower," *Icarus*, Vol. 281, pp. 417–443, 2017.

Armitage, T.; and Campbell-Brown, M.D.: "Using High-resolution Observations to Constrain the Grain Mass Distribution of Small Meteoroids," *Meteoroids*, pp. 1–1, 2019.

Ayers, W.G.; McCrosky, R.E.; and Shao, C.Y.: "Photographic Observations of 10 Artificial Meteors," *SAO Special Report #317 (1970)*, pp. 317, 1970.

Blaauw, R.C.: "The Mass Index and Mass of the Geminid Meteoroid Stream as Determined with Radar, Optical and Lunar Impact Data," *Planetary and Space Science*, Vol. 143, pp. 83–88, 2107.

Blaauw, R.C.; Campbell-Brown, M.D.; and Weryk, R.J.: "Mass Distribution Indices of Sporadic Meteors Using Radar Data," *Monthly Notices of the Royal Astronomical Society*, Vol. 412, No. 3, pp. 2033–2039, 2011.

Borovička, J.; Spurný, P.; and Koten, P.: "Atmospheric Deceleration and Light Curves of Draconid Meteors and Implications for the Structure of Cometary Dust," *Astronomy and Astrophysics*, Vol. 473, No. 2, pp. 661–672, 2007.

Campbell-Brown, M.D.: "High Resolution Radiant Distribution and Orbits of Sporadic Radar Meteoroids," *Icarus*, Vol. 196, No. 1, pp. 144–163, 2008.

Campbell-Brown, M.D.; Blaauw, R.C.; and Kingery, A.: "Optical Fluxes and Meteor Properties of the Camelopardalid Meteor Shower," *Icarus*, Vol. 277, pp. 141–153, 2016.

Campbell-Brown, M.D.; Borovička, J.; Brown, P.G.; and Stokan, E.: "High-resolution Modelling of Meteoroid Ablation," *Astronomy and Astrophysics*, Vol. 557, p. A41, 2013.

Campbell-Brown, M.D.; and Brown, P.G.: "A 13-year Radar Study of the η-Aquariid Meteor Shower," *Monthly Notices of the Royal Astronomical Society*, Vol. 446, No. 4, pp. 3669–3675, 2015.

Campbell-Brown, M.D.; and Jones, J.: "Annual Variation of Sporadic Radar Meteor Rates," *Monthly Notices of the Royal Astronomical Society*, Vol. 367, No. 2, pp. 709–716, 2006.

Campbell-Brown, M.D.; and Koschny, D.: "Model of the Ablation of Faint Meteors," *Astronomy and Astrophysics*, Vol. 418, pp. 751–758, 2004.

Campbell-Brown, M.D.; and Wiegert, P.A.: "Seasonal Variations in the North Toroidal Sporadic Meteor Source," *Meteoritics & Planetary Science*, Vol. 44, No. 1, pp. 1837–1848, 2009.

Christou, A.A.; Killen, R.M.; and Burger, M.H.: "The Meteoroid Stream of Comet Encke at Mercury: Implications for MErcury Surface, Space ENvironment, GEochemistry, and Ranging Observations of the Exosphere," *Geophysical Research Letters*, Vol. 42, No. 1, pp. 7311–7318, 2015.

Crismani, M.M.J.; Schneider, N.M.; Plane, J.M.C.; et al.: "Detection of a Persistent Meteoric Metal Layer in the Martian Atmosphere," *Nature Geoscience*, Vol. 10, pp. 401–404, 2017.

Dai, Z.; Ren, H.; Zhuang, X.; and Rabczuk, T.: "Dual-Support Smoothed Particle Hydrodynamics for Elastic Mechanics," *International Journal of Computational Methods*, Vol. 14, No. 4, pp. 1750039–29, 2017.

DeLuca, M.; Munsat, T.; Thomas, E.; et al.: "The Ionization Efficiency of Aluminum and Iron at Meteoric Velocities," *Planetary and Space Science*, Vol. 156, pp. 111–116, 2018.

Drolshagen, G.; and Moorhead, A.V.: "The Meteoroid Impact Hazard for Spacecraft," *Meteoroids: Sources of Meteors on Earth and Beyond*, pp. 255–274, 2019.

Egal, A.; Wiegart, P.; Brown, P.G.; et al.: "The Draconid Meteoroid Stream 2018: Prospects for Satellite Impact Detection," *The Astrophysical Journal Letters*, Vol. 866, No. 1, p. L8, 2018.

Egal, A.; Wiegart, P.; Brown, P.G.; et al.: "Meteor Shower Modeling: Past and Future Draconid Outbursts," *Icarus*, Vol. 330, pp. 123–141, 2019.

Evans, S.W.; Finchum, A.; Hubbs, W.; et al.: "NASA Marshall Impact Testing Facility Capabilities Applicable to Lunar Dust Work," *Engineering Directorate*, NASA Marshall Space Flight Center, Huntsville, AL, 2008.

Flynn, G.J.; Durda, D.D.; Patmore, E.B.; et al.: "Hypervelocity Impact Cratering of Chondritic Meteorites: Implications for Asteroid Recoil," *Procedia Engineering*, Vol. 204, pp. 146–153, 2017.

Fulle, M.; Corte, V.D.; Rotundi, A.; et al.: "Density and Charge of Pristine Fluffy Particles from Comet 67P/Churyumov-Gerasimenko," *The Astrophysical Journal Letters*, Vol. 802, No. 1, p. L12, 2015.

Fulle, M.; Levasseur-Regourd, A.C.; McBride, N.; and Hadamcik, E.: "*In Situ* Dust Measurements From within the Coma of 1P/Halley: First-Order Approximation with a Dust Dynamical Model," *The Astronomical Journal*, Vol. 119, No. 4, pp. 1968–1977, 2000.

Grün, E.; Zook, H.A.; Fechtig, H.; and Giese, R.H.: "Collisional Balance of the Meteoritic Complex," *Icarus*, Vol. 62, No. 2, pp. 244–272, 1985.

Hayashida, K.B.; and Robinson, J.H.: "Single Wall Penetration Equations," NASA-TM-103565, NASA Marshall Space Flight Center, Huntsville, AL, pp. 1–22, 1991.

Heisler, J.; Tremaine, S.; and Alcock, C.: "The Frequency and Intensity of Comet Showers from the Oort Cloud," *Icarus*, Vol. 70, No. 2, pp. 269–288, 1987.

Hill, K.A.; Rogers, L.A.; and Hawkes, R.L.: "High Geocentric Velocity Meteor Ablation," *Astronomy and Astrophysics*, Vol. 444, No. 2, pp. 615–624, 2005.

Hou, J.P.; and Ruiz, C.: "Soft Body Impact on Laminated Composite Materials," *Composites Part A: Applied Science and Manufacturing*, Vol. 38, No. 2, pp. 505–515, 2007.

Hu, K.; and Schonberg, W.P.: "Ballistic Limit Curves for Non-spherical Projectiles Impacting Dual-wall Spacecraft Systems," *International Journal of Impact Engineering*, Vol. 29, No. 1–10, pp. 345–355, 2003.

Humes, D.H.; Alvarez, J.M.; Kinard, W.H.; and O'Neal, R.L.: "Pioneer 11 Meteoroid Detection Experiment - Preliminary Results," *Science*, Vol. 188, No. 4187, pp. 473–474, 1975.

Janches, D.; Pokorny, P.; Sarantos, M.; et al.: "Constraining the Ratio of Micrometeoroids From Short- and Long-Period Comets at 1 AU From LADEE Observations of the Lunar Dust Cloud," *Geophysical Research Letters*, Vol. 45, No. 4, pp. 1713–1722, 2018.

Janches, D.; Swarnalingam, N.; Carillo-Sanchez, J.D.; et al.: "Radar Detectability Studies of Slow and Small Zodiacal Dust Cloud Particles. III. The Role of Sodium and the Head Echo Size on the Probability of Detection," *The Astrophysical Journal*, Vol. 843, No. 1, 2017.

Jones, W.: "Theoretical and Observational Determinations of the Ionization Coefficient of Meteors," *Monthly Notices of the Royal Astronomical Society*, Vol. 288, No. 4, pp. 995–1003, 1997.

Kikwaya, J.B.; Campbell-Brown, M.D.: and Brown, P.G.: "Bulk Density of Small Meteoroids," *Astronomy and Astrophysics*, Vol. 530, p. 17, 2011.

Killen, R.M.; and Hahn, J.M.: "Impact Vaporization as a Possible Source of Mercury's Calcium Exosphere," *Icarus*, Vol. 250, pp. 230–237, 2015.

Kim, H.; Welch, D.A.; and Kedward, K.T.: "Experimental Investigation of High Velocity Ice Impacts on Woven Carbon/epoxy Composite Panels," *Composites Part A: Applied Science and Manufacturing*, Vol. 34, No. 1, pp. 25–41, 2003.

Love, S.G.; and Allton, J.H.: "Micrometeoroid Impact Crater Statistics at the Boundary of Earth's Gravitational Sphere of Influence," *Icarus*, Vol. 184, No. 2, pp. 302–307, 2006.

Marshall, R.A.; Brown, P.G.; and Close, S.: "Plasma Distributions in Meteor Head Echoes and Implications for Radar Cross Section Interpretation," *Planetary and Space Science*, Vol. 143, pp. 203–208, 2017.

McNamara, H.; Jones, J.; Kauffman, B.; et al.: "Meteoroid Engineering Model (MEM): A Meteoroid Model For The Inner Solar System," *Earth, Moon, and Planets*, Vol. 95, No. 1, pp. 123–139, 2004.

Mihaly, J.M.: *Investigation of Hypervelocity Impact Phenomena Using Real-Time Concurrent Diagnostics*, PhD Dissertation, California Institute of Technology, Pasadena, California, 2013.

Moorhead, A.V.; Brown, P.G.; Spurny, P.; et al.: "The 2014 KCG Meteor Outburst: Clues to a Parent Body," *The Astronomical Journal*, Vol. 150, No. 4, p. 122, 2015.

Moorhead, A.V.; Blaauw, R.C.; Moser, D.E.; et al.: "A Two-population Sporadic Meteoroid Bulk Density Distribution and Its Implications for Environment Models," *Monthly Notices of the Royal Astronomical Society*, Vol. 472, No. 4, pp. 3833–3841, 2017a.

Moorhead, A.V.; Brown, P.G.; Campbell-Brown, M.D.; et al.: "Fully Correcting the Meteor Speed Distribution for Radar Observing Biases," *Planetary and Space Science*, Vol. 143, pp. 209–217, 2017b.

Moorhead, A.V.; Cooke, W.J.; and Campbell-Brown, M.D.: "Meteor Shower Forecasting for Spacecraft Operations," in *Proceedings of the 7th European Conference on Space Debris*, pp. 1–11, 2017c.

Moorhead, A.V.: "Deconvoluting Measurement Uncertainty from the Meteor Speed Distribution," *Meteoritics & Planetary Science*, Vol. 53, No. 6, pp. 1292–1298, 2018.

Moorhead, A.V.; Egal, A.; Brown, P.G.; et al.: "Meteor Shower Forecasting in Near-Earth Space," *Journal of Spacecraft and Rockets*, Vol. 866, No. 1, pp. 1–15, 2019a.

Moorhead, A.V.; Kingery, A.; and Ehlert, S.: "NASA's Meteoroid Engineering Model (MEM) 3.0 and Its Ability to Replicate Spacecraft Impact rates," *Journal of Spacecraft and Rockets*, pp. 1–38, 2019b, <http://arc.aiaa.org/doi/abs/10.2514/1.A34561>.

Moser, D.E.: and Cooke, W.J.: "MSFC Stream Model Preliminary Results: Modeling Recent Leonid and Perseid Encounters," *Earth, Moon, and Planets*, Vol. 95, No. 1, pp. 141–153, 2004.

Moser, D.E.; and Cooke, W.J.: "Updates to the MSFC Meteoroid Stream Model," *Earth, Moon, and Planets*, Vol. 102, No. 1, pp. 285–291, 2008.

NASA: "Mariner-Venus 1967," NASA-SP-190, NASA Headquarters, Washington, D.C., pp. i–301, 1971.

Nesvorný, D.; Janches, D.; Vokrouhlicky, D.; et al.: "Dynamical Model for the Zodiacal Cloud and Sporadic Meteors," *The Astrophysical Journal*, Vol. 743, No. 2, p. 129, 2011.

Pokorný, P.; Brown, P.G.: "A Reproducible Method to Determine the Meteoroid Mass Index," *Astronomy and Astrophysics*, Vol. 592, pp. A150–12, 2016.

Pokorný, P.; Sarantos, M.; and Janches, D.: "A Comprehensive Model of the Meteoroid Environment around Mercury," *The Astrophysical Journal*, Vol. 863, No. 1, p. 31, 2018.

Pokorný, P.; Sarantos, M.; and Janches, D.: "Reconciling the Dawn–Dusk Asymmetry in Mercury's Exosphere with the Micrometeoroid Impact Directionality," *The Astrophysical Journal Letters*, Vol. 842, No. 2, 2017.

Rudawska, R.; Toth, J.; Kalmancok, D.; et al.: "Meteor Spectra from AMOS Video System," *Planetary and Space Science*, Vol. 123, No. C, pp. 25–32, 2016.

Schneider, N.M.; Deighan, J.I.; Stewart, A.I.F.; et al.: "MAVEN IUVS Observations of the Aftermath of the Comet Siding Spring Meteor Shower on Mars," *Geophysical Research Letters*, Vol. 42, No. 1, pp. 4755–4761, 2015.

Spurný, P.; Borovička, J.; and Shrbený, L.: "Automation of the Czech part of the European Fireball Network: Equipment, Methods and First Results," *Near Earth Objects*, Vol. 236, No. S236, pp. 121–130, 2007.

Subasinghe, D.; and Campbell-Brown, M.D.: "Luminous Efficiency Estimates of Meteors. II. Application to Canadian Automated Meteor Observatory Meteor Events," *The Astronomical Journal*, Vol. 155, No. 2, 2018.

Szalay, J.R.; and Horányi, M.: "Annual Variation and Synodic Modulation of the Sporadic Meteoroid Flux to the Moon," *Geophysical Research Letters*, Vol. 42, No. 2, pp. 10–, 2015.

Thomas, E.; Simolka, J.; DeLuca, M.; et al.: "Experimental Setup for the Laboratory Investigation of Micrometeoroid Ablation Using a Dust Accelerator," *Review of Scientific Instruments*, Vol. 88, No. 3, pp. 034501–13, 2017.

Thomas, E.; Janches, D.; Munsat, T.; et al.: "Measurements of the Ionization Coefficient of Simulated Iron Micrometeoroids," *Geophysical Research Letters*, Vol. 43, No. 8, pp. 3645–3652, 2016.

Verniani, F.: "On the Luminous Efficiency of Meteors," *Smithson. Contrib. Astrophys.*, Vol. 8, pp. 141–, 1965.

Watts, A.J.; and Atkinson, D.R.: "Dimensional Scaling for Impact Cratering and Perforation," A. S. Levine (ed.), *Third LDEF Post-Retrieval Symposium*, NASA-CP-3275, pp. 522–535, 1995.

Weryk, R.J.; and Brown, P.G.: "Simultaneous Radar and Video Meteors—II: Photometry and Ionisation," *Planetary and Space Science*, Vol. 81, No. C, pp. 32–47, 2013.

Wiegert, P.A.; Brown, P.G.; Weryk, R.J.; and Wong, D.K.: "The Return of the Andromedids Meteor Shower," *The Astronomical Journal*, Vol. 145, No. 3, p. 70, 2013.

Wiegert, P.A.; Vaubaillon, J.J.; and Campbell-Brown, M.D.: "A Dynamical Model of the Sporadic Meteoroid Complex," *Icarus*, Vol. 201, No. 1, pp. 295–310, 2009.

Williamsen, J.; and Evans, S.: "Predicting Orbital Debris Shape and Orientation Effects on Spacecraft Shield Ballistic Limits Based on Characterstic Length," *Internaitonal Journal of Impact Engineering*, Vol. 33, No. 1–12, pp. 862-871, 2006.

Ye, Q.; Brown, P.G.; Campbell-Brown, M.D.; and Weryk, R.J.: "Radar Observations of the 2011 October Draconid Outburst," *Monthly Notices of the Royal Astronomical Society*, Vol. 436, No. 1, pp. 675–689, 2013.

Zook, H.A.: "Deriving the Velocity Distribution of Meteoroids from the Measured Meteoroid Impact Directionality on the Various LDEF Surfaces," in LDEF: 69 Months in Space, First Post-Retrieval Symposium, Part 1, NASA Langley Research Center, pp. 569–579, 1991.

REPORT DOCUMENTATION PAGE

Form Approved
OMB No. 0704-0188

1. REPORT DATE *(DD-MM-YYYY)*	2. REPORT TYPE	3. DATES COVERED *(From - To)*
01–12–2019	Technical Memorandum	

4. TITLE AND SUBTITLE

A Meteoroid Handbook for Aerospace Engineers and Managers

5a. CONTRACT NUMBER

5b. GRANT NUMBER

5c. PROGRAM ELEMENT NUMBER

6. AUTHOR(S)

A. Moorhead, B. Cooke, R. Blaauw*, D. Moser*, S. Ehlert*,**

5d. PROJECT NUMBER

5e. TASK NUMBER

5f. WORK UNIT NUMBER

7. PERFORMING ORGANIZATION NAME(S) AND ADDRESS(ES)

George C. Marshall Space Flight Center
Huntsville, AL 35812

8. PERFORMING ORGANIZATION REPORT NUMBER

M–1494

9. SPONSORING/MONITORING AGENCY NAME(S) AND ADDRESS(ES)

National Aeronautics and Space Administration
Washington, DC 20546–0001

10. SPONSORING/MONITOR'S ACRONYM(S)

NASA

11. SPONSORING/MONITORING REPORT NUMBER

NASA/TM—2019–220142

12. DISTRIBUTION/AVAILABILITY STATEMENT

Unclassified-Unlimited
Subject Category 91
Availability: NASA STI Information Desk (757–864–9658)

13. SUPPLEMENTARY NOTES

Prepared by Marshall Space Flight Center, Alabama,
*Jacobs Space Exploration Group, Huntsville, Alabama, **Qualis Corporation, Huntsville, AL

14. ABSTRACT

The purpose of this document is to provide aerospace engineers and managers with a general understanding of meteoroids and the hazards they pose to spacecraft. Topics covered include basic meteoroid terminology, meteoroid measurement techniques, the current state of knowledge of the meteoroid environment, the effects of meteoroid impacts on spacecraft and on the ground, and key areas of planned or needed future work.

15. SUBJECT TERMS

meteor, meteoroid, fireball, hypervelocity impacts, spacecraft safety

16. SECURITY CLASSIFICATION OF:			17. LIMITATION OF ABSTRACT	18. NUMBER OF PAGES	19a. NAME OF RESPONSIBLE PERSON
a. REPORT	b. ABSTRACT	c. THIS PAGE			STI Help Desk at email: help@sti.nasa.gov
U	U	U	UU	136	19b. TELEPHONE NUMBER *(Include area code)* STI Help Desk at: 757–864–9658

National Aeronautics and
Space Administration
IS02
George C. Marshall Space Flight Center
Huntsville, Alabama 35812